APPLICATION OF GIS AND REMOTE SENSING IN FLOOD MANAGEMENT IN THE LAKE VICTORIA BASIN

CHARLES ONYANGO GAYA

DOCTOR OF PHILOSOPHY

(Geomatic Engineering and GIS)

JOMO KENYATTA UNIVERSITY OF

AGRICULTURE AND TECHNOLOGY

2019

Application of GIS and Remote Sensing in Flood Management in the Lake Victoria Basin

Charles Onyango Gaya

Thesis Submitted in partial fulfillment for the degree of Doctor of Philosophy in Geomatic Engineering and Geospatial Information Systems in the Jomo Kenyatta University of Agriculture and Technology

2019

DECLARATION

This thesis is my original work and has not been presented for a degree in any other university.

Signature……Date……

Charles Onyango Gaya

This thesis has been submitted for examination with our approval as the University supervisors

Signature……...Date……

Prof. Moses K. Gachari, PhD.

DeKUT, Kenya

Signature……...Date……

Prof. John M. Gathenya, PhD.

JKUAT, Kenya

DEDICATION

I dedicate this work to my family for their understanding and for bearing with me during its realization and compilation.

ACKNOWLEDGEMENT

Foremost, I would like to express my sincere gratitude to the German Academic Exchange Service (DAAD) for the providing the research funds that enabled me undertake the study. I wish to thank my Supervisors, Prof. M.K. Gachari and Prof. J.M. Gathenya for their invaluable contribution and support in the process of the research work. I would also like to acknowledge. the Jomo Kenyatta University of Agriculture and Technology and the Department of Geomatic Engineering and Geospatial Informatin Systems (GEGIS) led by the long-term Chairman Prof. E.H. Waithaka, the current Chairman Dr. F.N. Mutua, The Dean of the school of Civil, Environmental and Geomatic Engineering, Prof Z. Abiero-Gariy and the entire GEGIS staff for the guidance and support provided while undertaking the project. Last but not least, I acknowledge the Kenya Metereological Department, the Survey of Kenya, t he Regional Centre for Mapping of Resources for Development (RCMRD), The Ministry of Water and Irrigation and the World Agroforestry Centre (formerly ICRAF) for providing the data that has been used in this research.

TABLE OF CONTENTS

DECLARATION ..... **ii**

DEDICATION ..... **iii**

ACKNOWLEDGEMENT ..... **iv**

TABLE OF CONTENTS ..... **v**

LIST OF TABLES ..... **x**

LIST OF FIGURES ..... **xii**

LIST OF APPENDICES ..... **xv**

ACRONYMS AND ABBREVIATIONS ..... **xvi**

ABSTRACT ..... **xviii**

CHAPTER ONE **1**

INTRODUCTION **1**

1.1 Background 1

1.2 Motivation and problem statement 3

1.3 Research identification 5

1.4 Research objectives 6

1.5 Research questions 6

1.6 Scope and Limitations of the Study 6

1.7 Study outline.....7

CHAPTER TWO 8

LITERATURE REVIEW.....8

2.1 Introduction 8

2.2 The Hydrologic Process 8

2.3 Determination of Discharge from Watershed.....10

2.3.1 Rational Method 12

2.3.2 SCS Curve Number Method.....13

2.3.3 Empirical Methods.....20

2.3.4 Frequency Analysis.....21

2.4 Developing Hydrologic Models 22

2.4.1 Distributed Hydrologic Modelling.....23

2.4.2 Watershed Analysis 24

2.4.3 Factors Influencing Watershed Analysis 29

2.5 DEM Generation 30

2.5.1 DEMs from Satellite Data.....32

2.6 Rainfall Estimation 36

2.7 Areal rainfall from Point Rainfall 41

2.8 Use of Satellite imagery in Flood Hazard Monitoring 42

2.9 Classification of Satellite Imagery in Flood inundation Mapping 45

2.9.1 Visual Image interpretation 45

2.9.2 Multispectral Image Classification and Analysis 45

2.9.3 Radar Image Interpretation 46

2.10 Flood Hazard Forecasting 47

2.11 Flood Management 48

CHAPTER THREE 50

MATERIALS AND METHODS 50

3.1 Materials: Site Location, Characteristics and Data Description 50

3.1.1 Study area 50

3.1.2 Data 56

3.2 Methodology 65

3.2.1 Introduction 65

3.2.2 Validation of Satellite Rainfall Estimates 66

3.2.3 Derivation of Runoff Parameters 70

3.2.4 Simulation of Surface Runoff Volumes from Rainfall Estimates 80

3.2.5 Flood Hazard Forecasting 81

3.2.6 GIS Database for Flood Management 82

3.2.7 Classification of Satellite Imagery 83

CHAPTER FOUR 85

RESULTS 85

4.1 Rainfall Estimation 85

4.2 Rainfall-Runoff Simulation 89

4.3 Flood Inundation Mapping 93

CHAPTER FIVE 94

DISCUSSION 94

5.1 Introduction 94

5.2 Evaluation of Satellite-Derived Rainfall Estimates (RFE) 94

5.3 GIS-Based Derivation of Runoff Parameters 95

5.4 GIS and Remote Sensing Integration for Flood Management 96

CHAPTER SIX 97

CONCLUSION AND OUTLOOK 97

6.1 Conclusions 97

6.1.1 Evaluation of Satellite-Derived Rainfall Estimates (RFE) 97

6.1.2 GIS-Based Derivation of Runoff Parameters 98

6.1.3 GIS and Remote Sensing Integration for Flood Management 99

6.2 Recommendations 100

REFERENCES 102

APPENDICES 114

LIST OF TABLES

Table 2.1: Comparison of selected satellite sensors that produce DEMs from optical satellite data ..... - 33 -

Table 2.2: Typical terrain features and signatures on radar images (Source: Jr. Sabins, 1997) 47

Table 3.1: Translation of LCCS Code into meaningful description.....60

Table 3.2: Grouping labels into major land cover types and assigning LU-Code 61

Table 3.3: The Satellite data used in this study 65

Table 3.4: The main land cover types over the Nyando basin 73

Table 3.5: Soil properties (Source: Artan et al., 2007).....74

Table 3.6: Generic conditions for soil classification (according to the Curve Number method).....75

Table 3.7: CN Runoff Curve Numbers as estimated from land cover classes and hydraulic soil groups. Source: 77

Table 4.1: Results of the pairwise analysis between dekadal satellite rainfall estimates and the observed station data for the selected period.....86

Table 4.2: Degree of association between the observed data and the satellite rainfall estimates at each station. 87

Table 4.3: Comparison of performance of RFE against rain gauges grouped by elevation of gauges.....88

Table 4.4: Degree of association between the simulated runoff volume and the daily stream levels at 1GD03 between 2006 and 2012 91

Table 4.5: Accuracy assessment for ASTER using Landsat as reference image. 93

LIST OF FIGURES

Figure 2.1: The Hydrologic Process (Source: Lance, 2004).....9

Figure 2.2: Relationship between the rainfall *P*, runoff *Q*, initial abstraction *Ia*, and reservoir capacity *S* according to the Curve Number Method (Source: Das, 2008).....14

Figure 2.3: Relationship between the rainfall *P* and runoff *Q* by curve numbers, when initial abstraction I_a = 2.2 (Source: USDA, 1986).....16

Figure 2.4: Schematic of a synthetic triangular runoff hydrograph (Source: Cornell University (2008) after SCS (1972)) 19

Figure 2.5: Distributed and lumped catchment parameters (Source: van Dijk et al., 1999).....23

Figure 2.6: Watersheds for each section of a stream network (Source: ESRI, 2014).....25

Figure 2.7: Satellite rainfall estimates (RFE) over Africa on 1st January 1995 (Source: USGS FEWSNET, n.d.) 39

Figure 3.1: Nyando Basin (Source: JICA, 2009) 52

Figure 3.2: Location of Rain and Flow Gauges in the Nyando Basin 57

Figure 3.3: RFE Grid for 2nd August 2003 overlaid with gauging stations over the Nyando Basin. 58

Figure 3.4: Time-series comparison of observed and satellite-derived estimates of daily rainfall at Station 8935186, Kimwani A.D.C. Farm.....59

Figure 3.5: Map generated from the major land cover types 62

Figure 3.6: A GIS display of soil data (Courtesy of FAO SOTER) 63

Figure 3.7: DEM of the Nyando Basin Overlaid with the Hydrology 64

Figure 3.8: Generalised workflow for utilising ground and remotely sensed data to support flood forecasting, management, and inundation mapping in a GIS environment 66

Figure 3.9: Comparison of annual rainfall between observed and satellite-derived estimates at the positions of 12 stations for the year 1999 67

Figure 3.10: Time series plot of average study area rainfall (millimetres per dekad) for the 37 dekads of 2003 for the rain gauges (observed) and satellite RFE .68

Figure 3.11: Workflow for Deriving Runoff Parameters (ESRI, 2014) 71

Figure 3.12*:* Flow accumulation and runoff volume.....72

Figure 3.13*:* This illustration shows a grid of soil hydraulic groups in the Nyando Basin 76

Figure 3.14: Grid of curve numbers assigned for each cell in the basin from land cover and soil hydraulic class grids.....78

Figure 3.15: Runoff volume for the study area on 20th April 1996 81

Figure 3.16: A GIS Database of Nyando district compiled from topographic maps and updated by field surveys. 83

Figure 4.1: Time series plot of average study area rainfall (millimetres per dekad) for the from 1996 t0 2003 for the rain gauges and satellite RFE.....85

Figure 4.2: Scatter plots of decadal (10-day) average rain gauges (observed) rainfall versus satellite RFE for 1999 and 2003.....88

Figure 4.3: A graphical comparison between the simulated runoff volume and observed river levels at flow gauge 1GB11 for the year 1996. 90

Figure 4.4: Graphical comparisons between the simulated runoff volume and observed river levels at flow gauge 1GD03 for (a) 2006 and (b) 2012. 92

LIST OF APPENDICES

Appendix I: VBA Code for Extraction of RFEValues at Rain Gauge Positions.....114

Appendix II: The Procedure of Using Satellite Rainfall Estimates (RFE) to Simulate Surface Runoff in GIS.....122

ACRONYMS AND ABBREVIATIONS

CN	Curve Number
CCD	Cold Cloud Duration
DEM	Digital Elevation Model
DMCN	Drought Monitoring Centre, Nairobi
DSS	Decision Support System
DTM	Digital Terrain Model
EDC	USGS EROS Data Centre
FAO	Food & Agriculture Organization
FEWS	Food Early Warning System
GIS	Geographical Information System
GPI	GOES Precipitation Index
GPCP	Global Precipitation Climatology Project
GPS	Global Positioning Systems
GTS	Global Telecommunications System
HEC-HMS	Hydrologic Engineering Center - Hydrological Modelling System
LiDAR	Light Detection and Ranging

LCCS	Land Cover Classification System
LP DAAC	Land Processes Distributed Active Archive Center
NASA	National Aeronautics and Space Administration
NOAA	National Oceanographic and Atmospheric Administration
NRCS	Natural Resources Conservation Service
RFE	Rainfall Estimates
SCS	Soil Conservation Service
SRTM	Shuttle Radar Topography Mission
SWAT	Soil and Water Assessment Tool
TRMM	Tropical Rainfall Measuring Mission
USDA	United States Department of Agriculture
USAID	U.S. Agency for International Development
USGS	United States Geological Survey
VBA	Visual Basic for Applications
WMO	World Meteorological Organization

ABSTRACT

Floods are the most common and widespread climate-related hazard in the Lake Victoria region. However, significant delays in ground data availability have made it unfeasible to use traditional flood forecasting systems. Satellite rainfall estimates have been identified as readily and economically available data that can be used as input to run hydrologic models and produce flood-warning systems. The aim of the study therefore is develop a simple and locally viable alternative approach to circumvent the absence of reliable ground measurements by using satellite rainfall estimates for forecasting and management of floods in the study area. The satellite-derived rainfall estimates (RFE) were first evaluated using historical rainfall data for the Nyando basin corresponding to the locations of 35 gauging stations in the basin for the period 1995 to 2005. A Digital Elevation Model (DEM) of the basin was used to generate the drainage patterns of the basin. The land cover of the study area and the digital soil map are incorporated in the system. The study applies daily driven satellite-derived rainfall and the pixel based Curve Number method for spatially distributed hydrologic streamflow modelling and flood forecasting. Rainfall–runoff relationships results of the area obtained in a spatial scale are then tested on their capabilities as a flood early-warning system by comparing them with historical streamflow. The approach was further tested using RFE for the period 2006 to 2012. The results for comparisons at daily accumulations of RFE with observed rain gauge data are not satisfactory but they performed reasonably well in detecting the occurrence of rainfall. The products show significant results for 10-day accumulation where regression analysis yielded on average, a correlation coefficient (r) of 0.78. While graphical plots of daily-observed stream flow against simulated streamflow show a poor agreement, there is indication that when there is a drastic surge in the runoff volume, a rise in the river level is to be expected and it enables the prediction of the occurrence of floods and the issuance of early warnings.

CHAPTER ONE

INTRODUCTION

1.1 Background

Floods are considered one of the most common natural hazards in the Lake Victoria basin (Otiende, 2009). Damage from flooding has been increasing each year resulting in loss of lives, property and production as well as affecting activities in the flooded areas (Nyakundi, Mogere, Mwanzo, & Yitambe, 2012). According to Otiende (2009), these losses will continue to increase as the population of the area increases and more people reside in the areas that are subject to the flood hazard. The flood prone areas of Western Kenya are located around the Lake Victoria Basin in the Nzoia and Nyando river basins. The two river systems pose the greatest dangers in that they drain very large low-lying plains that are also very heavily populated before entering the lake. The rivers are responsible for the flooding downstream in Budalangi area and Kano plains, respectively (DMCN, 2004; Opere, 2013)

Solutions that are normally put in place for coping with the floods mostly involve structural flood protection devices especially dams and dykes (Olugunorisa, 2011). However, an additional strategy using non-structural methods of mitigation of flood hazards has increasingly found favour with countries prone to flood hazards (Kourgialas & Karatzas, 2011). Modern flood forecasting techniques and the association with real-time hydrologic data collection systems is one such non-structural method (Jain et al., 2018; WMO, 2011b). The strategy involves the integration of streamflow forecasting models with a GIS (WMO, 2011a).

GIS has proven to be an effective tool in flood modelling. It has been used for describing, analysing, modelling and integrating forecasted flood levels with other related information such as topographic, thematic and attribute information. GIS

provides the essentials for Digital Elevation Models (DEMs), river and floodplain surface geometry (Li, 2014). It also provides the tools for visual interpretation and evaluation of flood distribution and inundation maps. It offers new opportunities to develop and implement a user-friendly, interactive decision support system for flood forecasting and monitoring using dynamic spatial modelling (Levy, Gopalakrishnan, & Lin, 2005).

Remote Sensing provides an effective means of obtaining a synoptic view of areas affected by floods for monitoring the progress of a flooding event (García-Pintado et al., 2015). The availability of remote sensing data from earth observation satellites offers an opportunity for continuous observation of flood events. This makes it possible to monitor the progress of flood in near real-time and to produce accurate, rapid and cost effective mapping of floods (de Groeve, 2010; Jung, Kim, Kim, Kim, & Lee, 2014). Additionally, remote sensing derived products are increasingly being used to estimate precipitation, which is the core data input to hydrological forecasting (Bajracharya, Shrestha, & Shrestha, 2014; Budhakooncharoen, 2014; Harris et al., 2007).

The coupling of GIS and Remote Sensing techniques would therefore provide a hybrid tool for simulation of flood events (Dang & Kumar, 2017; Sindhu & Durga Rao, 2017; Tehrany, Pradhan, Mansor, & Ahmad, 2015) and thus offer an important disaster management strategy for coping with the perennial floods in Lake Victoria Basin and for reducing vulnerability to such natural disasters.

The development of a GIS for flood management entails the use of a numerical representation of the relief of the earth's surface, i.e. a DEM of the area. This, in conjunction with digital input maps of existing rainfall data and drainage patterns, soil types, land use as well as daily rainfall estimation is used in simulating streamflow for forecasting flood events (Y. B. Liu & De Smedt, 2005).

1.2 Motivation and problem statement

Non-structural methods of mitigation of flood hazards such as flood forecasting can be cost-effective in the long run and compliment structural ones (dams and dykes) in undertaking measures for coping with floods which are a natural component of climate variability and will continue to recur in the low-lying plains of Western Kenya. A simple spatial analysis of the basin drainage parameters integrated with rainfall estimates over the basin can be used to predict the increase in stream levels that may lead to occurrence of floods (Gaya, Gachari, & Gathenya, 2009a).

The resulting system can be queried and manipulated by disaster management teams to enhance decision making. It will store data for historical records on flood water levels that will assist the management team in planning for sites of construction of dykes. Short term flood level prediction will aid in advising on stop-gap measures while long term prediction will be used to advice on long term preventive measures.

With prediction of the expected flood levels in relation to predicted rainfall patterns, the engineers will know how high they need to construct the dykes and if the existing dykes will be sufficient for impending flood levels or if otherwise they may require to be raised. Kilometres of dykes along both sides of the main rivers (and if necessary their tributaries) up to Lake Victoria will be more meaningful if the engineers are aware of the expected flood levels more accurately.

Land management efforts will benefit from informed decision from such a system through the identification of the flood plains to be set aside for purely agricultural use and higher grounds for settlement. It has also been the experience that most schools in the affected areas get flooded and thus have to remain closed until the floods subside, forcing pupils to miss precious school days. Identification of safe areas for construction of such crucial facilities as schools, hospitals and even emergency camping sites, etc, can also be part of the long term re-planning and restructuring of the area's land use.

The road network and other infrastructure will be better routed with accurate information on the topography and drainage of the area. If vital links are going to be impassable during a forthcoming rainy season, advance measures will be made to prepare alternative routes.

During floods rescue workers will be armed with vital and accurate information on the safe grounds and how to get there so that they will best guide the flood victims who would otherwise not know how deep the waters are that they have to wade through while looking for their way to safety. They will also be able to reposition the food items and medical supplies to more accessible areas.

Furthermore, the GIS will be utilised to improve production of the main crops of these areas such as rice and cotton, by providing geo-referenced digital base maps with topography and climatic data that will be merged with other data that are pertinent to their growth. Such factors as rainfall, temperature, humidity have a major effect on crop growth. If such information is geographically compared to other factors that affect crop growth and production such as soil properties, fertilizer, weeds, diseases etc., the resulting geographical analysis will provide the vital information for enhanced production, thus contributing towards increased food production and poverty alleviation.

The long term results include:

- Development of a simple model of the hydrologic process that overcomes the problem of insufficient time-variant data to produce a good representation of the real processes.
- A GIS based user-friendly flood management system for the Lake Basin floodplains.
- An effective early-warning system that can release warning up to several days before the actual flooding.
- A substantial change in the existing scenario that will render informed decision making in adopting proper measures towards disaster preparedness, mitigation, control, planning and management. This kind of advance warning will assist the

authorities in better flood preparedness and also effective flood management.

The main problem in sub-Saharan Africa is that significant delays in ground data availability have made it unfeasible to use traditional flood forecasting systems in this region (Thiemig, de Roo, & Gadain, 2011). Accurate data is very often either not readily available or is expensive to obtain. Thus, the main challenge is to identify and use readily and economically available information to produce a flood warning system.

Spatially distributed rainfall is an important input for accurate flood forecasting. Conventional rain gauge estimation of rainfall requires a dense network of gauges to accurately characterize precipitation over an area such as a watershed. The gauges should be reliable to avoid gaps in continuous data collection. However, in our area of interest, as in most parts of sub-saharan Africa, rain gauge data is expensive to obtain and the reliability of rain gauges is questionable. Furthermore, the number of rain gauges throughout Africa is small and unevenly distributed, and the gauge network is deteriorating (Funk et al., 2015). Satellite rainfall estimates have therefore been identified as readily and economically available data that can be used as input to run hydrologic models and produce flood-warning systems in this area.

1.3 Research identification

The main aim of this research is to develop a simple and locally viable scientific approach for the forecasting and management of floods in the flood plains of the Lake Victoria basin.

This is achievable through the following specific objectives:

1.4 Research objectives

1) To evaluate satellite-derived rainfall estimates (RFE) for assessing their reliability in the simulation of the hydrologic processes instead of rain gauge data.
2) To formulate a GIS-based simulation of the hydrologic processes of the area that can be used for forecasting flood events.
3) To investigate the potential of analytic capacity of GIS and remote sensing techniques for long-term monitoring and management of floods in the study area.

1.5 Research questions

The following questions are formulated with respect to aforementioned objectives:

1) How do satellite rainfall estimates perform when compared with rain gauge measurements in the study area?
2) Can satellite-derived rainfall estimates (RFE) be used in the absence of rain gauge data for simulation of the hydrologic processes?
4) How can GIS and remote sensing techniques be utilised in monitoring and management of floods in the study area.

1.6 Scope and Limitations of the Study

The study area selected is the Nyando Basin. Using Nyando Basin as a test site, the developed system can be applied elsewhere in the Lake Victoria basin. The approach develops a simulation of the hydrological processes in the basin using readily available data, forming a foundation for future development of a simple hydrological model for flood management in the Lake Victoria basin.

Due to unavailability of sufficient historical cloud-free satellite imagery of the study area, the aspect flood inundation mapping is limited to an investigation of the potential of use of satellite imagery in flood management.

1.7 Study outline

This proposal is organized into 6 chapters. The first chapter is an introduction giving a background of the study, motivation and statement of the problem, objectives of the study, research questions and organization of the thesis. Chapter 2 provides a theoretical context for the work described herein.

The methodology employed in utilising the satellite rainfall estimates to forecast runoff and the relationship with stream levels is defined in Chapter 3. The study region, rain gauge data used and the preprocessing involved are discussed herein. RFE is compared with rain station data over the study area in this chapter. The classification techniques used for flood extent mapping satellite imagery are also discussed

In Chapter 4, the results for satellite rainfall validation runs are discussed. Plots are provided, as are statistics which describe the fit between satellite estimates and observed data sets. The results of simulation of streamflow driven by the satellite rainfall estimates are presented here.

Chapter 5 discusses the results are presented in Chapter 4 and the strengths and weaknesses of the approach outlined therein. Chapter 6 presents the conclusions of the research presented herein and recommendations on areas for further research.

CHAPTER TWO

LITERATURE REVIEW

2.1 Introduction

In the recent past, developments in the field of geospatial technologies; which integrates acquisition, modelling, analysis and management of spatially referenced data, i.e. data identified according to their locations, has seen rapid progress and increased the visibility of these technologies (Ulubay & Altan, 2002). This has been made possible by the advances that have been achieved and continue to be realised in computer technology, computer science, and software engineering, as well as airborne and space observation remote sensing technologies since the 1990s (Keenan & Jankowski, 2019).

One of the areas where geospatial technologies have been found useful in providing practical solutions is in disaster risk reduction and response (Mitsova, n.d.). Flooding hazard is one of the natural hazards that can be characterized using geospatial technologies (Levy et al., 2005). The flood process can be considered as the result of many contributing factors such as the type of soil, surface water and groundwater characteristics, vegetation, precipitation (quantity and time), weather condition etc. Considering the spatial character of these parameters controlling the hydrologic process, GIS offers an effective method for modelling of the process.

2.2 The Hydrologic Process

The hydrologic cycle is a continuous natural process of transportation of water from the reservoirs and oceans to the atmosphere, then to the land surface, and finally back to the reservoirs and oceans. Water, in the form of liquid in reservoirs and oceans, evaporates and converts itself into gaseous state to form clouds; water then precipitates in the form of liquid as rain, and solid in the form of snow and hail. The major part of this

precipitation finds its way to the streams through surface and subsurface flow known as the runoff (Chow, Maidment, & Mays, 1988).

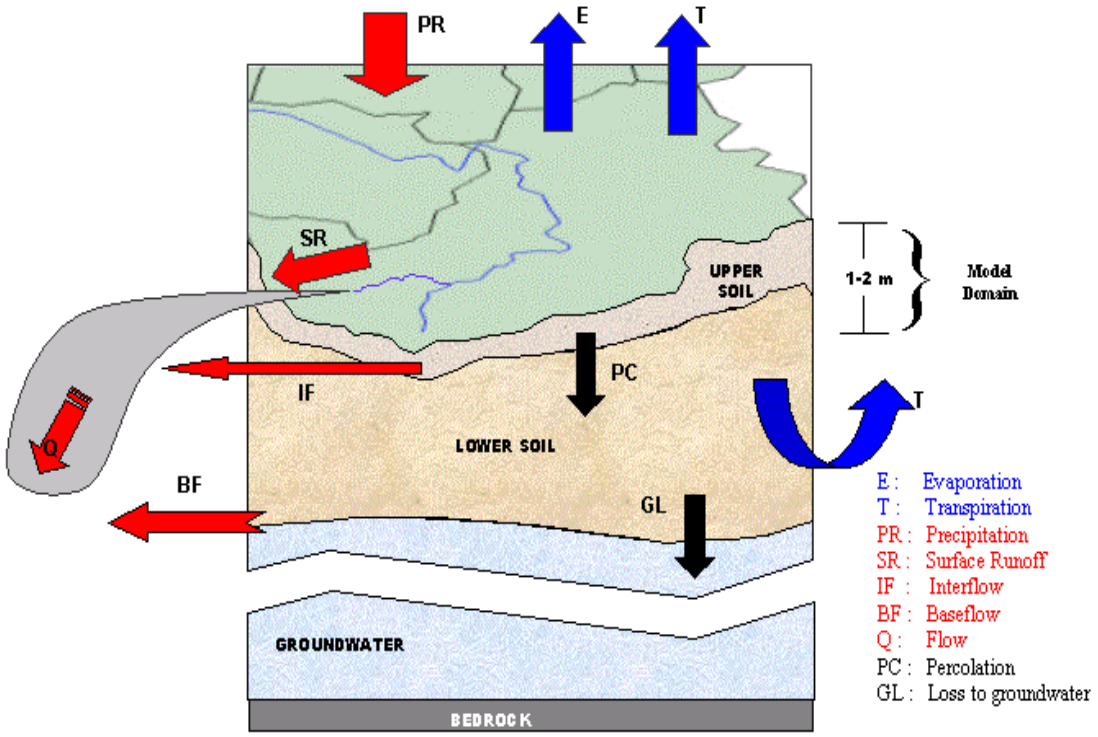

Figure 2.1: The Hydrologic Process (Source: Lance, 2004)

The hydrologic cycle is thus a complex relationship between precipitation and runoff. The heat due to solar radiation raises the temperature of the atmosphere and the land surface, which results in evaporation and transpiration of water from the surface, reservoirs, oceans and plants. Water in the gaseous form is transported upwards to higher altitudes, where it condenses and forms the clouds, and then precipitates. A part of this precipitation is intercepted by the plant leaves, buildings and other objects on the land surface, and the rest is lost to infiltration – a portion of which is used by the plants for their transpiration processes and the balance either percolates downwards and joins the groundwater reservoir, or passes off as subsurface flow (baseflow and interflow) to the streams as shown in Figure 2.1. The remaining portion of the precipitated water on

the land surface, after the above abstractions, flows out to the streams as surface runoff. The streams then flow down into reservoirs and oceans. This water evaporates and the again and the cycle thus continues (Das, 2008).

2.3 Determination of Discharge from Watershed

After a storm event, the precipitation drains from the catchment, flowing along the catchment's natural drainage channels as runoff. Not all the water received from rainfall flows out as runoff. Some amount is lost to natural processes called abstraction losses, which consist of infiltration, evaporation and evapotranspiration. Infiltration is the downward flow of the water into the soil medium. The infiltration characteristics of soil constitute an important attribute which influences the absorption of a part of rainwater in the soil medium and the consequent runoff to the rest of the streams. Infiltration characteristics of a soil are determined by ponding the water in a metal cylinder after installing it on the ground surface, and then measuring the rate of absorption of ponded water into the ground surface by registering the rate of fall of water level in the cylinder (Das, 2008).

Evaporation is the process by which a liquid on a free surface is transformed into gaseous state at a temperature less than the boiling point through the transfer of heat energy. The evaporation rate is influenced by atmospheric and water quality factors. To determine evaporation, there is need to make direct flux measurements using evaporimeters. It is also possible to estimate evaporation from ponded water; namely lakes and reservoirs, etc using the so called bucket (or budget) method. Treating the lake as a bucket, the analysis involves careful and correct accounting for all inflows and outflows from the lake (Das, 2008).

Transpiration is the process by which water vapour leaves the living plant body and enters the atmosphere. The process involves collection of water, circulation of water in the plant body and finally, the evaporation of water from the stomata of the leaves. The

process helps in transportation of soil nutrients to the plant body and the cooling of leaves. Transpiration from plants is influenced by solar radiation, air temperature, vapour pressure difference between the leaf and air, atmospheric pressure, wind velocity, plant type, soil properties, and availability of water. The water used by plants is through the processes of evaporation and transpiration. The combined form of the two is known as water use by evapotranspiration. Evapotranspiration of crops is either estimated from climatological data or found by conducting measurements in the field. It may also be possible to infer potential evapotranspiration from remote sensing measurements (Chow et al., 1988)

The balance of water that remains on the earth's surface after the abstraction losses is runoff, which empties into lakes, rivers and streams and is carried back to the oceans, where the cycle begins again. The generation of runoff from the watershed entirely depends on the watershed characteristics and a choice of the method is based on the type of data available. Two components of a storm runoff that are generally required to be estimated are runoff volume and peak runoff rate. The most commonly adopted methods for their estimation are the Curve Number Method of the Soil Conservation Service (SCS) for estimation of both excess runoff volume and peak flow rate, and the Rational Method for the peak flow rate (Das, 2008). The United States Soil Conservation Service is now called the Natural Resources Conservation Service (NRCS). In application of SCS curve number method more reliable results are expected if rainfall runoff relationships are determined for a small area instead of averaging over the entire watershed (USDA, 2004).

Empirical relationships for determination of runoff can be applied to regions for which they have been developed (Das, 2008)This method mainly considers the area of a basin or a catchment. All other factors which influence peak flow are merged in a constant. Another important method involved in estimation of peak flow is Frequency Analysis. Frequency analysis is done to estimate various phenomena like annual runoff variations,

frequencies of floods, droughts, rainfall etc. The primary objective of frequency analysis is therefore to relate the magnitude of extreme events to their frequency of occurrence through the use of probability distributions (Chow et al., 1988). In this method, data observed over an extended period of time in a river system are analysed. The data are assumed to be independent and identically distributed as well as time and space dependent.

2.3.1 Rational Method

The Rational Method was originally developed for urban catchments though it can be fairly applicable to small agricultural watersheds of 40 to 80 acres size (Chow V.T, 1964). The method is based on the assumption that a constant intensity of rainfall is uniformly spread over an area, and the effective rain falling on the most remote part of the basin takes a certain period of time, known as the time of concentration, to arrive at the basin outlet. In a drainage basin which has rainfall of uniform intensity and long duration, rate of runoff shows a gradual increase from zero to a constant value and thereafter a recession.

The relationship for peak runoff rate q_p is expressed as

$$q_p = \frac{1}{3.6} CIA \qquad \textbf{Eqn 2.1}$$

$q_p = \frac{1}{3.6} CIA$ where

q_p = peak runoff rate (m^3/s)

C = coefficient of runoff

I = mean intensity of precipitation (mm/h) for a duration equal to time of concentration, and for an exceedance probability

A = area of the drainage basin (km^2)

The runoff coefficient factor (C) depends several factors including vegetation, slope and soil type. Values of C for different soil conditions have been developed from several researches and tabulated (Das, 2008).

2.3.2 SCS Curve Number Method

The Runoff Curve Number Method was developed by the Soil Conservation Service of the USA in 1954 for determination of the rainfall excess (agricultural runoff) of agricultural watersheds. Abstraction of rainfall is caused by many factors as explained in Section 2.3 Considering these factors, the United States Geological Survey (USGS) developed the Runoff Curve Number Method for application to large agricultural watersheds to predict surface runoff from daily rainfall data.

The most widely available data is that of daily rainfall recorded by non-recording gauges (Das, 2008) These rain gauges record the total rainfall occurring in a calendar day, and do not record the time distribution of rainfall. A plot of the relationship between surface runoff Q (mm) and rainfall P (mm) on a per storm basis is shown in Figure 2.2, where I_a is the initial abstraction (mm); which consists of interception losses, depression storage, and infiltration before runoff begins; and S is the potential maximum retention of the rainwater at any time (mm).

No runoff occurs when precipitation is less than the initial abstraction ($P < I_a$), i.e., when all the precipitated water is lost to infiltration, interception, etc. The curve, Q versus P, approaches asymptotically a straight line, parallel to the line $P = Q$. The straight-line curve, P = Q, is a hypothetical relationship between P and Q for rainfall occurring on a paved area where the total rainfall has been lost as the total runoff and no initial abstraction has occurred. The vertical distance, S, between these two lines is the

maximum amount of rainfall that the basin can absorb, and is known as the potential maximum retention.

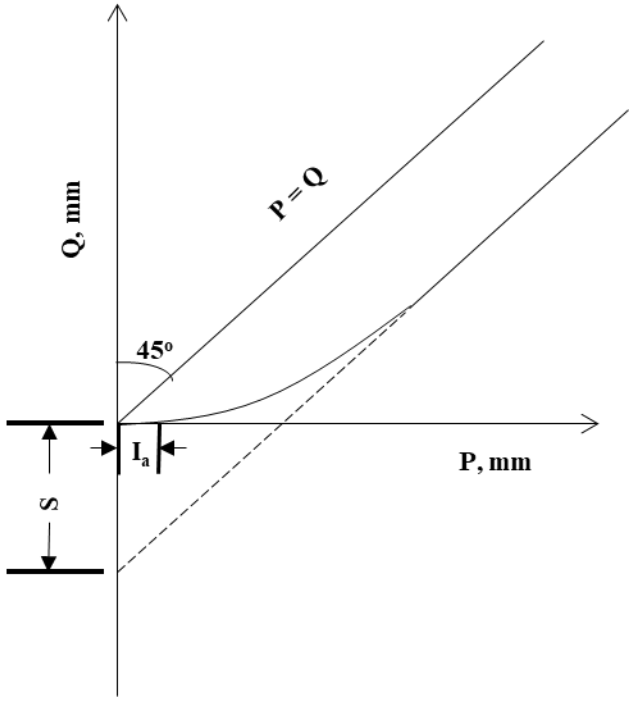

Figure 2.2: Relationship between the rainfall *P*, runoff *Q*, initial abstraction *Ia*, and reservoir capacity *S* according to the Curve Number Method (Source: Das, 2008).

Surface runoff depends on the amount of rainfall, initial abstraction and moisture retention by the soil, whereas moisture retention is a function of the curve number and is dependent on soil conditions and crop cover. Assume that:

$$q_p = \frac{1}{3.6} CIA \qquad \textbf{Eqn 2.2}$$

the actual moisture retention by the soil = $P - I_a - Q$,

the potential maximum retention = S [where $S \geq (P - I_a - Q)$],

the actual runoff taking place = Q,

and the potential maximum runoff = $P - I_a$ [where $(P - I_a) \geq Q$].

The ratios between the actual and potential moisture retained and the actual and potential surface runoff should be equal, i.e,

$$\frac{P - I_a - Q}{S} = \frac{Q}{P - I_a} \qquad \textbf{Eqn 2.3}$$

Solving the above equation for Q, we obtain

$$Q = \frac{(P - I_a)^2}{(P - I_a) + S} \qquad \textbf{Eqn 2.4}$$

The US Soil Conservation service has found by experience that

$$I_a = 0.2S \qquad \textbf{Eqn 2.5}$$

Therefore

$$Q = \frac{(P - 0.2S)^2}{(P - 0.2S) + S} = \frac{(P - 0.2S)^2}{P + 0.8S} \qquad \textbf{Eqn 2.6}$$

For I_a, P and Q in inches, S (the maximum potential difference between P and Q) in inches is obtained from

$$S = \frac{1000}{CN} - 10 \qquad \textbf{Eqn 2.7}$$

where CN is the runoff curve number.

Taking the value of *S* in millimetres (mm), the curve number is

$$CN = \frac{25400}{254 + S} \qquad \textbf{Eqn 2.8}$$

Figure 2.3 shows the graphical solution of Eqn 2.4, indicating values of runoff depth *Q* as a function of rainfall depth, *P* for selected values of Curve Numbers.

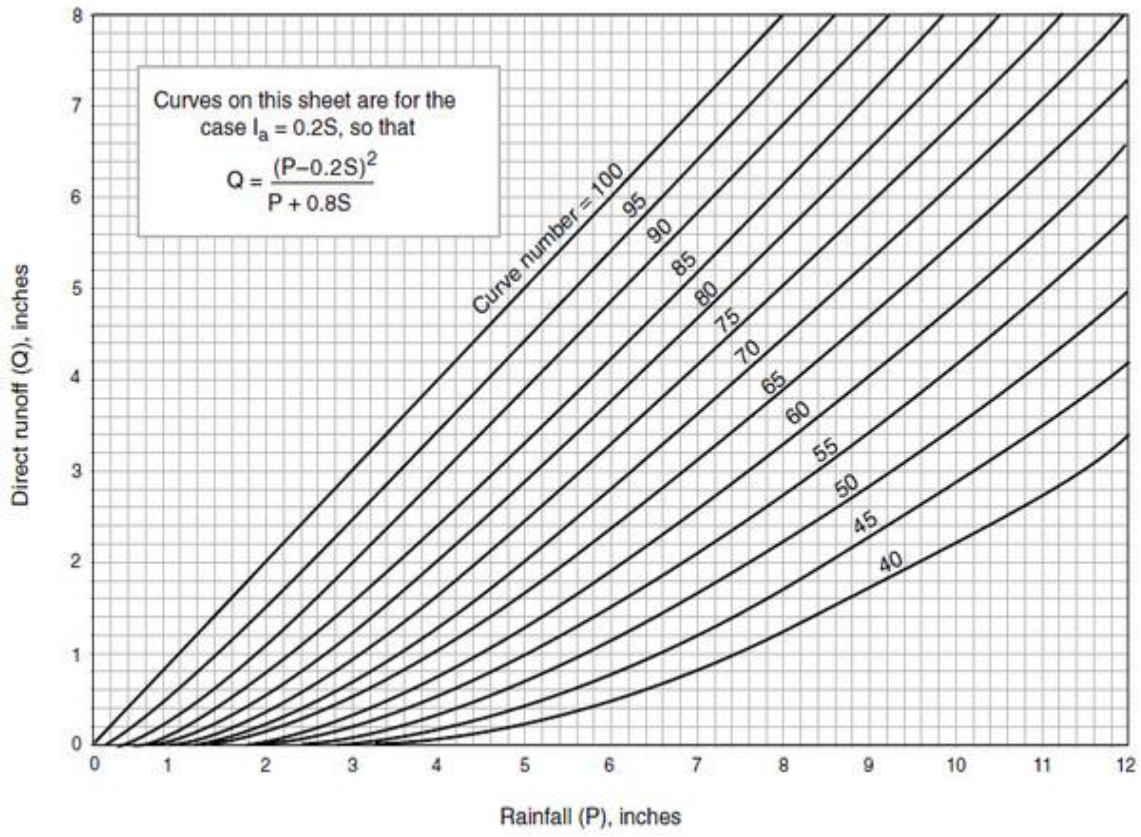

Figure 2.3: Relationship between the rainfall *P* and runoff *Q* by curve numbers, when initial abstraction I_a = 2.2 (Source: USDA, 1986)

The *CN* depends on the basin characteristics and soil moisture conditions at the time of the occurrence of rainfall. It can be evaluated from tables as a function of the hydrologic soil group, antecedent rainfall, land use pattern, density of plant cover and conservation

practices. In paved areas, for example, S = 0 and CN = 100; all rainfall will become runoff. For highly permeable, flat-lying soils, $S = \infty$ and CN = 0; all rainfall will infiltrate and there will be no surface runoff. In drainage basins, the actual scenario will be somewhere in between.

The Curve Number method holds several advantages due to it's; simplicity, predictability, stability, dependence on one parameter and responsiveness to runoff producing watershed properties. It has also opportunistically combined with computer driven models, satellite data collection, and GIS (Hawkins, Ward, & Woodward, 2009). Associated disadvantages are; its marked sensitivity to *CN*, unclear description on how to vary antecedent conditions, varying accuracy due to variation in biomass, lack of provisions to account for spatial scale effects and the fixed initial abstraction ratio at 2.2 (Ponce & Hawkins, 2002). Knowing that the calculated runoff *Q* is more sensitive to CN than to the rainfall depth *P*, enlightened practice should seek CNs from local data for local situations (Hawkins et al., 2009).

Determination of Peak Runoff

The Curve Number Equation is actually a relationship between runoff volume and rain volume but because this method is universally used, especially for rural areas, associated methods have been developed to estimate peak runoff too.

Ogrosky and Mockus (1957) developed the method for determination of peak runoff rate by using the Curve Number Method. They suggested employing the following formula to determine the peak rate of runoff by using the 6-hour rainfall as the design frequency of small watersheds.

$$q_p = \frac{0.0208 \times A \times Q}{t_p} \qquad \textbf{Eqn 2.9}$$

where

q_p = peak runoff rate (m^3/s)

A = area (ha)

Q = runoff depth (cm)

t_p = time to peak

$= 0.6\ t_c + \sqrt{t_c} = ½$ (duration of excess rainfall) $+ 0.6\ t_c$

where

t_c = time of concentration (h)

The time of concentration, t_c is the time required for runoff to travel from the hydraulically most distant point in the watershed to the outlet. Several methods are in use for computing the time of concentration, depending on basin characteristics. The SCS Lag equation is used to calculate time of concentration for agricultural watersheds under 2000 acres. However, it tends to overestimate the flow for mixed areas of pervious and impervious covers.

$$t_c = \frac{1.67L^{0.8}\left(\frac{1000}{CN} - 9\right)^{0.7}}{1900S^{0.5}}$$

Eqn 2.10

In the above equation,

CN = SCS runoff curve number

S = average watershed slope (%)

L = hydraulic length of the watershed - longest flow path, ft

The SCS Triangular Unit Hydrograph method estimates peak runoff from runoff volume by assuming a synthetic hydrograph shape to relate volume and peak geometrically as shown in Figure 2.4.

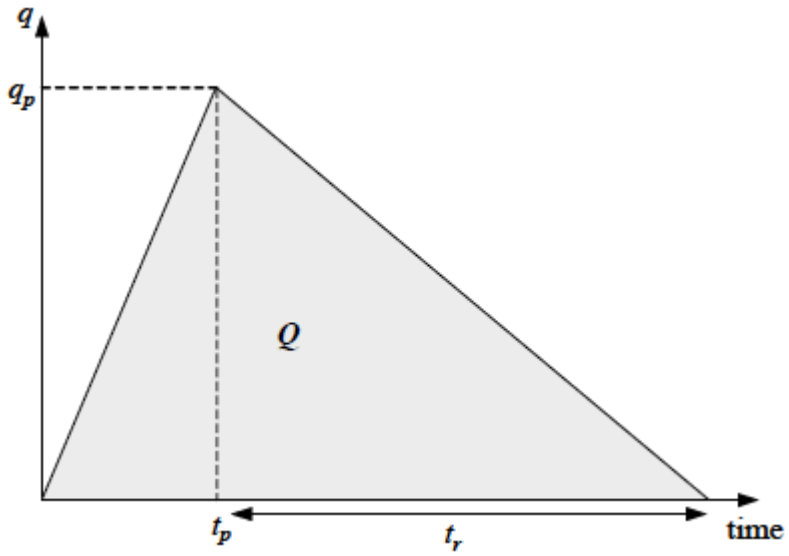

Figure 2.4: Schematic of a synthetic triangular runoff hydrograph (Source: Cornell University (2008) after SCS (1972))

From Figure 2.4 it is obvious that the peak discharge is simply:

$$q_p = \frac{2Q}{(t_p + t_r)} \qquad \textbf{Eqn 2.11}$$

where Q is in units of volume and the equation is unit consistent. Commonly, $t_p = 1.1t_c$ and the recession time, $t_r = 1.67t_p$. Eqn 2.13 is then:

$$q_p = \frac{2Q}{2.937t_c}$$ **Eqn 2.12**

The SCS developed a highly empirical approach for computing peak discharge from rural and

urban areas. The Graphical method was developed from hydrograph analyses using the TR-20

computer program (SCS, 1992). It uses the following equation:

$$q_p = q_u A_m QP$$ **Eqn 2.13**

where q_u is a coefficient called the unit peak discharge (read from a graph), A_m is the watershed area (mi^2), and Q is the runoff from the 24-hr design event calculated with Eqn 2.6. In this approach the impact of the watershed's time of concentration is incorporated into the q_u factor rather than the design storm duration. Charts for q_u as a function of t_c, *P, and* I_a that is appropriate for particular areas are available in the TR-55 manual or various texts by using t_c, rainfall distribution type, and I_a / P ratio. The pond and swamp adjustment factor is obtained from the TR-55 manual. If pond and swamp areas are spread throughout the watershed and are not considered in the t_c computation, an adjustment for pond and swamp areas is also needed.

2.3.3 Empirical Methods

A general equation may be written in the form:

$$q^p = CA^n$$ **Eqn 2.14**

where q_p is peak flow or rate of maximum discharge

C is a constant for the catchment

A is area of the catchment and *n* is an index

The constant for a catchment depends on basin characteristics such as area, shape, and slope and storm characteristics such as intensity, duration and distribution. Fixing of constant is complex and exact theory cannot be put forth for its selection. This method does not take frequency of flood into consideration.

2.3.4 Frequency Analysis

Frequency analysis is a method which involves statistical analysis of recorded data to estimate flood magnitude of a specified frequency. Research on flood frequency analysis has taken place with varying intensity over the last couple of decades (Rao & Hamed, 2000). Several methods have been developed over the years to estimate the frequency of floods (Condie & Lee, 1982; Kidson & Richards, 2005).

Overall, as new distributions and estimation methods are introduced for flood frequency analysis, researches are increasingly realizing that the lack of sufficiently long data series (Bobée & Rasmussen, 1995) and the imprecision of regional relationships imposes an upper limit on the degree of sophistication that can reasonably be justified in at-site flood frequency analysis (Stedinger & Griffis, 2011)

In this study, Curve Numbers have been identified as a useful input in Geographical Information Systems. They are determined on a table look-up basis which is compatible with spatial analysis methods and they can be overlaid with GIS-based soil and land cover information.

2.4 Developing Hydrologic Models

The flood process can be considered as the result of many contributing factors such as the type of soil, surface water and groundwater characteristics, vegetation, precipitation (quantity and time), weather condition etc. The parameters of the hydrologic cycle which can be observed and recorded are precipitation, evaporation, lake and river levels, streamflow and groundwater. Precipitation (rainfall) estimation can be obtained from the meteorological department while the hydrologic data can be obtained from the water department. The storage capacity (infiltration) of the soil is a major determinant of how much rainfall becomes runoff. Infiltration depends on the soil type, topography, natural vegetation and land use of the area.

Hydrologic models for flood forecasting are classified according either how catchment processes are represented – deterministic or data driven; or how the catchment is spatial discretized – lumped or distributed (Jain et al., 2018). Deterministic models solve a set of equations representing the different watershed processes that produce a single model output for a given set of parameters. Data-driven models depend upon the statistical or cause–effect relationships between hydrologic variables without considering the physical processes that underlie the relationships (Luchetta & Manetti, 2003).

The concept of ensemble forecasting overcomes the limitations associated with the deterministic models. In this system, a set of possible future states of the variable are provided through small changes in the initial conditions, different representations of the physical processes, and changes in parameterization schemes and solution schemes. Instead of just a single deterministic forecast, the EPS offers an ensemble prediction of hydrological variables, such as streamflow or river level, allowing the identification of the most likely scenario (Jain et al., 2018).

2.4.1 Distributed Hydrologic Modelling

A catchment area is divided into sub-basins with defined stream reaches and junctions. For modelling purposes, the infinite variability of the real world processes is averaged to some degree of finite elements (e.g. square grids) which is then assumed to have uniform parameters (altitude, slope, land cover, soils, etc). The model can be lumped when all parameters (A, B, C …) are assumed to be homogenous within the whole catchment as shown in Figure 2.5 (van Dijk, Boekelman, & Rientjes, 1999).

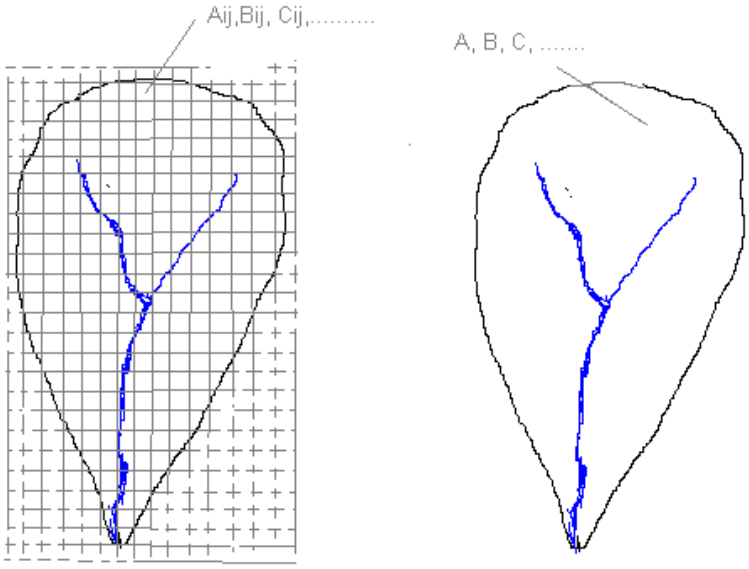

Figure 2.5: Distributed and lumped catchment parameters (Source: van Dijk et al., 1999).

The physical characteristics of the terrain data are used to estimate the parameters of the hydrologic runoff process i.e. land use and land cover, soils, topography, satellite-derived rainfall estimation and evaporation. These parameters are used to run the hydrologic model for each sub-basin to simulate the dynamics of the runoff processes.

Historical practice has been to use lumped representations because of computational limitations or because sufficient data was not available to populate a distributed model database. Also, though contour lines are the traditional way of mapping topography, distributed hydrological modelling requires a DEM (Vieux, 2004). With a DEM at reasonable resolution and the utilisation of GIS procedures and remotely sensed data including accurate rainfall input, it is possible to develop a model for distributed runoff routed through the hydrologic network to determine the spatial and temporal distribution of flooding depth and discharge.

GIS-Based Hydrologic Modelling

Considering the spatial character of the parameters controlling the hydrologic process, GIS offers an effective method to model the process. It requires spatial and temporal distribution of the inputs and parameters controlling surface runoff. GIS maps describing topography, land use, land cover, soils, rainfall and meteorological variables become inputs in the simulation of hydrologic processes. Land cover and land use map layers are available from classification of satellite images. The infiltration can be estimated through GIS analysis of these map layers overlaid with the elevation layer and existing digital soil maps. Surface runoff can then be generated as infiltration excess.

In this study, GIS-based hydrologic modelling based on distributed catchment is adopted. The catchment is divided into small cells (square grids) in which each cell is assigned a value for each parameters required to simulate the dynamics of the runoff process.

2.4.2 Watershed Analysis

Defined by topographic divides, a watershed (or basin or catchment) is an area that drains surface water to a common outlet. Watershed analysis refers to the process of using DEMs and raster operations to delineate watersheds and to derive topographic

features such as stream networks. Traditionally watershed boundaries are drawn manually onto a topographic map. The person who draws the boundaries uses topographic features on the map to determine where a divide is located. Today, using computer technology we can generate preliminary watershed boundaries, such as those shown in Figure 2.6, in a fraction of the time needed for the traditional method.

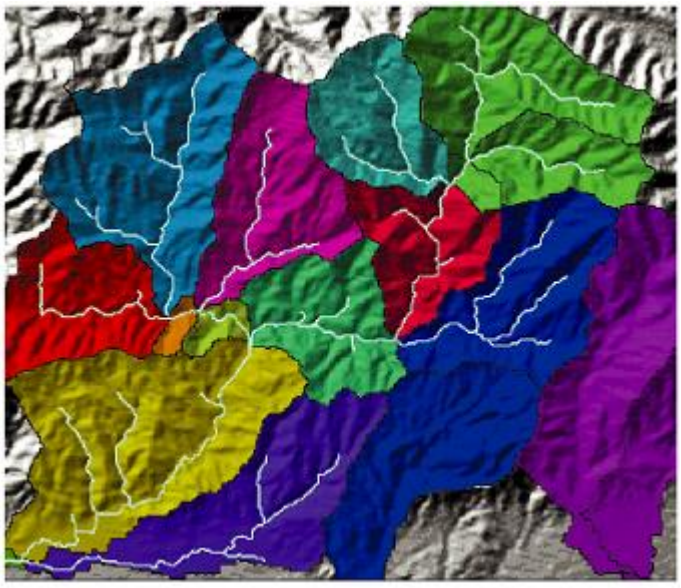

Figure 2.6: Watersheds for each section of a stream network (Source: ESRI, 2014)

Delineation of watersheds can take place at different spatial scales (Band, Tague, Brun, Tenenbaum, & Fernandes, 2000). A large watershed might cover an entire stream system and, within the watershed, there may be smaller watersheds, one for every tributary in the stream system. Delineation of watersheds can also be area-based or point-based. An area-based method divides a study area into a series of watersheds, one for each stream section. A point-based method, on the other hand, derives a watershed for each select point. The select point may be an outlet, a gauge station, or a dam. Whether area- or point-based, the automated method for delineation watersheds follows a series of steps, starting with a filled DEM.

Filled DEM

A filled DEM is void of depressions. A depression is a cell or cells in an elevation raster that are surrounded by cells of higher elevation values, and thus represents an area of inward drainage. Although some depressions are real, such as quarries, many are imperfections in the DEM. Therefore depressions must be removed from an elevation raster. Fernandez, Adamowski, & Petroselli (2016) pointed out that that fill correction processes are strongly influenced by the relief and the size of the predominant and neighbouring depressions. They consequently argued that there is no one computational procedures that works optimally for every type of correction, given that the majority of basins have diverse topographical conditions. A common method of removing depressions is to increase the cell value to the lowest overflow point out of the sink (Jenson & Domingue, 1988). The flat surface resulting from the sink filling still needs to be interpreted to define the drainage flow. One approach is to impose shallow gradients and to force flow away from higher terrain surrounding the flat surface toward the edge bordering lower terrain (Garbrecht & Martz, 1999).

Flow Direction

A flow direction raster displays the direction water will flow out of each cell of a filled elevation raster. A widely used approach for deriving flow direction in GIS is the D8 (deterministic eight nodes) method. This technique involved assigns a cell's flow direction to the one of its eight surrounding cells that has the steepest distance-weighted gradient (O'Callaghan & Mark, 1984). The approach does not allow flow to be distributed to multiple cells. Freeman (1991) found that the D8 method produces good results in zones of convergent flows and along well-defined valleys but fails to represent adequately divergent flows over convex slopes and ridges. It also tends to produce flows in parallel lines along principal directions (Moore, 1996). Other algorithms have been proposed to allow flow divergence or flow bifurcation (Endreny & Wood, 2003; Gallant & Wilson, 2000). An example is the D∞ (D infinity) method, which partitions flow from

a cell into two adjacent cells (Tarboron, 1997). The D∞ method first forms eight triangles by connecting the centres of the cell and its eight surrounding cells. It selects the triangle with the maximum downhill slope as the flow direction. The two neighbouring cells that the triangle intersects receive the flow in proportion to their closeness to the aspect of the triangle.

Flow Accumulation

A flow accumulation raster tabulates and records the number of upstream cells that will flow to into each cell, thereby contributing drainage to it. The tabulation is dependent on the flow direction raster. A flow accumulation raster can be interpreted in two ways. First, cells having high accumulation values generally correspond to stream channels, whereas cells having accumulation values of zero generally correspond to ridge lines. Secondly, if multiplied by the cell size, the accumulation value equals the drainage area.

Stream Network

A stream network can be generated from a flow accumulation raster. This is based on a threshold accumulation value. A threshold value of 500, for example, means that each cell of the drainage network has a minimum threshold of 500 contributing cells. For the same flow accumulation raster, a higher threshold value will result in a less dense stream network with fewer internal watersheds than a lower threshold value. The threshold value is a necessary input to watershed analysis. But the choice of the threshold value can be arbitrary. Ideally, the resulting stream network from a threshold value should correspond to a network obtained from traditional methods such as from high resolution topographical maps or field mapping (Tarboton, Bras, & Rodriguez-iturbet, 1991)

Stream Links

After a stream network is derived from a flow accumulation raster, each section of the stream raster line is assigned a unique value and is associated with a flow direction. A stream link raster therefore resembles a topology-based stream layer: the intersections or junctions are like nodes, and the stream sections between junctions are like arcs or reaches.

Area-wide Watersheds

The final step is to delineate a watershed for each stream section. This operation uses the flow direction raster and the stream link raster as inputs. A denser stream network (i.e., based on a smaller threshold value) will have more, but smaller, watersheds.

Point-Based Watersheds

Instead of deriving a watershed for each identified stream section, the task for some projects is to delineate individual watersheds based on points of interest. These points may be stream gauge stations, dams or surface drinking water intake locations. In watershed analysis these points are called *pour points* or *outlets*.

Delineation of individual watersheds based on pour points follows the same procedure as for delineation of area-wide watersheds. The only difference is to substitute a point raster for a stream link raster. In the point raster, a cell representing a pour point must be located over a cell that is part of the link. If a pour point is not located directly over a stream link, it will result in a small, incomplete watershed for the outlet.

The algorithm for deriving a point-based watershed varies according to the location of the pour point. If the pour point is located at a junction, then the watersheds upstream from the junction are merged to form the watershed for the pour point. If the pour point is located between two junctions, then the watershed assigned to the stream section

between the two junctions is divided into two, one upstream from the pour point and the other downstream. The upstream portion of the watershed is then merged with watersheds further upstream to form the watershed for the pour point.

2.4.3 Factors Influencing Watershed Analysis

Several factors can influence the outcome of watershed analysis. As the primary data source, DEMs play a crucial role in watershed analysis. DEMs can vary both in resolution and quality. A 30-meter DEM is likely to be too course to provide detailed topographic features for geomorphic and hydrologic modelling. A higher-resolution DEM also tends to generate a slightly smaller watershed area than a lower resolution DEM (Beard et al., 2004). For studies of small catchments, researchers have advocated DEMs with a 10-meter resolution (Zhang & Montgomery, 1994) and even higher.

The quality of DEMs is also important. Many depressions are examples of imperfections in DEMs. Accuracy of elevation data is especially important in low-relief areas. Whenever possible, one should choose better quality DEMs for watershed analysis.

The algorithm for deriving flow directions is another important factor. The D8 method is widely used because it is simple (Boonklong & Jaroensutasinee, 2007) and useful for a number of applications (Wang, Li, Hao, & Gourley, 2011). The method produces good results in mountainous topography with convergent flows but does not do as well in highly variable topography with floodplains and wetlands (Liang & MaCkay, 2000).

Automated watershed delineation typically uses the stream network derived from a flow accumulation raster. But the stream network can deviate from that on a topographic map, especially in areas of low relief. A method that can integrate a vector-based stream layer into the process of watershed delineation is commonly referred to as “stream burning” (Kenny & Matthews, 2005). But the method requires extensive data pre-processing, and

the hydrography-enhanced DEM may produce distorted watershed boundaries (Saunders, 2000).

From the foregoing, it is clear that a DEM is a crucial input in GIS-based hydrologic modelling. In the construction of a DEM for flood simulation, consideration must be made to generate a high resolution and high quality DEM.

2.5 DEM Generation

Hydrological modelling for the simulation of flood levels requires a Digital Elevation Model (DEM)/ Digital Terrain Model (DTM). A DEM is a matrix where every cell value represents the elevation of the centre point in the corresponding area on the Earth's surface. It represents a topographic surface in terms of a set of elevation values and contains terrain features of morphologic importance such as valleys, ridges, peaks and pits.

The most accurate method of acquisition of DEM is through intensive field survey methods. These require the use of expensive survey equipment such as Global Positioning Systems (GPS) or Total Stations to collect spot heights. However, this approach is very labour intensive, expensive and can be hampered by inaccessibility to some remote areas on the ground. It is mostly preferred for large scale (small area) projects.

The next best possible method is the use of aerial photography. It involves flying over the area and taking photographs with special cameras mounted on the aircraft. When viewed stereoscopically in pairs, the photographs produce three-dimensional images of the ground from which numerical plan and elevation data can be produced, with the aid of stereoplotting machines and lately, Digital Photogrammetric Workstations (DPWs). Photogrammetry is the most common method of producing topographical maps. Photogrammetric methods are more accurate than field methods in rugged, steep, terrain

where the ground is not concealed by vegetation. The method is also considerably expensive, tedious and time consuming and also requires a high level of expertise.

DEMs have traditionally been generated from contour lines and spot heights of existing topographic maps. This is in spite of the arguments that digitizing existing contours produces poorer quality DEMs than the direct photogrammetric measurements (Yoeli, 1982). The process is very slow and tedious, and there are some cases where the quality of acquired DEM is not satisfactory. Even though the digitization of the scanned topographic map templates ("repromats") can be made easier and faster by use of raster-to-vector conversion techniques, careful editing must always be done to the resulting vector data.

Unsatisfactory results are often obtained when people attempt to create their own DEMs by digitizing contours and then using local interpolation methods like inverse distance weighting and kriging to interpolate the digitized contours to a regular grid. The main problem is the assumption that smooth contour lines are true representations of terrain. A better solution is to use another interpolation method that is designed to deal with the kinds of data yielded by digitizing contours. The best strategy is to thin the digitized contours to the very minimum, to add extra points to the data set to indicate peaks, ridges, valley bottoms, and breaks of slope, and to interpolate with a large search window that uses many data points. This will be computationally more demanding but it provides better results than the simple interpolation methods (Burrough, McDonnell, & Lloyd, 2015). Clerici (1980) and (Yoeli, 1984) described algorithms that were specifically designed for interpolating contour lines to altitude matrices. In 1984, Oswald and Raetzsch presented a system, known as the Graz Terrain Model for generating discrete altitude matrices from sets of polygons representing contours that have been digitized either manually or by raster scanning supplemented by drainage and ridge lines. Commercial GIS may include procedures for DEM interpolation from

contours but do not disclose the algorithms, so the user has no idea of the quality of the result (Burrough et al., 2015).

2.5.1 DEMs from Satellite Data

Another approach of DEM generation involves the use of remotely-sensed satellite imagery to generate DEMs in a digital photogrammetric system. This is dependent on availability of imagery and equipment. The spatial resolution of the imagery needs to be fine enough in both plan and the derived elevation to be suitable for the project considering that the study area is fairly flat in the lowlands. DEM can only be extracted from satellite imagery if two or more overlapping images are available. Producing DEMs from satellite data has been a research and development topic for the last three decades. Remote sensing uses stereoscopy for elevation modelling in the same way as traditional photogrammetry. To obtain stereoscopy with images from satellite scanners, two solutions are possible:

- Along-track stereoscopy from the same orbit using fore and aft images
- Across-track stereoscopy from two different orbits

Table 2.1 was compiled from a review of the common optical satellite data.

Table 2.1: Comparison of selected satellite sensors that produce DEMs from optical satellite data

Sensor	Producer	Launch Date	Ground Coverage (km)	Ground Pixel Size (m)		Base/ Height Ratio	Stereo Acquisition		DEM Accuracy Z, XY (m)
				Pan	MS		Along-Track	Cross-Track	
Landsat TM	NASA, US	1982- 84	185 x 170	~	30, 120	0.2*	no	yes	40, 30
JERS -1 OPS	NASDA, JP	1992	75 x 75	~	18	0.27	0º/ +15.3º	no	35, 35
SPOT HRV	CNES, F	1986 - 93	60 x 60	10	20	Up to 1.0	no	±27º	10, 10
IRS - 1 C/D	ISRO, IND	1995 - 97	70 x 70	6	23	Up to 1.0	no	±26º	5, 5
SPOT 4 HRVIR	CNES, F	1998	120 x 120	~	10, 20	0.8	no	no	10,10
Terra - ASTER	NASA, US & MITI, JP	1999	185 x 170	~	15 - 90	0.6	0º/ -27.7º	±24º/ ±8.55º	15, 15
Ikonos 2	SpaceImaging Inc, US	1999	11 x 11	1	4	Variable	yes	yes	2, 1
Quickbird	DigitalGlobe, US	2001	16.5 x16.5	0.61	2.40	Variable	yes	yes	?
SPOT 5 1) HRG	CNES, F	2002	60 x 60	2.5 or 5	10 – 20	0.8	no	±31º	5, 2
2) HRS			120 x 60	5 - 10	~		yes	no	

* From narrow overlap area of adjacent swaths where available

The latter solution has been applied more often since 1980 - first with NASA's Landsat from two adjacent orbits, then with the French *Sytẻme Pour l'Observation de la Terre (*SPOT) using across-track steering capabilities, and finally with Indian Remote Sensing system IRS-1C/D by "rolling" the satellite. In the last several years, the first solution has gained renewed popularity due to the Japanese JERS-1's Optical Sensor (OPS), the German Modular Opto-Electronic Multi-Spectral Stereo Scanner (MOMS), and now ASTER (Advanced Spaceborne Thermal Emission and Reflection Radiometer)

Landsat, in addition to producing imagery of relatively course spatial resolution at 30 m, has no stereo coverage capabilities for complete coverage as it relies on the overlap between adjacent ground swaths. It can therefore be only applied for areas in latitude higher than 45° to 50° north and south; far outside the area of interest which lies a couple of degrees astride the equator.

The cost and difficulty of obtaining cloud-free, cross-track SPOT stereo coverage for many areas of the world limited the possibilities of producing DEMs of large, contiguous areas. Consequently, attention has turned other sensor configurations, including an along-track stereo sensor system incorporated in the SPOT-5 satellite launched in May 2002. It carries a High Resolution (HRS) instrument with fore-and-aft stereo collection of panchromatic imagery that facilitates the preparation of DEMs at a resolution of 10 m.

Even though the Indian Remote Sensing Satellites IRS-1C and IRS-1D offer high ground resolution, it seems difficult to obtain stereo images outside of India. The high resolution commercial satellite imagery such as Quickbird and Ikonos offer higher resolution stereo products but the cost per square kilometre is still high and uneconomical for such a project.

ASTER is an imaging instrument that is flying on Terra, a satellite launched in December 1999 as part of NASA's Earth Observing System (EOS). ASTER has along-

track stereo-capability that allows acquisition of 15 m data in near infrared bands 3N and 3B. ASTER consists of three different subsystems: the Visible and Near Infrared (VNIR 15 m), the Shortwave Infrared (SWIR 30 m), and the Thermal Infrared (TIR 90 m). The release of ASTER data has two significant impacts. First, the data can be downloaded free of charge from the web (LP DAAC, n.d.). Second, it provides a new alternative for mapping at medium-to-large scales and for generating DEM from the along-track stereo data. ASTER has the capability to provide both across-track and along-track stereo. In fact, the same-date along-track stereo-data acquisition gives a strong advantage versus the multi-date across-track stereo-data acquisition. It reduces the radiometric image variations (refractive effects, sun illumination, temporal changes) and thus increases the correlation success rate in any image matching (Hijazi & Geomatics, 2001).

DEM can be generated from satellite stereo imagery using remote sensing or digital photogrammetry software such as Erdas Imagine, PCI Orthoengine, Z/I Imaging, etc. High precision DEMs can also be derived from LiDAR (Light Detection And Ranging)

NASA launched the Shuttle Radar Topography Mission (SRTM) in February 2000 to map DEMs of 16 m height accuracy from SAR data. SRTM uses the Shuttle Imaging Radar C (SIR-C) antenna. Approximately 80% of the earth's landmass (between 60º N and 56º S latitudes) is imaged in 1000 scenes. For the United States, these DEMs have elevation data spaced 1-arc-second (about 30 m) apart. For other countries, SRTMs at a coarser spatial resolution of 3-arc-seconds (90 metres) are available in public domain on the website of the Consortium for Spatial Information of the Consultative Group for International Agriculture Research (CGIAR) (CGIAR-CSI, n.d.).

Other existing global DEM products include the GTOPO30 and the HYDRO1k, each with horizontal grid spacing of 30-arc-second (approximately 1-kilometer). The GTOPO30, with a reported vertical accuracy of 70 m, is distributed at low or no charge through the USGS EROS Data Centre (EDC). The EDC has also developed the HYDRO1k dataset for use in hydrologic and morphometric studies. The HYDRO1k datasets were developed from the GTOPO30 on a continental basis to provide a suite

raster and vector datasets. HYDRO1K is a hydrological corrected DEM which implies that it is devoid of spurious pits that interrupt hydraulic connectivity over the land surface. These pits are artifacts of the interpolation procedure used in the creation of DEMs, and they result in breaks in the flow network unless they are removed. The raster datasets are the hydrologically correct DEM, derived flow directions, flow accumulations, slope, aspect, and a topographic (wetness) index. The derived streamlines and basins are derived as vector datasets. The datasets are available over the internet for download from the EDC's Distributed Active Archive Centre (NASA, n.d.).

For the study area, a locally generated DEM is preferred to the globally available DEMs due to the better resolution and quality obtainable at larger scales. In the absence of field surveyed elevations and aerial photography of the area, DEMs produced from contours, which are products of earlier aerial surveys are sufficient.

2.6 Rainfall Estimation

Spatially distributed precipitation is an important input for accurate hydrologic modelling. Precipitation is the water that returns to the earth from the atmosphere in the form of rainfall, snowfall, hail, frost and dew. In the Lake Victoria basin, rainfall is the only significant source of precipitation. Depth of rainfall is measured as the distribution of rainfall per unit time in terms of day, month, year, etc using rain gauges. The most common rain gauges are the standard non-recording rain gauges, recording rain gauges that record a continuous plot of rainfall depth against time and the storage rain gauges that are read at weekly or monthly intervals. Precipitation is expressed in terms of the total water obtained from the precipitation which would stand in an area. For example, 1 cm deep sheet of rainwater, spread over an area of 1 sq km represents 10,000 m^3 of volume of rainwater.

Conventional rain gauge estimation of rainfall requires a dense network of gauges to accurately characterize precipitation over an area such as a watershed. This method can be hindered by the insufficient number of gauges as we have on the ground, some of

which break down and take time to replace, thereby causing gaps in continuous data collection. Satellite rainfall estimates have therefore been identified as having the potential to provide reliable and cost-effective rainfall data that can be used as input to run hydrologic models and produce flood-warning systems.

Satellite rainfall estimation based on Cold Cloud Duration (CCD) derived from remotely sensed data such as Meteosat thermal infrared imagery as a surrogate for rainfall (Grimes and Drop, 2003) was first suggested in the 1970's by Arkin. In 1987 Arkin and Meisner showed that rainfall in the tropical Atlantic could be related to the fractional coverage of cold cloud using a threshold of -38° C (P. A. Arkin & Ardanuy, 2002). This work led to the development of the GOES Precipitation Index (GPI), where it is assumed 3 mm of rainfall occurs for every hour of cold cloud over a pixel. The GPI is still widely used for climatological studies of global precipitation. The GPI technique was developed primarily to estimate rainfall over tropical regions of the globe where more conventional surface observations are unavailable.

The most common initiatives of satellite rainfall estimation include Global Precipitation Climatology Project (GPCP) Multi-Satellites (GPCP-MS), GPCP Satellite and Gauge (GPCP-SG), National Oceanographic and Atmospheric Administration Climate Prediction Center (NOAA-CPC) Merged Analysis (CMAP), and the Tropical Rainfall Measuring Mission (TRMM) all with 2.5° grid spatial resolution and monthly temporal resolution, which are considered low resolutions. TRMM-3B43 has higher spatial resolution (0.25°). High spatial (0.1° to 1°) and temporal (three-hourly to 10-daily) resolution products include the NOAA-CPC African Rainfall Estimation Algorithm (RFE), NOAA-CPC African Rainfall Climatology (ARC), GPCP one-degree daily (1DD), the TRMM-3B42, Tropical Applications of Meteorology using Satellite (TAMSAT), and a relatively new product from NOAACPC called the CPC morphing technique (CMORPH) (Dinku, Chidzambwa, Ceccato, Connor, & Ropelewski, 2008).

The theoretical basis for satellite rainfall estimation derives from the fact that rainfall forms when moisture in the atmosphere is cooled to condensation. In the absence of

condensation nuclei, moisture condenses at temperatures of 235 Kelvin and below. By monitoring the temperature of cloud tops from infrared imagery from geostationary satellites such as Meteosat 7, scientists are able to determine areas where moisture condensation and consequently rainfall is occurring. Infrared satellite imagery gives a good indication of the spatial distribution of convective rainfall (Griffith, Augustine, & William, 2014; Tarruella & Jorge, 2003). Microwave imagery from sensors such as the Special Sensor Microwave/Imager (SSM/I) of Defense Meteorological Satellite Program and the Advanced Microwave Sounding Unit (AMSU) from NOAA are also incorporated to identify other types of non-convective rainfall. However, satellite imagery do not give a good indication of the rainfall rate, and consequently, other sources of rainfall rate information must be incorporated in order to calculate a daily rainfall accumulation.

The RFE technique for estimation of precipitation over Africa was developed to augment the rainfall data available from the relatively sparse observational network of rain gauge stations over this region. The method utilizes Meteosat satellite data, Global Telecommunication System (GTS) rain gauge reports, model analyses of wind and relative humidity, and orography for the computation of estimates of accumulated rainfall (Herman, Kumar, Arkin, & Kousky, 1997). The inclusion of ground observations in these rainfall estimates provides a means of ground-truthing satellite observations on a daily basis, thus minimizing inaccuracies in the estimate (North, 1994). These satellite-derived rainfall estimates can be generated for most parts of the world since weather satellites have global coverage (Kidd & Huffman, 2011).

Figure 2.7 shows a grid of the inaugural satellite rainfall estimates for one product, commonly known by the abbreviation RFE, over Africa on 1st January 1995.

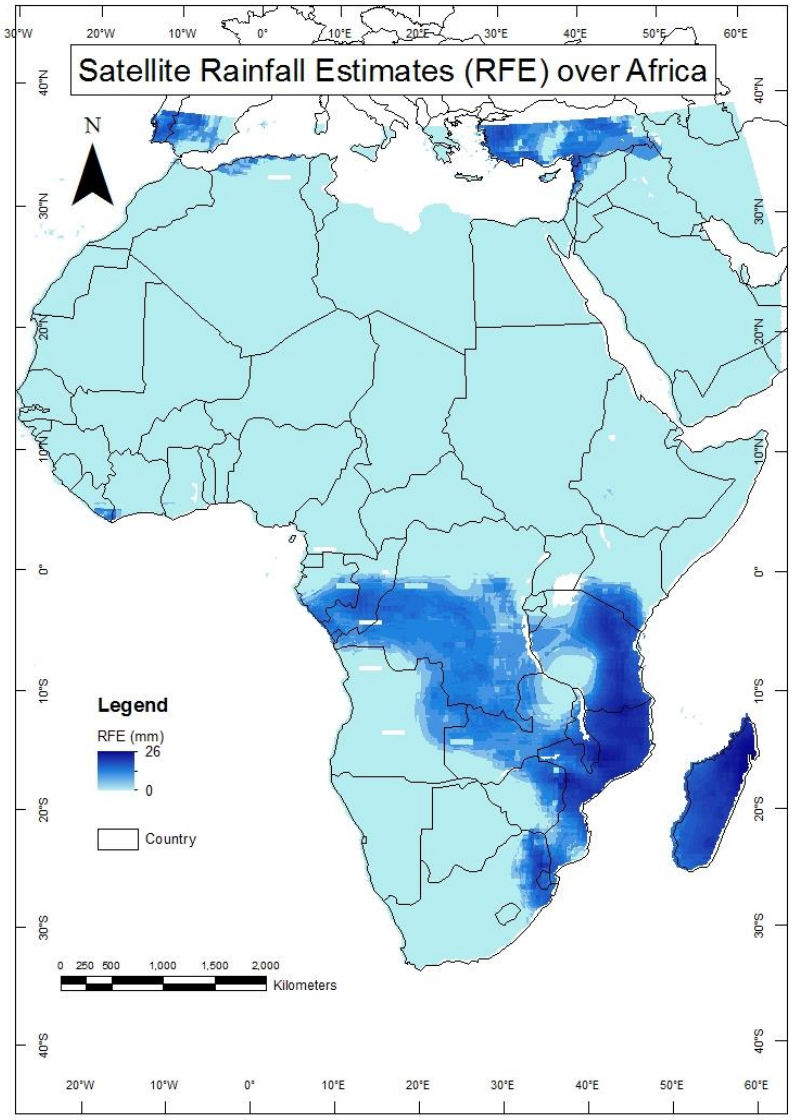

Figure 2.7: Satellite rainfall estimates (RFE) over Africa on 1st January 1995 (Source: USGS FEWSNET, n.d.)

The World Meteorological Organization (WMO) collects and archives weather information (including rainfall accumulations) from around the world on a daily basis. National meteorological agencies throughout the world obtain readings of weather conditions for the previous 24 hours through their network of ground-based synoptic

weather stations. These data are transmitted daily through WMO's GTS to a central archive, and a consolidated archive documenting global weather conditions is redistributed via the same system to the member countries. Barring any transmission errors, these data provide an accurate assessment of the quantity of rainfall at selected points throughout the world. By combining observed rainfall from the GTS system with satellite rainfall estimates, scientists at NOAA have produced an RFE product which captures both the spatial and quantitative distribution of rainfall. The resulting RFE product has a spatial resolution of 8 kilometers and can be produced for virtually any part of the world (Maidment et al., 2017).

The U.S. Agency for International Development (USAID) Famine Early Warning System (FEWS) has been supporting the production of 10-day Rainfall Estimate (RFE) data for Africa since 1995. The RFE 1.0 algorithm, implemented from 1995 to 2000, uses an interpolation method to combine Meteosat and GTS data, and warm cloud information for the 10-day estimations. The RFE 2.0 algorithm, implemented as of January 1, 2001, uses additional techniques to better estimate precipitation while continuing the use of cold cloud duration and station rainfall data. The RFE subsets are flat binary images of 8 km square pixels, with the cell value rainfall units in millimetres (Maidment et al., 2017).

Rigorous validation is necessary to have some level of confidence in using the satellite products for different applications. Some global and regional validations have been reported for different satellite rain products(A. Arkin & Xie, 1997; Krajewski, Ciach, McCollum, & Bacotiu, 2000; Petty, Morissey, Adler, Goodman, & Kidd, 2002; Gebremichael, Krajewski, Huffman, Morrissey, & Adler, 2005). In many parts of Africa, where these products are arguably needed most, there has been minimal validation work. Few studies validate rainfall over the African continent due to the lack of appropriate dense rain gauge networks (Toté et al., 2015). The evaluation studies have mainly been over western Africa ((Laurent, Jobard, & Toma, 1998; Grimes, Pardo-Iguzquiza, & Bonifacio, 1999; Nicholson et al., 2003a, 2003b; Ali, Amani, Diedhiou, & Lebel, 2005; Amekudzi et al., 2016) and southern Africa ((Thorne, Coakeley, Grimes, &

Dugdale, 2001). Most of these validation exercises have been limited to few products, particularly to monthly estimates at a spatial resolution of 2.5° x 2.5° latitude/longitude. (Adeyewa & Nakamura, 2003) compared TRMM products over most of Africa, but their validation was based mainly on Global Precipitation Climatology Project (GPCC) gauge data received through the Global Telecommunication System (GTS), which is very sparse over most of Africa. Validation over the Horn of Africa, particularly over the complex topography, has been relatively limited. Among those who have undertaken studies in the region are Asadullah, McIntyre & Kigobe (2008), Dinku et al. (2007), Hermance & Sulieman (2014) and Abtew & Melesse (2014) . Tucker & Sear (2001) compared two rainfall products over Kenya but with a limited number of gauges and only 1 year of data. Njoroge, Muthama, Ouma, & Lukorito, (2010) compared TRMM's monthly rainfall estimates over Kenya between 1998-2008 with gridded monthly rainfall totals from 26 meteorological stations for the same period. Their results suggested that satellite rainfall estimates can be modeled to represent areal rainfall in areas with inadequate ground based rainfall observations. Gaya, Gachari, & Gathenya (2009b) evaluated RFE satellite rainfall estimates at the positions of the gauging stations for the period 1995 to 2005 corresponding to the locations of 35 gauging stations in the Nyando basin in western Kenya.

2.7 Areal rainfall from Point Rainfall

Historically, rainfall data has mostly been obtained from a sparse network of rain gauges. Such gauges sample rain at distinct points. However, a distributed approach to modelling a watershed would consist of a grid representation of topography, precipitation, soils and land use. Point estimates of rain gauge accumulations can be distributed in space over a river basin by spatial interpolation.

Spatial interpolation is a process in which the investigator attempts to make a reasonable estimate of the value of a continuous field at places where the field has not actually been measured. Spatial interpolation finds application in many areas including in precipitation

and other attributes at places that are not weather stations and where no direct measurements of these variables are available.

The principle that underlies all spatial interpolation is the Tobler Law - “all places are related but nearby places are more related than distant places” (Tobler, 1970). In other words, the best guess as to the value of a field at some point is the value measured at the closest observation points. For example, the rainfall here is likely to be more similar to the rainfall recorded at the nearest weather stations than to the rainfall recorded at more distant weather stations. This means that in the absence of better information, it reasonable to assume that any continuous field exhibits relatively smooth variation – fields tend to vary slowly and exhibit strong positive correlation. The three most common methods of spatial interpolation are Nearest Neighbour, Inverse-Distance Weighting (IDW) and Kriging.

While interpolation of areal rainfall would be useful for running hydrological models in GIS, the very lack of point data of observation gauges for the purpose negates this approach and therefore in this study, readily available satellite-derived areal rainfall is used.

2.8 Use of Satellite imagery in Flood Hazard Monitoring

Even though structural measures such as dams and dykes can control flood hazards, there is little that can be done to prevent their occurrence. However the actions to minimize their effect may include analyzing the risk that flood hazards will occur in a given area, providing an advance warning for specific hazardous events and assessing the damage caused by hazards. An early evaluation of damage caused by floods is essential in carrying out rescue, relief, and rehabilitation efforts (Tobler, 1970).

Accurate knowledge of flood extent for locating flood prone areas is a crucial consideration in improving flood management and mitigating its catastrophic effects. Traditional methods of flood mapping are based on ground surveys and aerial

observations. However, when the phenomenon is widespread, such methods are time-consuming and expensive; furthermore timely aerial observations can be impossible due to prohibitive weather conditions. An alternative option is offered by satellite remote sensing technology to detect flooded areas at their peak (Brivio et al., 2002). Remote sensing is becoming increasingly valuable for analyzing, warning about, and assessing damage related to natural hazards such as floods. Floods have been monitored by successive generations of remote sensing technology. From the early 1970s Landsat data made it possible to easily measure the extent of flooding (Deutsch & H. Ruggles Jr, 1978). A decade later, in the 1980s floods were analyzed by comparing Landsat images acquired before and during the high water (Jr. Sabins, 1997). However, the use of optical sensors for flood mapping is limited by cloud cover present during a flooding event. Since the 1990s floods have been analyzed with satellite radar images, digital terrain data and repeated Landsat TM images ((M. Lillesand, Kiefer, & W Chipman, 2004)

One of the main benefits of radar sensors is that they are daylight and weather independent. In principle, they utilize their own energy to generate signals with long wavelengths that penetrate clouds. This allows for effective sensing during cloudy periods or even at night. This benefit is particularly valuable in areas characterized by high frequency of cloud cover, as is the case in many equatorial regions. Examples of radar satellite systems include ERS- 1 and 2, Radarsat-1, Envisat-1, JERS-1, SIR-C and X-SAR. Synthetic aperture Radar (SAR) from ERS and Radardsat have been proven to be very useful for mapping flood inundation areas, due to their bad weather capability (van Westen, 2002). Sentinel-1, launched in April 2014, is the first of satellites series from the Copernicus programme, previously known as GMES (Global Monitoring for Environment and Security). It provides operational monitoring information for environmental and security applications. Sentinel-1 has been designed to address primarily medium-resolution to high-resolution applications through a main mode of operation that features both a wide swath (250 km) and high geometric (5 × 20 m) and radiometric resolution. Sentinel-1's revisit frequency and coverage are better than those of the ERS-1/2 SAR and the ENVISAT ASAR. The two-satellite constellation offers 6-

day exact repeat and daily full coverage from North of 45°N to South of 45°S. Quick data delivery allows near real time data to be delivered within 3 hours of observation, as well as emergency operations to be completed typically within 24 hours. Most importantly, Sentinel-1's open and free data policy would be extremely beneficial for scientific users across the world, particularly for developing countries. Sentinel-1 operations shall fill the gaps left by the finished operational lifetimes of ERS/ENVISAT and last for a period of at least 7 years (Torres et al., 2012).

Radar provides information that is different from optical and near infrared (NIR) remote sensing. Optical/ NIR remote sensing is based on differential scattering and absorption by the target. this captures biochemical properties of a target. In contrast, radar portrays structural and physical properties. The radar return signal, or backscatter, is determined by the structure and roughness of the target and the spatial distribution of the terrain feature. It also captures soil surface characteristics, such as roughness and moisture content. One significant characteristic of radar images is that the reflections of radar signals are very complex functions of the physical and structural properties, as well as water content of target objects. This means that the interpretation of radar images is completely different from the interpretation of optical images (van der Meer, Schmidt, W., & W., 2002).

Apart from the difficulty of obtaining cloud-free satellite data during floods, other factors might be expected to constrain flood impact assessments. First, the timing of the satellite data coverage relative to river conditions frequently leads to underestimates of the severity and areal extent of flood inundation (Blasco, Bellan, & Chaudhury, 1992). In addition, accuracy assessments generally require reliable post-flood ground truth data, adequate digital elevation models, or other data that are often lacking or inadequate (Michener & Houhoulis, 1997).

This study explores the various options available for inundation mapping in the study area for purposes of flood monitoring and management.

2.9 Classification of Satellite Imagery in Flood inundation Mapping

2.9.1 Visual Image interpretation

Visual image interpretation may be used in flood inundation mapping. In general, when electromagnetic radiation interacts with a clear water body, it is absorbed within about 2 m of the surface. The degree of absorption is highly dependent on the wavelength. Near-infrared wavelengths are absorbed in only a few centimetres of water, resulting in very dark image tones of even shallow water bodies in near-infrared images. Absorption in the visible portion of the spectrum varies considerably with the characteristics of the water body under study ((M. Lillesand et al, 2004).

Aerial and satellite images can help determine the extent of flooding. During flooding, deep floodwaters can easily be detected in satellite imagery. Thereafter, dark soil tones will be seen in poorly drained areas that are still wet, days after flooding. A few weeks after flooding, it may be possible to see on the images, the widespread crop damage even though the soil moisture conditions may have returned to normal. In composite images of the near- and mid-infrared bands of satellite imagery such as Landsat TM, water appears very dark as contrasted to any surrounding vegetation data. Using multi-temporal images of the affected areas, the flood progress can be effectively monitored.

2.9.2 Multispectral Image Classification and Analysis

The most common approach to map land cover types from satellite imagery is the use of digital image classification. Digital image classification uses the spectral information represented by the digital numbers in one or more spectral bands, and attempts to classify each individual pixel based on this spectral information. This type of classification is termed spectral pattern recognition. In either case, the objective is to assign all pixels in the image to particular classes or themes (e.g. water, coniferous forest, deciduous forest, maize, wheat, etc.). The resulting classified image is comprised of a mosaic of pixels, each of which belong to a particular theme, and is essentially a

thematic "map" of the original image. In this approach, patterns of spectral reflectance, or spectral signatures, are associated with different land cover types. Some a-priori knowledge about classes in imagery is essential and separation of classes is selected by the operator. The thresholds are defined by the human observer and we may not expect 100% accuracy by this procedure. Different classes show very different behaviour. This means that the spectral signatures display larger or smaller variances according to the classes they have been assigned to (Bähr, 1999).

2.9.3 Radar Image Interpretation

Table 2.2 lists the terrain features together with their signatures and tones in a radar image. The table also summarizes the causes of the signatures and tones.

However, tone alone (bright, intermediate, or dark) is insufficient to identify terrain features on radar images. Topographic scarps facing away from the antenna and specular surfaces both have dark tones but are completely different features. Radar signatures, however, are determined not only by tone but also by size, shape, texture, and associations of the image feature. The size and shape of specular features are different from radar shadows. Radar shadows are generally associated with highlights, which are absent from specular features (Jr. Sabins, 1997).

Table 2.2: Typical terrain features and signatures on radar images (Source: Jr. Sabins, 1997)

Image signature	Image tone	Terrain feature	Cause of signature
Highlights	Bright	Steep slopes and scarps facing *toward* antenna	Much energy is reflected back to antenna.
Shadows	Very dark	Steep slopes and scarps facing *away from* antenna	No energy reaches terrain; hence there is no return to antenna.
Diffuse surfaces	Intermediate	Vegetation	Vegetation scatters energy in many directions, including returns to antenna.
Corner reflectors	Very bright	Bridges and cities	Intersecting planar surfaces strongly reflect energy toward antenna.
Specular surfaces	Very dark	Calm water, pavement, dry lake beds.	Smooth, horizontal surfaces totally reflect energy, with angle of reflectance opposite to angle of incidence.

2.10 Flood Hazard Forecasting

Simulated streamflows driven by the daily estimates of meteorological variables are compared with observed streamflows observed at several locations along the main rivers and tributaries. The river gauge readings and hydrographs of previous flood events are used to determine flood warning levels. The hydrologic model is run daily to provide

several days' forecast of the river levels at the various river gauging stations. Using the forecast river levels in conjunction with recorded flood levels of each area, it is possible to predict the occurrence of floods and issue early warnings.

2.11 Flood Management

A GIS database is designed based on components and specifications resulting from considerations of the scope and purpose of the GIS. Digital maps of the river basin can be constructed from digitizing the physical features of scanned topographical maps at a scale of 1:50,000 (the largest topographical scale covering the area). This should include map layers for hydrologic data, administrative data, infrastructure data, settlements, etc which must all be georeferenced using GIS software.

Inundated areas can be mapped from satellite imagery such as Landsat TM and ASTER. Multi-temporal satellite imagery can be classified or traced to delineate flood extent and produce vector maps to be overlaid with administrative maps to show the flood movement. Flood coverage maps are thus produced and the evolution of a flood event can be studied.

Images from previous floods can be studied to guide on where dykes should be constructed. Rainfall estimates are input in the simulated process to monitor the sufficiency of the dykes and advice on necessary emergency measures. The GIS database should also contain agricultural, socio-economic, communication, population and infrastructure data. This is used, in conjunction with the flooding data, for an evacuation strategy, rehabilitation planning or damage.

There have been several hydrological modeling works in the study area. Muthusi, Gathenya, Gadain, Kaluli, and Lenga (2005) applied the USGS Streamflow Model to the basin with the aim of evaluating its performance as a tool for flood early warning. Olang and Fürst (2011) used the HEC-HMS to assess the effects of land cover change on flood peak discharges and runoff volumes. Gathenya, Mwangi, Coe and Sang (2011)

used the SWAT model to investigate climate- and land use-induced risks to watershed. They all used rain gauge data from the Kenya Meteorological Department (KMD).

This approach is on the plausibility of utilising increasingly available and unlimited daily satellite-derived rainfall estimation (RFE) to provide flood early warning. The rainfall estimates must be evaluated using existing rainfall data to assess their agreement with in situ data. Using RFE with the DEM of the area together with the soil types, land cover, a distributed hydrologic model is envisaged that applies the curve number method that is well suited for GIS-based spatial analysis. The DEM is used to derive the runoff characteristics. For the purposes of modelling the hydrologic processes using GIS, the area is divided into small cells representing the spatial distribution of the parameters controlling surface runoff i.e. topography (DEM), surface roughness, soil infiltration and rainfall. This can be integrated with a geospatial database of the area so that it can be used as a flood management tool for monitoring the flood-prone Kano plains of the Nyando river basin and providing early warning mechanisms for floods in the plains.

CHAPTER THREE

MATERIALS AND METHODS

3.1 Materials: Site Location, Characteristics and Data Description

3.1.1 Study area

The area of interest is the Nyando river basin where perennial floods in the lower Kano plains have been causing a recurrent humanitarian crisis in the area. The Nyando River is located in western Kenya and drains into Lake Victoria. The basin covers an area of approximately 3,600 km². The Nyando River basin is bounded by latitude 00 7' 8"N and 00 24' 36"S and longitude 340 51'E and 350 43' 12"E. Lake Victoria is to the west, Tinderet Hills to the east, Nandi Escarpment to the north and Mau Escarpment to the south east. Elevations within the Basin rise from approximately 1080 m above sea level in the plains to 3000 m above sea level in the surrounding highlands. The basin mainly lies in the Nyando District of Kisumu County, Nandi South District of Nandi County and Kericho District of Kericho County. The Basin has a total population of almost 1 million, based on the 2009 census (KNBS, 2009).

Lake Victoria Basin

Lake Victoria is situated between South Latitude 3º 0’ and North Latitude 0º 20’ and East Longitudes 31º 40’ and 34º 53’. It has a total catchment area of 194,000 km^2 shared between five countries – Uganda, Rwanda, Burundi, Kenya and Tanzania.

The Kenyan part of the Lake receives inflows from rivers Sio, Nzoia, Yala, Nyando, Sondu, Gucha/Migori, Mara and several small streams, with a total catchment area of 46, 229 km^2. In the North-Western part of the basin two small rivers Malaba and Malakisi flow into Uganda; their catchment areas in Kenya being 246 km^2 and 293 km^2 respectively. River Sio with a total length of 85 km has a catchment area of 1338 km^2. It is joined on the left bank by the Naliwatsi. River Nzoia in its 334 km long course up to

its outflow into the Lake is joined by four main tributaries on the left bank and six relatively smaller tributaries on the right bank, and has a catchment area of 12,709 km^2. The next river to the South-East of Nzoia is the Yala which together with its tributaries Mogong and Edzowa drains an area of 3280 km^2 into the Lake. The Nyando rises in the watershed dividing the Lake basin and the Rift Valley. In the upper reaches its main tributaries are the Ainamatua, Nomuting and Masaija. In its lower reaches the Awach Kano and the Asawa join it on the left bank. It drains an area of 3618 km^2 into the Lake. The river Sondu together with its main tributaries the Kopsonoi and the Itare has a catchment area of 3481 km^2. The last major river to the South, joining the lake in the Kenyan territory, is the Kuja with a catchment area of 6919 km^2. The Mara river which joins the lake in Tanzanian territory has a length of 270 km and catchment area of 8967 km^2 in Kenya. Besides these main rivers, six small streams Kibos, Awach Seme, Ndate, Kabondo Awach, Magushi and Olambwe have independent outfalls into the lake.

Nyando Sub-Basin

The Nyando River Basin covers an area of approximately 3600 km^2 in Western Kenya. About 1,000,000 persons reside within the Nyando Basin, occupying the Nyando District of Kisumu County in Nyanza Province and the Nandi and Kericho Counties in the Rift Valley Province. The Nyando River originates in the highlands of Kericho and Nandi Districts at an altitude of 1700 m above mean sea level and flows through Nyando District then drains into the Winam Gulf of Lake Victoria. Its main tributaries are Ombei, Miriu, Awasi and Asawo. The catchment has a steep gradient upstream but a gentle one downstream in the Kano plains where the river dissipates in a wetland area and finally discharges into the Nyakach Bay, Lake Victoria. The mean annual rainfall varies from 1200 mm close to Lake Victoria to 1500 mm at the foot of the Nandi Escarpment (Figure 3.1). The annual rainfall pattern shows no distinct dry season; it is bi-modal with peaks during the long rainy season of the region (March–May) and during the short rainy season (October– December).

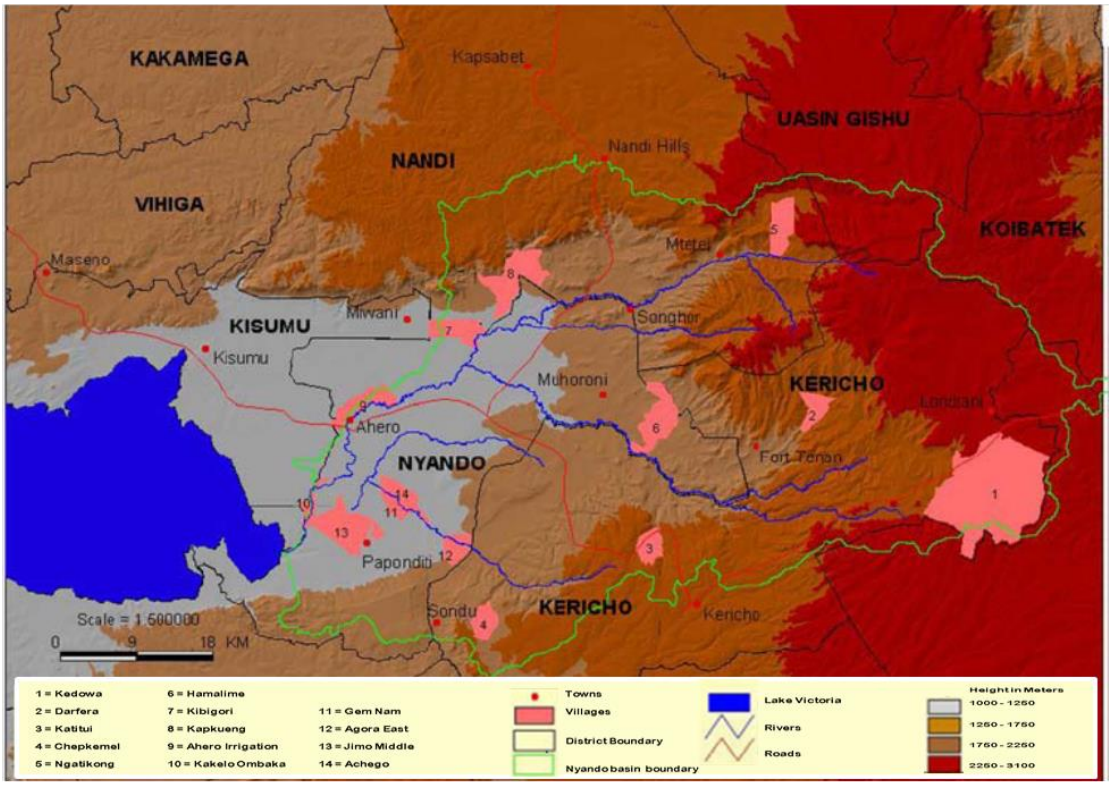

Figure 3.1: Nyando Basin (Source: JICA, 2009)

In its upper reaches from ü75 to 109 Km the Nyando river flows through a V-shaped valley in the mountain area of Londiani. The bed width is 20 m with a gradient of 1 in 45. There are few human settlements in the area. The prominent land uses are forests and subsistence agriculture. In its middle reaches from 45 to 75 Km it meanders on a narrow valley floor with a bed width of about 40 m and gradient of 1 in 160. The land use remains much the same as in the upper reaches except for cattle grazing which is quite significant. The lowermost 45 Km reaches is characterized by pronounced meandering over a wide flood plain. The bed width increases to about 50 m and the gradient flattens further to 1 in 700. The land use in this reach is predominantly agriculture, livestock farming and fishery with lot of human settlements. In its middle and lower reaches, the river flows through the Kano Plains with an area of about 73,000 ha. About 50,000 ha of the Kano Plains are arable and natural vegetation areas while an area of 13,000 ha in the lower reaches is under swamps. Approximately 50 per cent of the arable land has

been developed for paddy cultivation with supplemental irrigation supply from the Nyando and other small streams. An area of about 20,000 ha is prone to flooding from over bank spills of the river.

The Nyando River Basin has within it some of the most severe problems of agricultural stagnation, environmental degradation and deepening poverty found anywhere in Kenya. The percentage of individuals living below poverty line in the basin is high; ranging from an average of 34% in Kericho District, 44% in Nandi South District and 48% in Nyando District (KNBS, 2018).

Nyando District

More than a third of the population in Nyando River Basin resides in the Nyando District. The district has a population of 395,767 people; according to the 2010 projection by the Kenya National Bureau of Statistics. It has a geographical coverage of 1,168.4 km^2 and is divided into five administrative divisions: Upper Nyakach, Lower Nyakach, Nyando, Miwani and Muhoroni1. The district lies in the eastern part of the large lowland surrounding the Nyanza Gulf, much of it being in the Kano Plains. The topography can be generally classified into three land formations: the Nandi Hills, the Nyabondo Plateau, and the Kano Plains which are sandwiched between the hills. The Kano Plains comprise predominantly black cotton clay soils with moderate fertility and poor drainage. The rest of the district has sandy clay loam soils derived from igneous rocks. The area supports a large rural population (75 per cent) and the stage of economic growth is undermined by high absolute poverty levels, deteriorating infrastructure and the HIV pandemic (Swallow, Onyango, & Meinzen-Dick, 2003). The settlement patterns are mainly determined by the potential of the area; Upper Nyakach division has the highest population density with nearly 368 persons per km^2, while Muhoroni is the least populous with about 190 individuals per km^2. Muhoroni division is a high potential sugar-belt region, and is also the largest division in the district, covering an area of 334.8 km^2. The average density of the district is 284.6 people per km^2 with an annual growth rate of 3.4%.

Kano Plains

Floods are experienced in the lower course of the Nyando River covering approximately 50% of the Nyando district. This is the region referred to as the Kano Plains. The flat terrain of the Kano Plains does not allow easy drainage of water into the waterways. As a result of this, rainwater tends to remain on the land for considerably longer periods than would be the case where the gradient is steeper. The Black Cotton soils (Vertisols) found in the Kano Plains do not allow quick infiltration of surface water into the ground. This compounds the problem of drainage since surface drainage is already impeded by the gradient. Erosion as a result of inappropriate land use in the watershed and the flood plains leads to an increase in the sediment load of the river. The sediments fill up the channel in the lower course of the river where its speed is reduced by the gentle gradient. The channel's capacity to hold water is thus reduced and it becomes unable to hold the waters flowing through by the river and this leads to flooding. The upper reaches of the Nyando are in the Kericho and Nandi districts where annual rainfall is high and it is this rain that causes the most devastating of the floods in the basin. Reduced vegetation cover in the watersheds leads to less rainwater percolating into the soils, thus increasing surface run off which causes flash floods. The implication is that for the duration of the flash flood, the river channel is supplied with an unusually high volume of water, which it is not able to contain, thus causing floods (Onyango, 2004).

The Flooding Problem

Flooding in the Nyando District is a rapidly growing public health problem in the area. Floods have increased the incidence of a number of water associated diseases among people and animals, constrained crop type and tree species selection, made transportation more difficult, interrupted schooling and destroyed property and infrastructure. The residents of these flood-prone areas suffer every year due to damage caused by the floods. It should be noted that the small and medium size floods that occur perennially in the Nyando District have an equally devastating accumulative effect with annual damages of over 49 million Kenya shillings and annual relief and rehabilitation

cost over 37 million shillings (Otiende, 2009). The impacts of these extreme climatic events intertwined with socio-economic constraints have made populations living in these areas even more vulnerable (Nyakundi et al., 2012).

The limited intervention for disaster risk reduction has consisted mainly of conventional methods such as structural techniques and the provision of relief. Over 5,000 people are affected every year by floods in the area. This generally happens during the long and short rains, especially after spells of intense and heavy rainfalls in the catchments of the rivers.

Major floods documented in the area occurred in 1937, 1947, 1951, 1957-1958, 1961, 1964, 1985, 1988, 1997-1998, 2002, 2003, 2004, 2005 and 2006 (JICA, 2009). According to Opere (2013) and the DMCN-UNEP Report of 2004, the El Niño related floods of 1997/8 constituted one of the greatest flood episodes experienced in Kenya in recent years. The land degradation peaked during the heavy rains associated with El Niño events, of which there have been three in the Nyando over the past century. However, Nyando Basin continues being flooded every year during the long (April-June) and short (October-November) rainy seasons. The frequency of heavy precipitation events has increased especially in areas near Lake Victoria that experience warming and increases of atmospheric water vapour.

There were 3 major flood events in 1997-1998, 2002 and 2003. The 1997- 1998 flood was the consequence of El Nino related long and intensive rainfall during the months of October and November when precipitation was 300 percent of the normal. The floods had a tremendous impact on the environment and the population. A weir on Kipchoria river, a tributary of the Nyando, was washed away and a water supply dam in Kericho district was silted up. Almost the entire Kano Plain was inundated and agricultural crops were completely destroyed. The protective dykes were over topped and breached at several places (Otiende, 2009).

The floods of 2002 and 2003 were of shorter duration. These events took place in April, May and November 2002 and April-May 2003 affected the Kano Plains. These floods were caused by heavy and concentrated rainfall in the upper catchment of Nyando River. The problem was aggravated due to breaches in the dykes caused during the 1997-1998 floods. The most recent floods were experienced in December 2011 as a result of persistent heavy rainfall which affected most parts of the country.

There is at present no systematic arrangement for assessment of flood damages and maintenance of damage data. Damage assessment is usually made by various line departments after every major flood but due to lack of coordination, the data is rarely compiled to have a comprehensive appreciation of the actual socio-economic and environmental impact of floods. According to Otiende (2009), an estimated 5,000 people are affected every year by flood spills of Nyando River. The average annual damage is about Ksh 49 million. Relief and rehabilitation measures cost KSh 37 million.

3.1.2 Data

Meteorological Data

Observed rainfall data for 35 stations were obtained from the Kenya Meteorological Department. Figure 3.2 indicates the locations of all stations in the basin, with the stations whose data was obtained marked in blue.

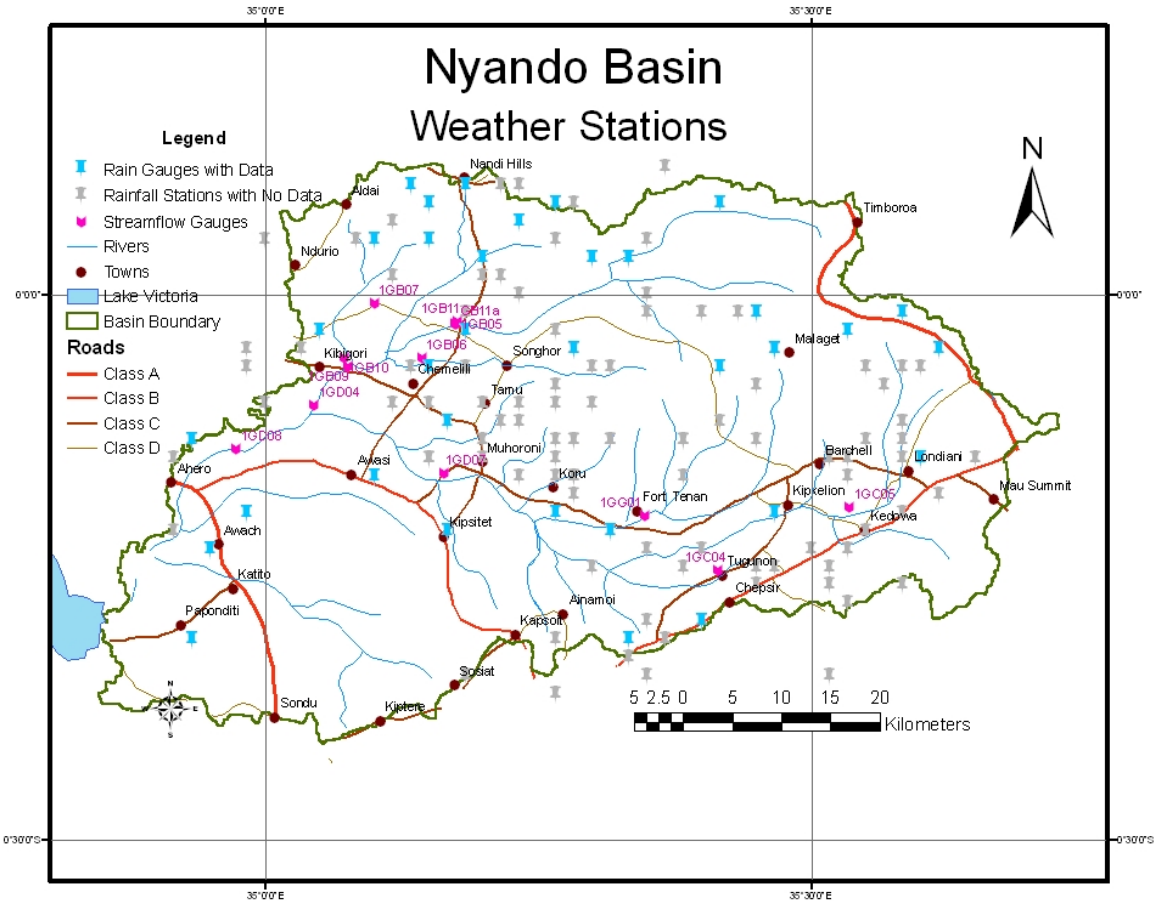

Figure 3.2: Location of Rain and Flow Gauges in the Nyando Basin

The stations used in the analysis are those with no missing days in observed data for any full year between 1995 and 2005. Though satellite rainfall estimates (RFE) data were obtained for the years 1995 to 2005, some years were left out of the analysis due to lack of concurrent RFE and station data. There was no station without gaps in 1995 while the RFE data in 2004 and 2005 had gaps. The RFE data for 2000 had unrealistic values for day 305 (ranging from 0 to 14848, in multiples of 256). Consequently, the years used in this study are 1997, 1998, 1999, 2001, 2002 and 2003. The number of stations used in the particular years ranged from 2 to 12 gap-free stations. A total of 18 stations in all were used.

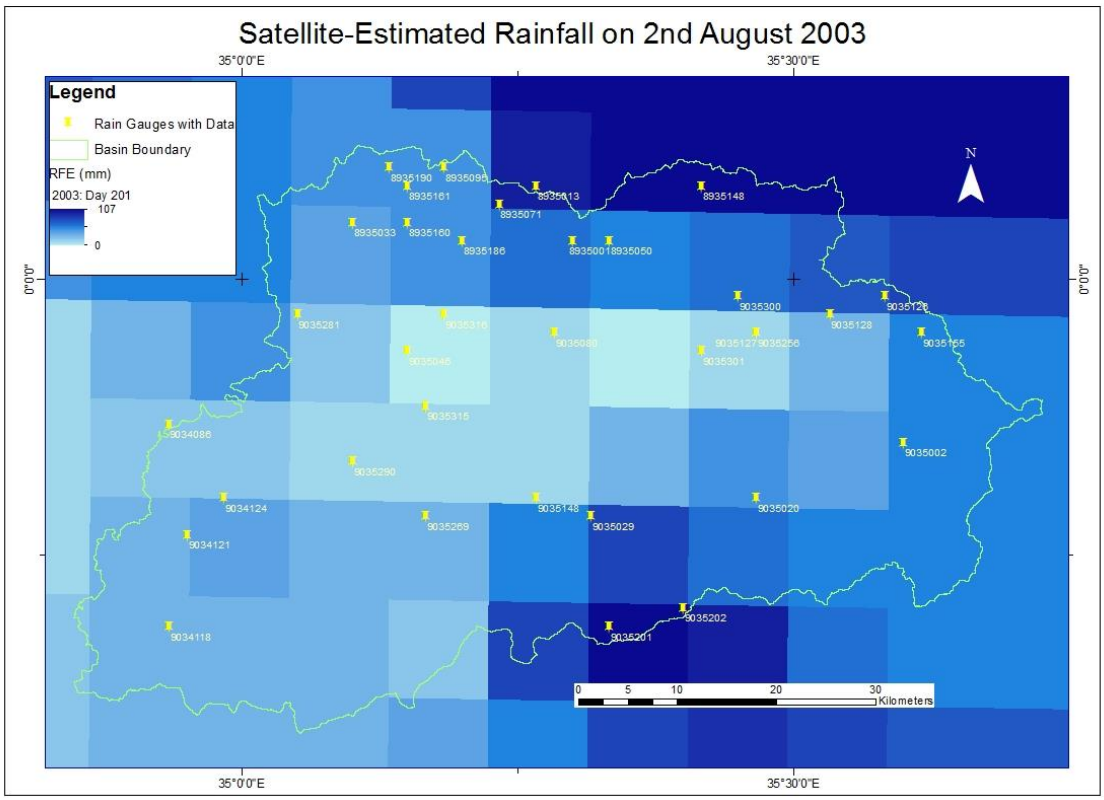

Figure 3.3: RFE Grid for 2nd August 2003 overlaid with gauging stations over the Nyando Basin.

Figure 3.3 illustrates the coverage of satellite rainfall estimates (RFE) over the Nyando Basin while Figure 3.4 is time-series plot comparing the daily RFE estimates alongside observed daily rainfall.

The streamflow data was obtained from the Ministry of Water and Irrigation. By the time of completion of this research, the Ministry was still in the process of transferring the historical streamflow data from analogue records into a digital database. Therefore most flow gauge stations had serious gaps that would not be useful in the study. Only one station had continuous data for a full calendar year. This station, 1GB11 is an outlet for a sub-basin of approximately 600 km² and had gap-free data for all the days of 1996. It is located immediately upstream of the flood-prone area.

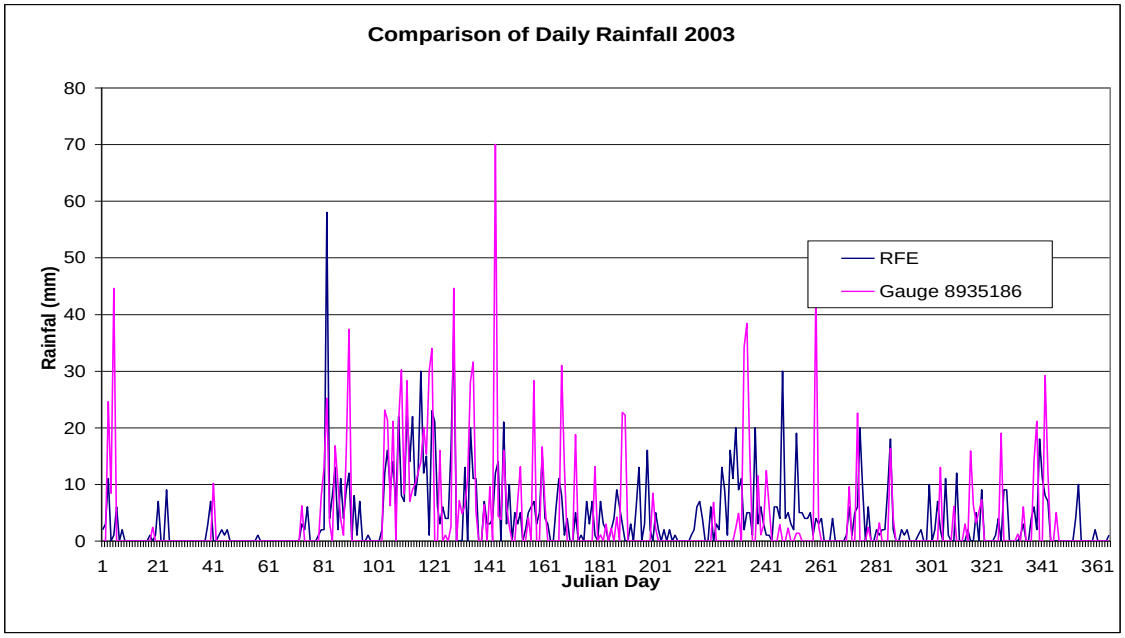

Figure 3.4: Time-series comparison of observed and satellite-derived estimates of daily rainfall at Station 8935186, Kimwani A.D.C. Farm

Land Cover Classification

The *Africover* Land Cover map of the area has descriptions of the land cover in LCCS (Land Cover Classification System) code. This had first to be translated into meaningful description using the translator in the LCCS software and the results were as shown in Table 3.1 below.

Table 3.1: Translation of LCCS Code into meaningful description

LCCS CODE	*LABEL1*
20268	Closed Woody Vegetation with Emergents
20304/10292	Open Woody Vegetation with Herbaceous Layer
8002-5	Perennial Natural Waterbodies (Standing)
3026-S0308	Continuous Large To Medium Sized Field(s) Of Graminoid Crops On Permanently Flooded Land
10154-11341-W7	Permanently Cropped Area With Rainfed Tree Crop(s)
3043-S0308/40055-R1	Continuous Small Sized Field(s) Of Graminoid Crops On Permanently Flooded Land
40055-R1	Closed Herbaceous Vegetation On Permanently Flooded Land
40056-R1	Closed Herbaceous Vegetation On Temporarily Flooded Land.
21455	Continuous Closed to Open Herbaceous Vegetation
21647	Closed to Open Herbaceous Vegetation with Trees and Shrubs
21648/40055-R1	Closed to Open Herbaceous Vegetation with Shrubs
42178-R1/10292	Closed to Open Herbaceous Vegetation With Sparse Shrubs On Temporarily Flooded Land.
10567-11341-S0804	Permanently Cropped Area With Rainfed Shrub Crop(s)
10613	Permanently Cropped Area With Small Sized Field(s) Of Rainfed Shrub Crop(s)
10613/10292/20862-1	Permanently Cropped Area With Small Sized Field(s) Of Rainfed Broadleaved Evergreen Shrub Crop(s)
10613-S0804/10292/20862-1	Permanently Cropped Area With Small Sized Field(s) Of Rainfed Shrub Crop(s)
20286	Trees with Shrubs
20286/10154-11341-W7	Trees with Closed Shrubs
20286/10292	Trees with Closed Shrubs
20286-13233-Zt1	Medium High Trees with Shrubs
20862-1	Broadleaved Deciduous ((70-60) - 40%) Woodland with Shrubs
20862-1/10292	Broadleaved Deciduous Woodland with Shrubs
20326	Woodland with Shrubs
10637	Rainfed Herbaceous Crop(s)
10655	Permanently Cropped Area With Irrigated Herbaceous Crop(s)
10655-12598	Permanently Cropped Area With Surface Irrigated Herbaceous Crop(s)
10223-11341	Rainfed Herbaceous Crop(s)
10765-13227-S13Zs2/10292	Permanently Cropped Area With Small Sized Field(s) Of Surface Irrigated Herbaceous Crop(s)
10282	Small Sized Field(s) Of Rainfed Herbaceous Crop(s)
20389	Shrubland with Herbaceous
20391-701	((70-60) - 40%) Medium To High Shrubland with Open Medium to Tall Herbaceous and Emergents
20391-701/10292	Shrubland with Herbaceous and Emergents
20391-3719/10302	Shrubland with Herbaceous and Emergents
5003-9	Urban Area(s)

The labels were then grouped into the major land cover types (Label 2) against the corresponding LU_Code as shown in Table 3.2.

Table 3.2: Grouping labels into major land cover types and assigning LU-Code

LABEL1	LABEL2	LU_CODE
Closed Woody Vegetation with Emergents	Mixed Forest	430
Open Woody Vegetation with Herbaceous Layer	Savannah	332
Perennial Natural Water Bodies (Standing)	Water Bodies	500
Continuous Large To Medium Sized Field(s) Of Graminoid Crops On Permanently Flooded Land	Herbaceous Wetland	620
Permanently Cropped Area With Rainfed Tree Crops, Plantation	Dryland Cropland and Pasture	211
Continuos Small-Sized Fields of Graminoid Crops On Permanently Flooded Land	Herbaceous Wetland	620
Closed Harbaceous Vegetation on Permanently Flooded Land, Fresh Water	Herbaceous Wetland	620
Closed Harbaceous Vegetation on Temporarily Flooded Land, Fresh Water	Herbaceous Wetland	620
Continous to Closed Harbaceous Vegetation	Grassland	311
Continous to Closed Harbaceous Vegetation with Trees and Shrubs	Mixed Shrubland/ Grassland	330
Continous to Closed Harbaceous Vegetation with Shrubs	Mixed Shrubland/ Grassland	330
Continous to Closed Harbaceous Vegetation with Shrubs on Temporarily Flooded Water, Fresh Water	Herbaceous Wetland	620
Permanently Cropped Area With Rainfed Shrub Crops	Cropland/ Grassland Mosaic	280
Permanently Cropped Area With Rainfed Shrub Crops, Plantation	Cropland/ Grassland Mosaic	280
Permanently Cropped Area With Small Sized Fields of Rainfed Shrub Crops	Cropland/ Grassland Mosaic	280
Permanently Cropped Area With Small Sized Fields of Rainfed Broadleaved Evergreen Shrub Crops	Cropland/ Grassland Mosaic	280
Trees With Shrubs	Savannah	332
Tree With Closed Shrubs	Savannah	332
Medium High Trees With Shrubs	Savannah	332
Broadleaved Decidous ((70-60)-40%) Woodland With Shrubs	Deciduous Broadleaf Forest	411
Broadleaved Decidous Woodland With Shrubs	Deciduous Broadleaf Forest	411
Woodland With Shrubs	Savannah	332
Rainfed Herbaceous Crops	Grassland	311
Permanently Cropped Area With Irrigated Herbaceous Crops	Mixed Dryland/ Irrigated Cropland and Pasture	213
Permanently Cropped Area With Surface Irrigated Herbaceous Crops, Other Food Crops	Mixed Dryland/ Irrigated Cropland and Pasture	213
Permanently Cropped Area With Small Sized Fields of Surface Irrigated Herbaceous Crops, Other Food Crops	Mixed Dryland/ Irrigated Cropland and Pasture	213
Small Sized Fields of Rainfed Herbaceous Crops	Grassland	311
Shrubland With Herbaceous	Shrubland	321
((70-60)-40%) Medium to High Shrubland With Open Medium To Tall Herbaceous and Emergents	Mixed Shrubland/ Grassland	330
Shrubland With Herbaceous and Emergents	Shrubland	321
(40- (20-10)%) Medium to High Shrubland With Open Medium To Tall Herbaceous and Emergents	Mixed Shrubland/ Grassland	330
Urban Area	Urban and Built-Up Land	100

The resulting map based on the major land cover types is shown in Figure 3.5.

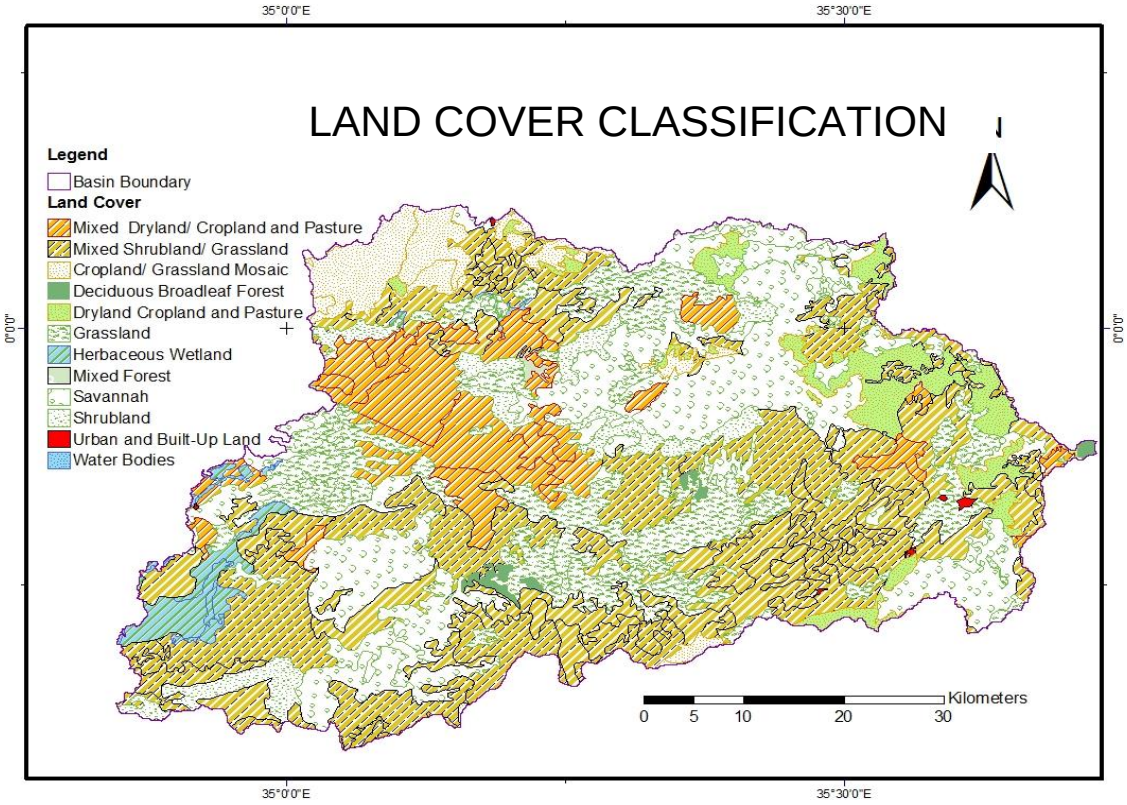

Figure 3.5: Map generated from the major land cover types

Soil Map

Figure 3.6 shows the soil map of the area obtained from the FAO SOTER project. The properties of the soil provided in the attributes include proportionate extent of the component soils, soil depth and hydraulic properties, which are necessary for estimating infiltration parameters from soil maps.

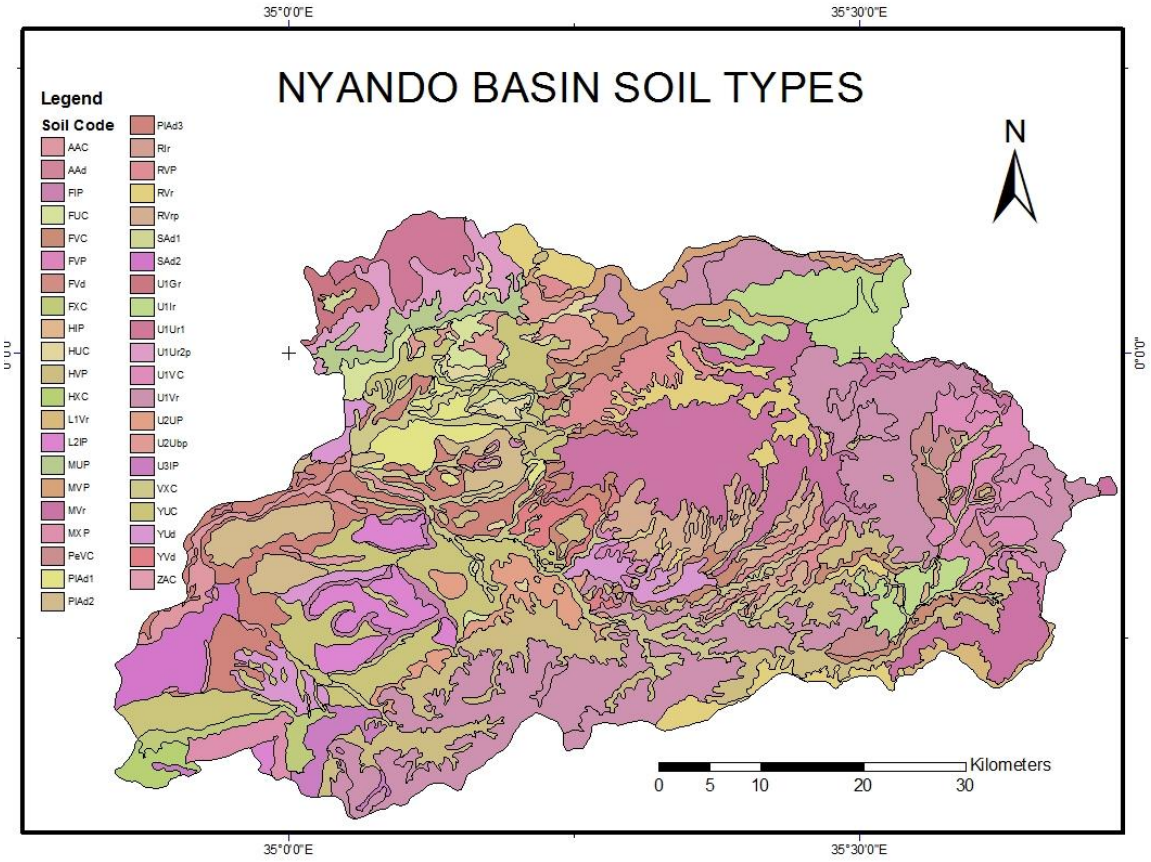

Figure 3.6: A GIS display of soil data (Courtesy of FAO SOTER)

Digital Elevation Model (DEM)

The DEM for the Nyando Basin (Figure 3.7) was acquired from the collaboration project between the Survey of Kenya and World Agroforestry Centre (formerly International Centre for Research in Agroforestry - ICRAF) that undertook to generate DEMs for western Kenya. The DEM was generated from contour lines and spot heights of existing topographic maps. This area is covered by topographic maps at a scale of 1:50,000 and contour interval of 20 m. The method involved the assembly of contour lines from different map sheets. The DEM was derived from digitizing the contour layer and the hydrographic features layer of the existing topographic maps. Scanned topographic map templates were digitized using of raster-to-vector conversion techniques and the

resulting vector data carefully edited manually. The sheets were finally merged together to produce a single terrain model of the area using.

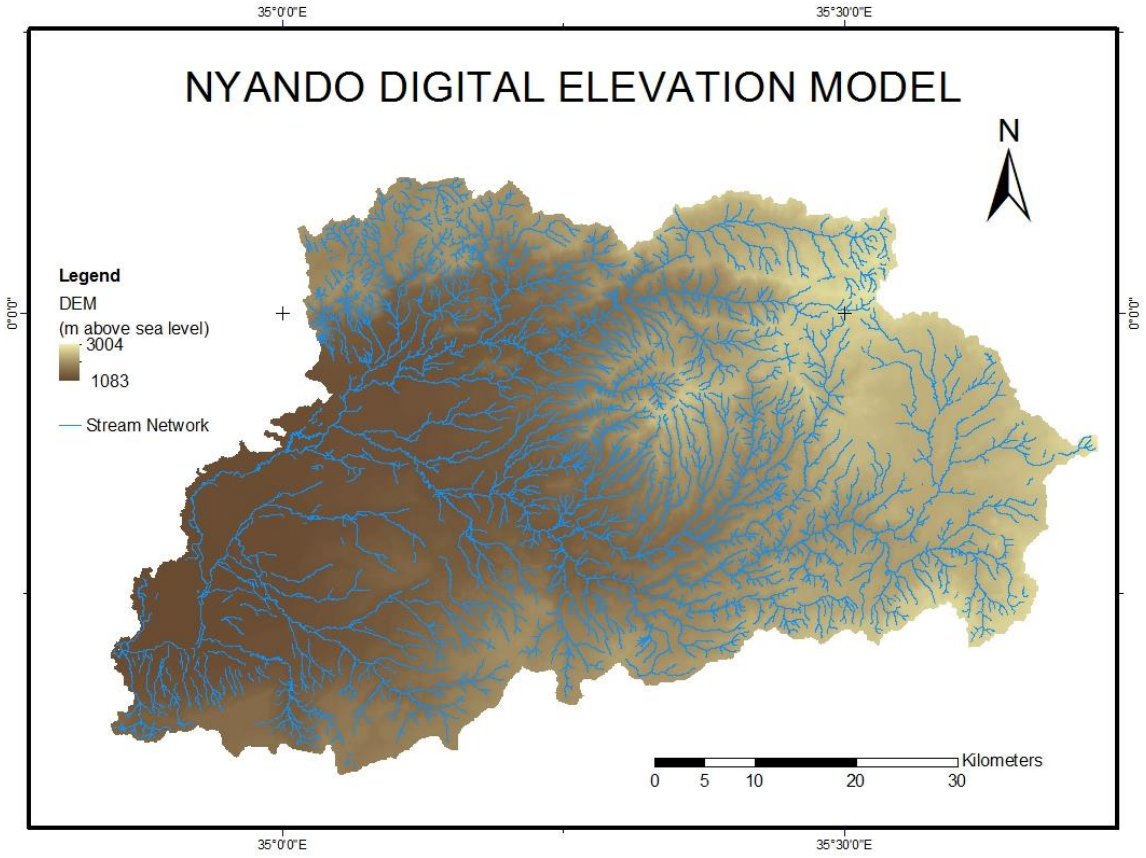

Figure 3.7: DEM of the Nyando Basin Overlaid with the Hydrology

Satellite Imagery

Images of the area were obtained from Landat for 1995, 2003 and 2005, ASTER for 2003 and 2005.

Table 3.3: The Satellite data used in this study

Date	ASTER	Landsat
02.04.1995		√
18.05.2003		√
19.11.2003	√	
26.12.2003	√	
21.04.2005		
12.05.2005		√
10.07.2005	√	
16.05.2005	√	
11.08.2005	√	

3.2 Methodology

3.2.1 Introduction

The use of GIS to model hydrologic processes requires the spatial and temporal distribution of the inputs and parameters controlling surface runoff. GIS maps describing topography, land cover, soils, rainfall and meteorological variables become inputs in the simulation of hydrologic processes.

Figure 3.8 is a summary of the methods employed in this study. The method involves the use of a DEM of the area together with the soil data, land cover and daily satellite-derived rainfall estimates (RFE) to drive a GIS-based hydrologic model which is used to estimate runoff volumes. Historical daily rainfall data were first used to validate the satellite rainfall estimates. The DEM is used to derive the runoff characteristics. For the purposes of modelling the hydrologic processes using GIS, the area is divided into small cells representing the spatial distribution of the parameters controlling surface runoff i.e. topography (DEM), surface roughness (land cover), soil infiltration and rainfall.

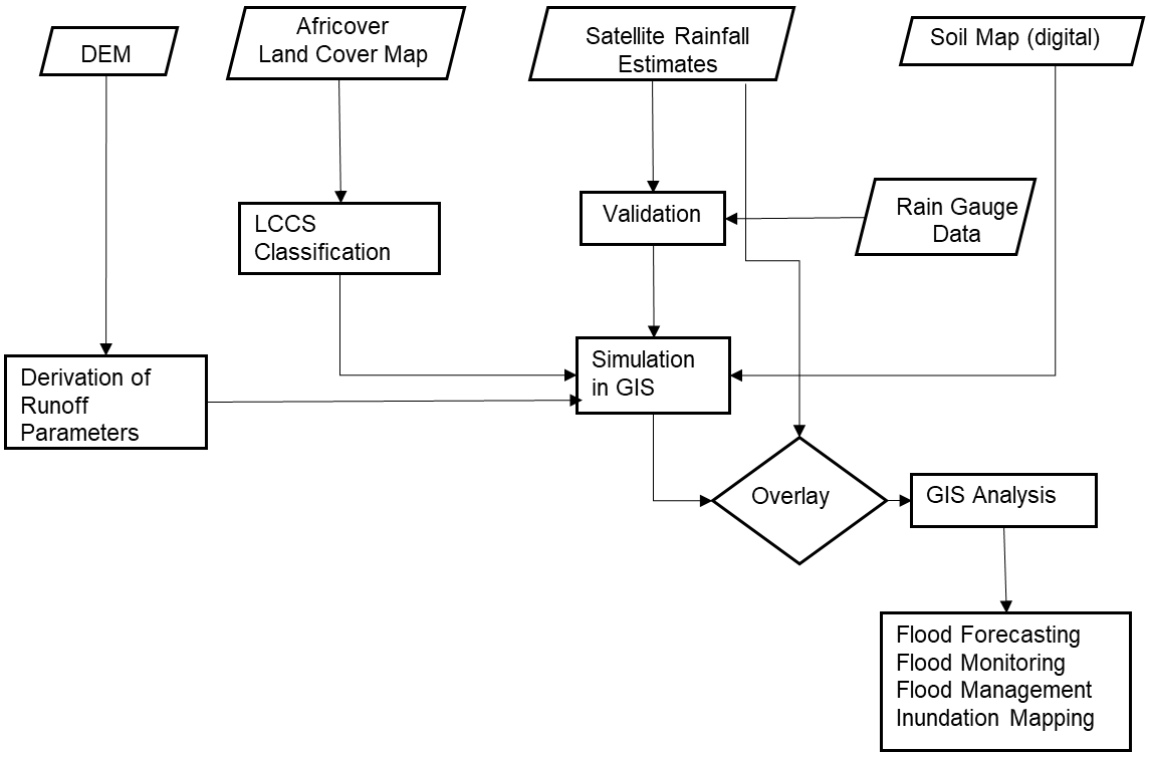

Figure 3.8: Generalised workflow for utilising ground and remotely sensed data to support flood forecasting, management, and inundation mapping in a GIS environment

3.2.2 Validation of Satellite Rainfall Estimates

Ground based gauges are widely considered to provide the most accurate measure of precipitation at any location. However, the spatial coverage of ground based gauges is very poor in this region and is therefore inadequate to support hydrologic modeling needs. RFE data was therefore used to estimate the precipitation. The RFE data was first validated against observed rainfall data.

A Visual Basic for Applications (VBA) program (see Appendix I) was developed to extract the values of the satellite rainfall estimates at the positions of the gauging stations. The stations are first displayed in the GIS user interface. The program retrieves each day's RFE raster dataset in turn and loops through each station in the point feature

class to obtain the cell value of the raster on that point. This routine was used to obtain the RFE data for the period 1995 to 2005 corresponding to the locations of 35 gauging stations in the basin. The values were compared with the observed gauge data for the same period. The elevations of the rain gauge stations were also obtained from the DEM of the study area and used to investigate any influence of topographical location on the satellite rainfall estimates.

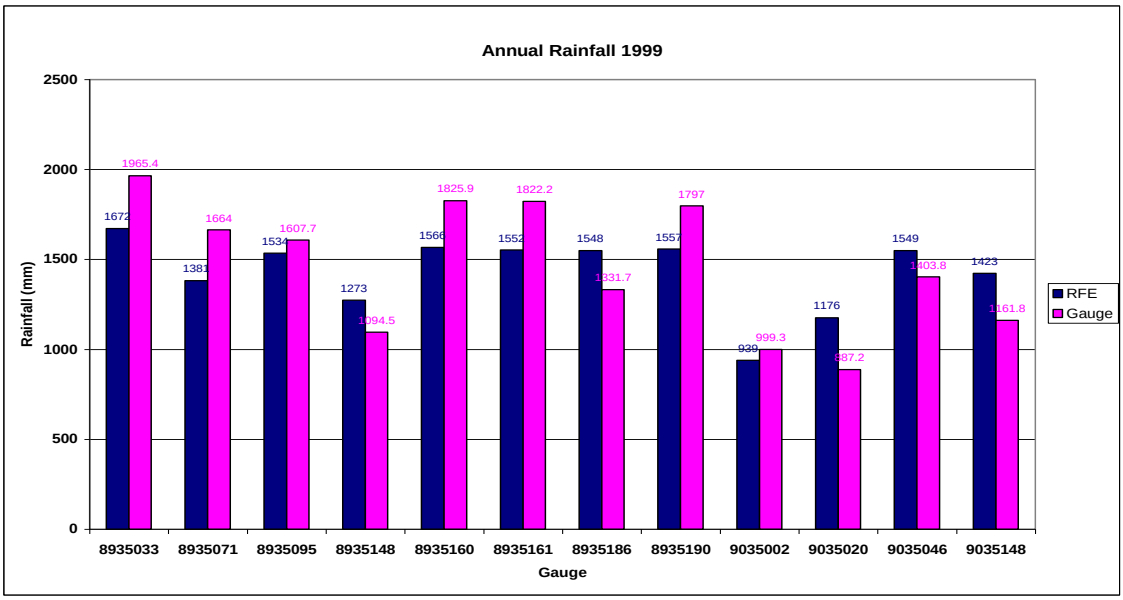

Figure 3.9: Comparison of annual rainfall between observed and satellite-derived estimates at the positions of 12 stations for the year 1999

Histograms were plotted of the annual rainfall for each year at each available station by summing the daily precipitation from both sets of data for a graphical comparison (Figure 3.9). Time-series graphs were also plotted for each station for daily (Figure 3.4), 10-day and monthly rainfall.

Daily precipitation fields were then summed up to into decadal (10-day) fields for both sets of data for each station. The arithmetic average of the included stations was then calculated for each dekad in both sets

Time series traces (Figure 3.10: Time series plot of average study area rainfall (millimetres per dekad) for the 37 dekads of 2003 for the rain gauges (observed) and satellite RFE). and scatter plots of the data were prepared to illustrate the results. Simple regression analysis was used to measure the degree of agreement between the observed rainfall and the satellite RFE (Gaya, Gachari, & Gathenya, 2012).

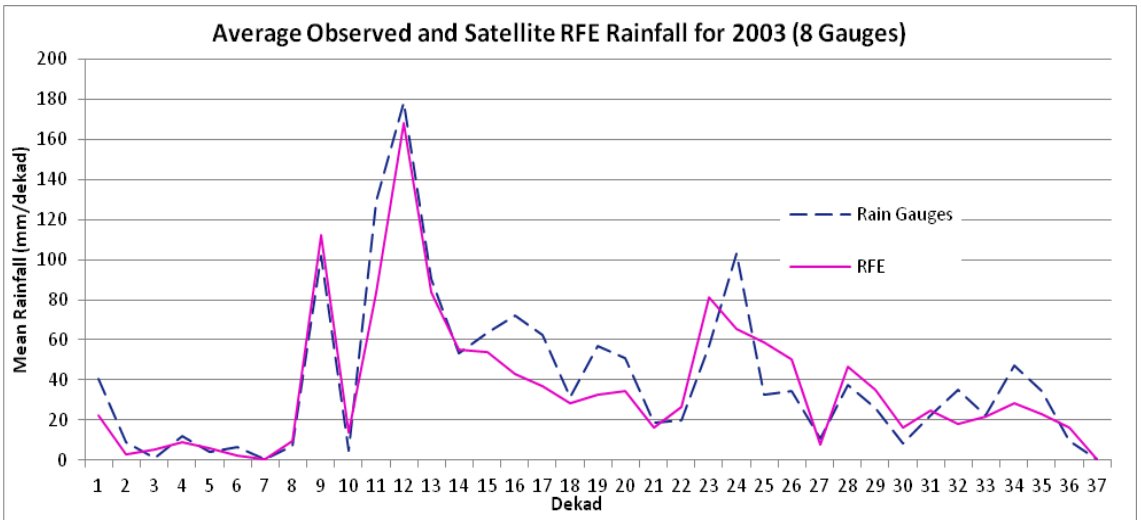

Figure 3.10: Time series plot of average study area rainfall (millimetres per dekad) for the 37 dekads of 2003 for the rain gauges (observed) and satellite RFE

The Pearson correlation coefficient *(r)* was used to evaluate how well the estimates corresponded to the observed values. The correlation coefficient is obtained from Eqn 3.1.

$$r = \frac{\sum(P_G - \overline{P_G})(P_S - \overline{P_S})}{\sqrt{(P_G - \overline{P_G})^2}\sqrt{\sum(P_S - \overline{P_S})^2}}$$

Eqn 3.1

where P_G = gauge rainfall measurement

$\overline{P_G}$ = average gauge rainfall measurement

P_S = satellite rainfall estimate

$\overline{P_G}$ = average satellite rainfall estimate.

Correlation coefficient varies from -1 to +1. A correlation coefficient of +1 indicates a perfect positive correlation.

The Mean Error *(ME)* and Relative Mean Absolute Error *(RMAE)* were used to assess the average estimation error in millimetres. The Mean Error is calculated by Eqn 3.2.

$$ME = \frac{\sum(P_S - P_G)}{N} \qquad \textbf{Eqn 3.2}$$

where N = number of data pairs.

The Relative Mean Absolute Error is calculated by Eqn 3.3.

$$RMAE = \left(\frac{\frac{1}{N}\sum |P_S - P_G|}{\overline{P_G}} \right) \qquad \textbf{Eqn 3.33}$$

The perfect score for both the Mean Error and Relative Mean Absolute Error is zero.

The Nash-Sutcliffe Efficiency coefficient *(NSE)* is a normalized statistic that determines the relative magnitude of the residual variance compared to the measured data variance (Nash & Sutcliffe, 1970). It varies from -∞ to 1: negative values mean that the gauge mean is a better estimate, zero means that the gauge mean is as good as the estimate, and 1 corresponds to a perfect match between gauge data and satellite based data. The Nash-Sutcliffe Efficiency coefficient is obtained from Eqn 3.4.

$$NSE = 1 - \frac{\sum(P_S - P_G)^2}{\sum(P_G - \overline{P_G})^2} \qquad \textbf{Eqn 3.4}$$

The *Bias* indicates how well the mean estimate and gauge mean correspond. It is obtained from Eqn 3.5.

$$Bias = \frac{\sum P_S}{\sum P_G}$$

Eqn 3.5

NSE and *Bias* do not have units and the perfect score for both is 1.

The Root Mean Square Error *(RMSE)* was also calculated to quantify the amount by which the satellite-derived rainfall estimates differ from the rain gauge-observed values for the 10-day accumulations. The Root Mean Square Error is calculated Eqn 3.6.

$$RMSE = \sqrt{\frac{\sum (P_S - P_G)^2}{N}}$$

Eqn 3.6

Lower values of *RMSE* indicate better fit, with zero being the perfect score.

3.2.3 Derivation of Runoff Parameters

The storage capacity (infiltration) of the soil is a major determinant of how much rainfall becomes runoff. Infiltration depends on the soil type, topography, natural vegetation and land use of the area. the land cover used for the study area was derived from the *Africover* Land Cover. The *Africover* Land Cover map layer was originally obtained from evaluation of satellite images by computer-assisted classification using remote sensing software. The infiltration was estimated through GIS analysis of these map layer overlaid with the elevation layer and existing digital soil maps. Surface runoff was generated as infiltration excess.

The Soil Conservation Service Curve Number (SCS-CN) Method was selected for derivation of runoff parameters because it considers the physiographic heterogeneity of the catchment (topography, soil and land use) to simulate the rainfall-runoff relationship

at catchment level ((X. Liu & Li, 2008; Hawkins et al., 2009). The model has been widely used with success providing consistently useful results (Soulis, Valiantzas, Dercas, & Londra, 2009: D'Asaro & Grillone, 2010).

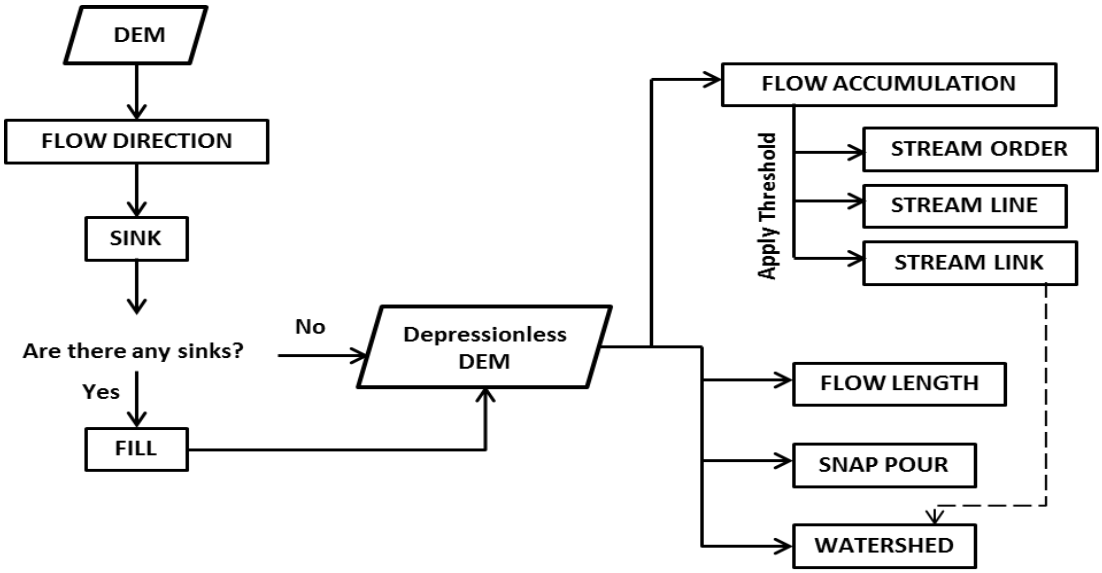

Figure 3.11: Workflow for Deriving Runoff Parameters (ESRI, 2014)

The DEM for the Nyando Basin was processed using the Hydrologic toolset of *ArcGIS* to derive the runoff characteristics of the basin as summarised in Figure 3.11.The DEM was first filled to remove depressions. A flow direction grid was derived using the D8 method, which assigns a cell's flow direction to the one of its eight surrounding cells that has the steepest distance-weighted gradient. This enabled the generation of a flow accumulation grid to record how many upstream cells contribute drainage to each cell in the basin.

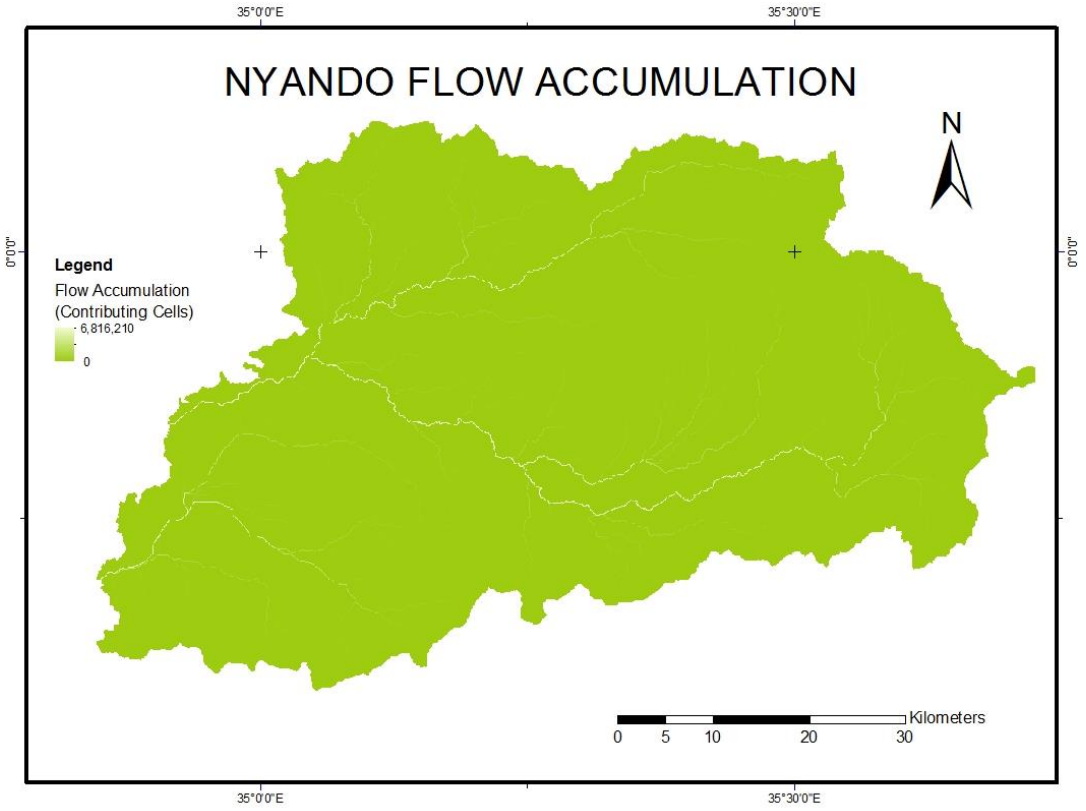

Figure 3.12*:* Flow accumulation and runoff volume

The stream network for the basin was then delineated using a threshold accumulation value of 500, i.e. if the flow accumulation at a cell is greater than 500, the cell is considered a stream cell. This threshold value was settled on as it gave the closest shape to the vectorized rivers from existing topographical maps. The resulting flow accumulation grid is shown in Figure 3.12. This is also done only once for the basin.

Evaluating Curve Number for the Study Area

Curve Number was evaluated for the study area on pixel basis using the landcover/ land use and soil map that are reclassified to hydrologic conditions and hydrologic soil group.

Reclassification of Land Cover

The *Africover* Land Cover map of the area with descriptions of the land cover in LCCS code was first translated into meaningful description using the LCCS software translator as described in Chapter 3. The labels were then grouped into the major land cover types as shown in Figure 3.5 and listed in Table 3.4.

Table 3.4: The main land cover types over the Nyando basin

S/No.	Land Cover Type
1.	Mixed Dryland/ Irrigated Cropland and Pasture
2.	Cropland/ Grassland Mosaic
3.	Deciduous Broadleaf Forest
4.	Dryland Cropland and Pasture
5.	Grassland
6.	Herbaceous Wetland
7.	Mixed Forest
8.	Mixed Shrubland/ Grassland
9.	Savanna
10.	Shrubland
11.	Urban and Built-Up Land
12.	Water Bodies

Reclassification of Soil Map to Soil Group

Application of the Curve Number method requires that the soils for the study area are reclassified to fit in one of four categories (A, B, C, and D). The condition to fit the soil classes to certain categories is subjective but depends highly on the infiltration rates and

the textural soil composition. These factors for the different soil classes are approximated during empirical field experiments and are available for use to classify the soils of the study area based on the generic conditions for soil classification. The soil hydraulic classes are found in Table 3.5 and their characteristics are as listed in Table 3.6

Table 3.5: Soil properties (Source: Artan et al., 2007)

Zobler Class Code	FAOTexture	Porosity	Matric Potential	Ks	Bslope	Soil Texture	Soil Hydraulic Class	Numeric soil HydraulicClass
1	Coarse	0.421	0.0363	**5.076**	4.26	loam sand	a	**88**
2	medium or coarse	0.43	4 0.1413	**1.882**	**4.74**	sandy loam	a	**88**
3	medium	0.439	0.3548	1.217	5.25	loam	b	**89**
4	fine or medium	0.404	0.1349	**1.602**	6.77	sandy clay or loam	c	**90**
5	fine	0.465	0.2630	**0.882**	8.17	clay or loam	d	**91**
6	ice	0.0	0.0	**0.0**	0.0	ice		
7	organic	0.439	0.3548	**1.217**	5.25	loam	b	**89**

Table 3.6: Generic conditions for soil classification (according to the Curve Number method).

Soil Hydraulic Class	Characteristics
Group "A"	Soils that have low runoff potential and high infiltration rates. The soil textures included in this group are sand, loamy sand, and sandy loam. The transmission rates of these soils are greater than 0.76 cm/hour.
Group "B"	Soils that have moderate infiltration rates. The soil textures included in this group are silt loam, and loam. The transmission rates of these soils are between 0.38 and 0.76 cm/hour.
Group "C"	Soils that have low infiltration rates. The soil texture included in this group is sandy clay loam. The transmission rates of these soils are between 0.13 and 0.38 cm/hour.
Group "D"	Soils that have very low infiltration rates. The soil textures included in this group are clay loam, silty clay loam, sandy clay, silty clay, and clay. The transmission rates of these soils are between 0.0 and 0.13 cm/hour.

The soil types were classified from their attributes according to the Soil Conservation Service (SCS) of the United States into four hydrologic soil groups according to their infiltration rate (D. R. Maidment, 1993). The resulting soil map categorised by hydraulic class is as shown in Figure 3 13.

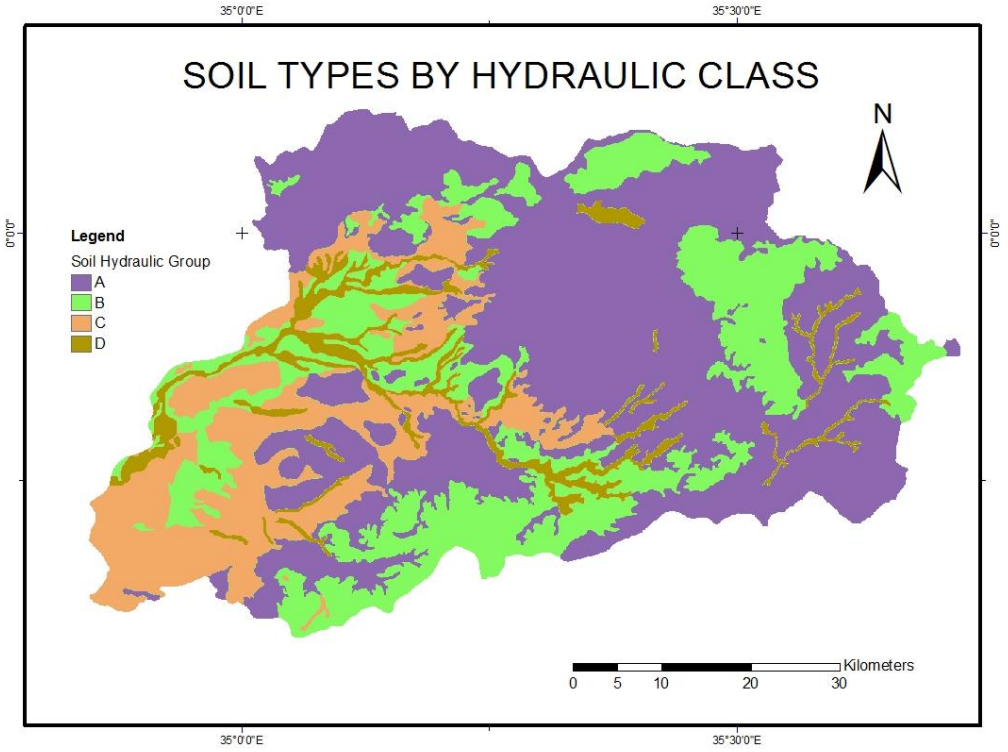

Figure 3.13*:* This illustration shows a grid of soil hydraulic groups in the Nyando Basin

Building up the Curve Number Grid

The SCS runoff curve number is based on the area's hydrologic soil group, land use, treatment and hydrologic condition. The SCS have developed tables of *CN* values for various land cover types against the four soil hydraulic groups under average moisture condition. Table 3.7 indicates the runoff curve numbers for characteristic land cover descriptions and a hydrologic soil group. From the table, from these four soil groups, numeric values were given to ease the grid creation process. The Numeric Soil Hydraulic classes, found in the last column of Table 3.5 are used when creating the Runoff Curve Number grid.

Hyd_a_mean = soil hydraulic class A
Hyd_b-mean = soil hydraulic class B

Hyd_c_mean = soil hydraulic class C

Hyd_d_mean = soil hydraulic class D.

Table 3.7: CN Runoff Curve Numbers as estimated from land cover classes and hydraulic soil groups. Source:

Lu_code	Description	Hyd_a_ mean	Hyd_b_ mean	Hyd_c_ mean	Hyd_d_mean
0	Unclassified	54.0	70.0	80.0	85.0
100	Urban and Built-Up Land	81.0	88.0	91.0	93.0
211	Dryland Cropland and Pasture	68.0	79.0	86.0	89.0
212	Irrigated Cropland and Pasture	62.0	71.0	78.0	81.0
213	Mixed dryland/ Irrigated crop land and pasture	65.0	75.0	82.0	85.0
280	Cropland/Grassland Mosaic	65.0	75.0	82.0	85.0
290	Cropland/Woodland Mosaic	45.0	66.0	77.0	83.0
311	Grassland	54.0	70.0	80.0	85.0
321	Shrubland	45.0	66.0	77.0	83.0
330	Mixed shrubland/grassland	49.5	68.0	78.5	84.0
332	Savanna	57.0	73.0	82.0	86.0
411	Deciduous Broadleaf Forest	45.0	66.0	77.0	83.0
412	Deciduous needleleaf Forest	45.0	66.0	77.0	83.0
421	Evergreen Broadleaf Forest	25.0	55.0	70.0	77.0
422	Evergreen needleleaf Forest	25.0	55.0	70.0	77.0
430	Mixed forest	35.0	60.5	73.5	80.0
500	Water Bodies	98.0	98.0	98.0	98.0
620	Herbaceous Wetland	30.0	58.0	71.0	78.0
610	Wooded Wetland	25.0	55.0	70.0	77.0
770	Barren or Sparsely Vegetated	68.0	79.0	86.0	89.0
820	Herbaceous Tundra	98.0	98.0	98.0	98.0
810	Wooded Tundra	98.0	98.0	98.0	98.0
850	Mixed tundra	98.0	98.0	98.0	98.0
830	Bare ground tundra	98.0	98.0	98.0	98.0
900	Snow or Ice	98.0	98.0	98.0	98.0

Since the CN value is dependent on the ground cover type and the hydrologic condition (see Table 3.7), the curve numbers grid was derived by assigning the corresponding value to each cell from the overlay of the land cover and soil hydraulic group grids. This is achieved using the Map Algebra Expression:

$$\text{con}([\text{soilhydgrp}] == 1, [\text{hyd\_a\_rcn}], \text{con}([\text{soilhydgrp}] == 2, \text{hyd\_b\_rcn}], \\ \text{con}([\text{soilhydgrp}] == 4, [\text{hyd\_c\_rcn}], \text{con}([\text{soilhydgrp}] == 3, [\text{hyd\_d\_rcn}], 0))))$$ **Eqn 3.7**

The resulting Curve Number map is shown in Fig 3.14 The grid is generated only once for the basin as long as the land cover and soil hydrologic conditions are considered unchanged.

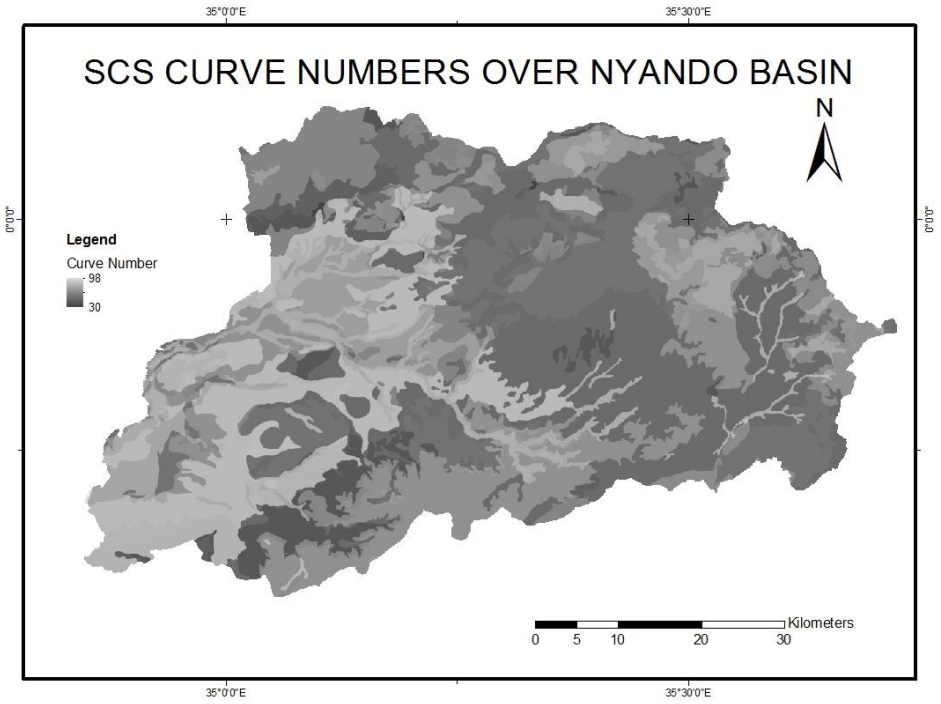

Figure 3.14: Grid of curve numbers assigned for each cell in the basin from land cover and soil hydraulic class grids

Determination of Runoff Using Curve Numbers (CN)

With the grids of soil hydraulic groups, land cover and rainfall estimates (RFE), surface runoff from each cell was estimated by the curve number method of the Soil Conservation Service. The approach estimates direct runoff *Q* in inches from rainfall *P* in inches and watershed storage *S* by:

$$Q = \frac{(P - I_a)^2}{P - I_a + S} \qquad \textbf{Eqn 3.8}$$

where I_a is the initial abstraction in inches and *S* is the maximum potential difference between *P* and *Q*. Both I_a and *S* are affected by factors such as vegetation and infiltration. No runoff occurs when the precipitation is less than the initial abstraction (*P* < *Ia*). Empirical evidence shows that *Ia* = 0.2 *S* so that

$$Q = \frac{(P - 0.2S)^2}{P + 0.8S} \qquad \textbf{Eqn 3.9}$$

The parameter *S* is defined by:

$$S = \left(\frac{1000}{CN} - 10\right) \qquad \textbf{Eqn 3.10}$$

where *CN* is an arbitrary runoff curve number ranging from 0 to 100. The RFE rainfall values, *P* for each cell were first converted from millimeters to inches.

From the grid of curve numbers, *CN* the grid of surface storage, *S* was derived for the basin. This is achieved in *ArcGIS* by applying Eqn 3.11 for each cell in the Raster Calculator with the grid of curve numbers, *CN* as the input and the grid of surface storage, *S* as the output. The grid is generated only once for the basin as long as the land cover is considered unchanged.

3.2.4 Simulation of Surface Runoff Volumes from Rainfall Estimates

The runoff depth, *Q* is calculated for each cell for each day to produce a continuous raster representing surface runoff from rainfall estimates, *P* for the basin for each day. This grid is used to weight the flow accumulation grid to estimate the amount of surface runoff that is incident on the surface, upslope from each cell.

Each day's satellite rainfall estimates was clipped to the Basin boundary to improve processing efficiency. The grid pixel values converted from millimetres (mm) to inches The runoff depth for each cell is computed in inches from the grid of surface storage, *S* and satellite rainfall estimates, *P* using the formula:

$$Q = \frac{(P - 0.2S)^2}{P + 0.8S} \qquad \textbf{Eqn 3.11}$$

in which rainfall *P* and runoff depth *Q* are in inches

The runoff depth for each upstream cell on each day was used to generate a weighted flow accumulation grid to record how much volume of runoff is incident to each cell for each day, the areal unit being one cell.

Finally, the runoff volumes so obtained at the positions of the flow gauges were extracted and tabulated for use in statistical comparisons. Routines were developed in the Model Builder in ArcGIS to undertake the above repetitive steps that are carried out on a cell-by-cell basis. The steps are described in details in Appendix B. The runoff grid for one day as a result of this process is presented in Figure 3.15.

.

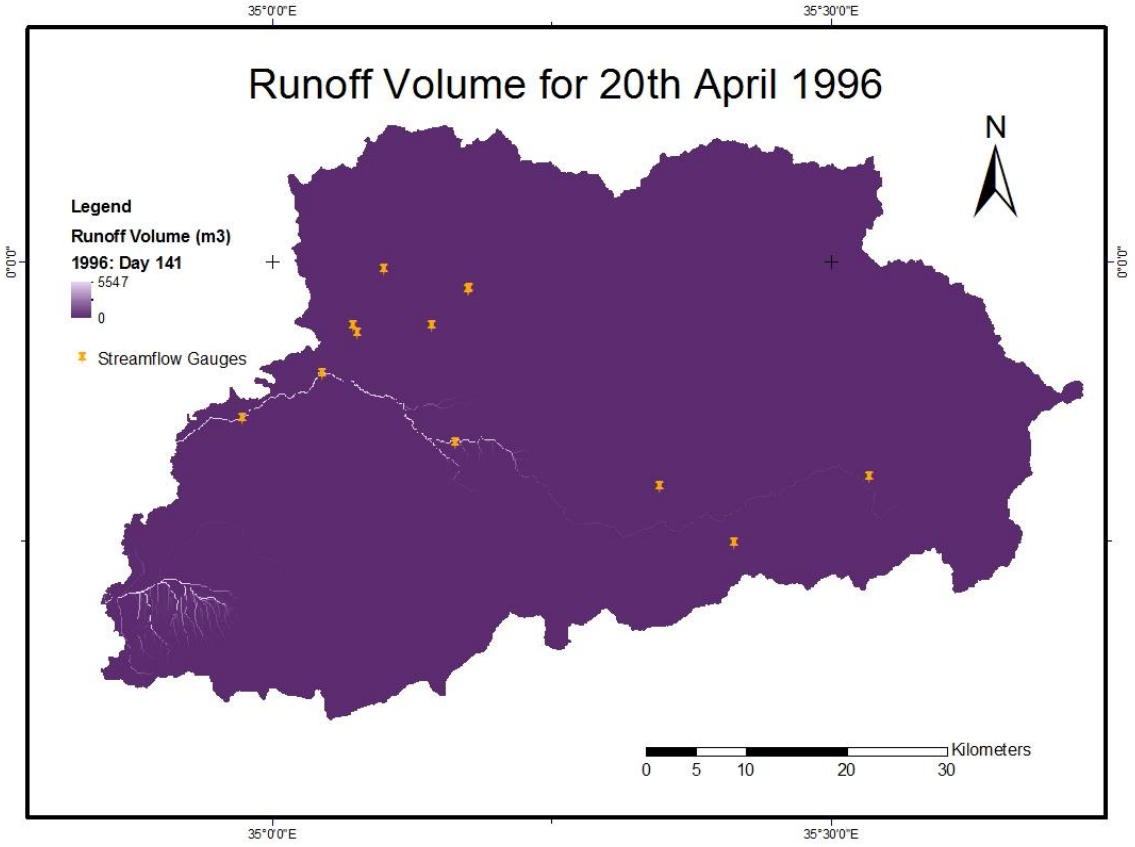

Figure 3.15: Runoff volume for the study area on 20th April 1996

The extracted runoff volume for each day for each gauge was exported to Excel spreadsheets for comparison with observed streamflow. The volumes obtained were compared with observed streamflow levels using time series plots and the correlation coefficient (*r*).

3.2.5 Flood Hazard Forecasting

The simulated accumulations of surface runoff volumes, driven by the daily rainfall estimates were extracted for a sub-basin of approximately 600 km² for 1996 and were then compared with that year's stream level records obtained from existing river gauging station1GB11 located at the sub-basin outlet (Gaya et al., 2009a).

Using the steps described in Section 5.4, the simulation of runoff volumes was performed for selected periods between 2006 and 2012 and related with observed stream levels at the river gauging station 1GD03.

3.2.6 GIS Database for Flood Management

Digital maps of the Kano flood plains were constructed from digitizing the physical features of scanned topographical maps at a scale of 1:50,000 and updated with field surveys. Public utilities such as schools, colleges, hospitals and markets in and around the flood zone were mapped (Figure 3.16) and their attribute information incorporated in shapefiles. Other shapefiles assembled are the administrative data for the area; including sub-locations, locations, former districts and divisions and counties within and neighbouring the basin, and the accompanying demographic data.

The geodatabase also consists of shapefiles of the road network and major towns, rain gauge and stream gauge stations with historical records and the stream network. Also assembled are gridded data in the form of a 20-m resolution DEM of the basin generated from contours of the area, *Africover* land cover map, soil map and clipped historical RFE data for the Nyando basin. The geodatabase is intended to facilitate a dynamic formulation of informed and relevant decisions and policies for reducing flood-induced disaster and alleviating the undesirable socio-economic effects of perennial flooding in the area (Gaya, Gachari, & Gathenya, 2011).

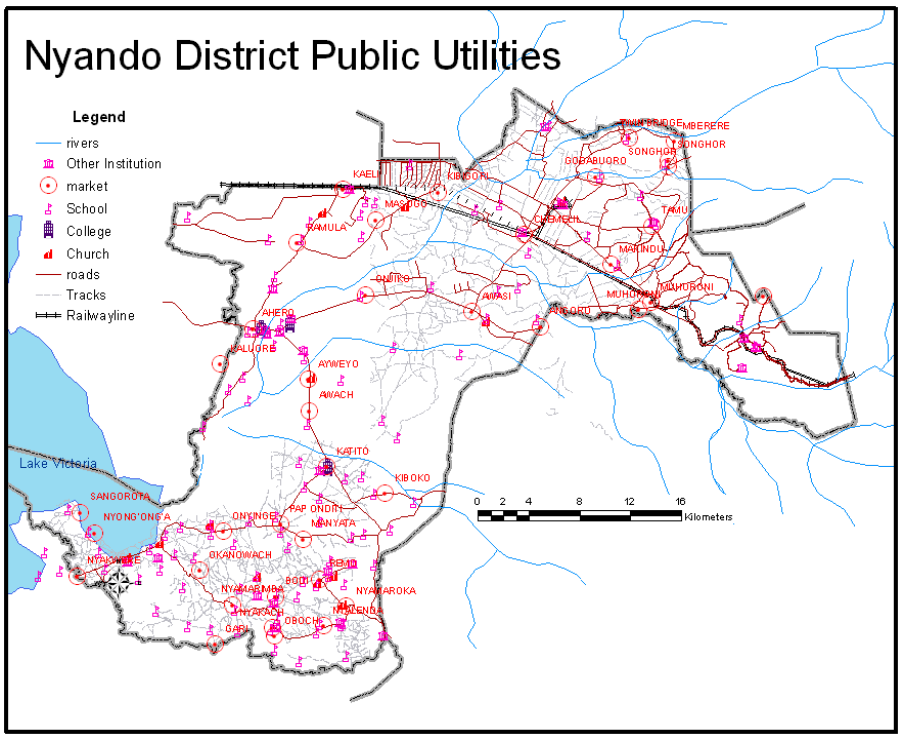

Figure 3.16: A GIS Database of Nyando district compiled from topographic maps and updated by field surveys.

3.2.7 Classification of Satellite Imagery

Classification was undertaken of satellite imagery from Landsat and ASTER. In order to aid visual interpretation, visual appearance of the objects was improved by image enhancement techniques such as grey level stretching to improve the contrast and spatial filtering for enhancing the edges.

Different land cover types in an image were discriminated through image classification using spectral features, i.e. the brightness and ‘’color’’ information contained in each pixel. In supervised classification, the spectral features of areas of known land cover types were extracted from the image. Every pixel in the whole image was then classified as belonging to one of the classes depending on how close its spectral features were to the spectral features of the training areas. In unsupervised classification, the computer

program automatically grouped the pixels in the image into separate clusters, depending on their spectral features. Each cluster was then assigned a land cover type.

CHAPTER FOUR

RESULTS

4.1 Rainfall Estimation

Results obtained in from the validation of satellite rainfall estimates, RFE give an indication of how the satellite derived rainfall amounts fit to the gauge measured rainfall. Figure 4.1 shows time-series comparison of basin-wide average of the mean 10-daily rainfall for the RFE data against gauge measurements for the 8 year period. Table 4.1 summarizes the results of a comparison of the satellite rainfall estimates with the observed station data as the reference standard.

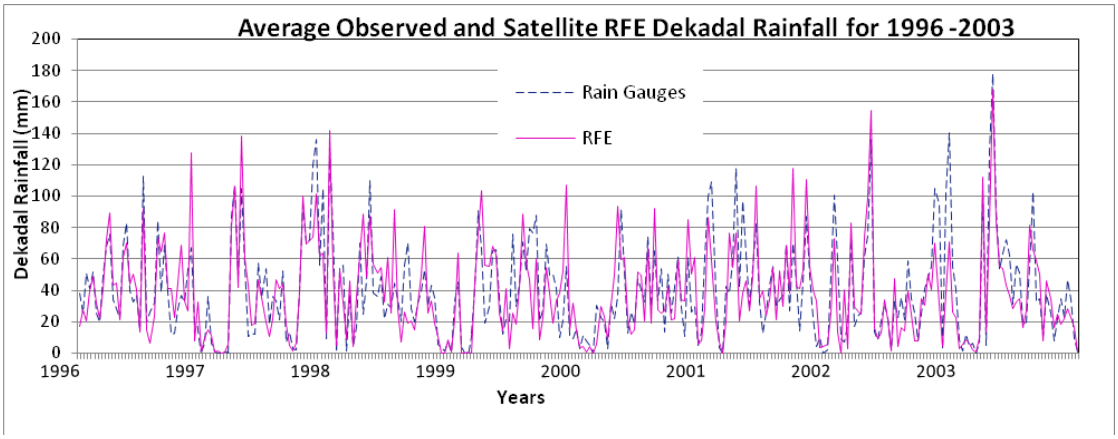

Figure 4.1: Time series plot of average study area rainfall (millimetres per dekad) for the from 1996 t0 2003 for the rain gauges and satellite RFE

Table 4.1: Results of the pairwise analysis between dekadal satellite rainfall estimates and the observed station data for the selected period.

Year	*No. of Gauges*	*Corr. Coeff. (r)*	*ME*	*RMAE*	*NSE*	*Bias*	*RMSE*
1996	9	0.774	2.44	0.62	0.50	1.07	6.07
1997	11	0.903	-2.25	0.51	0.61	0.98	5.17
1998	11	0.771	1.60	0.60	0.55	1.06	5.09
1999	12	0.629	-0.88	0.62	0.57	1.01	5.23
2000	10	0.736	2.38	0.57	0.57	1.40	4.19
2001	6	0.714	-1.05	0.54	0.63	1.01	5.21
2002	4	0.775	-9.77	0.57	0.63	0.81	6.99
2003	8	0.920	-4.14	0.50	0.69	0.91	4.72
Overall Mean		**0.778**	**-1.46**	**0.57**	**0.59**	**1.03**	**5.33**

Figure 4.1 shows a good agreement between the arithmetic averages of the two sets of data from dekadal accumulations. This is supported overall mean bias of 1.03 between the gauge data and the satellite estimates for dekadal rainfall as reported in Table 4.1. Regression analysis yielded on average a correlation coefficient *(r)* of 0.78 and a *RMSE* of 5.33 mm/dekad as presented in However, RFE underestimates rainfall in most stations as indicated by the negative mean errors *(ME)* in (Table 4.1).

Table 4.1 illustrates that the two years with the best match are 2003 and 1997. Incidentally, these two years saw some of the most extreme flood events of recent times in this region. Even for the year 2000 where Day 305 RFE data was suspicious, an arbitrary division of the cell values by 256 yielded a correlation factor of 0.74. The *RMSE* was on the order of 4.2 mm per dekad.

Figure 4.2: illustrates the correspondence between the two sets of data using scatter plots at two selected gauge stations. Table 4.2 ranks the rainfall stations according to the correlation between the observed data and the satellite rainfall estimates at each station.

Table 4.2: Degree of association between the observed data and the satellite rainfall estimates at each station.

Station ID	***Station Name***	***Elev. (m above sea level)***	***No. of years used***	***Corr. coeff. (r)***	***ME***	***RMAE***	***NSE***	***Bias***	***RMSE***
9035080	*Kamarero - Songhor*	1920	1	0.781	-0.45	0.50	0.69	0.99	3.96
9035127	*P.B.K Londiani Pyrethrum Office Nursery*	2524	1	0.768	-0.66	0.56	0.60	0.98	4.29
9035126	*P B.K Olenguruone Field Office*	2501	2	0.757	-14.04	0.57	0.71	0.65	5.43
					14.04				
8935071	*Siret Tea Co. Ltd. - Nandi*	2057	5	0.709	-9.18	0.50	0.72	0.81	5.52
9035148	*Koru Bible School*	1410	4	0.697	3.87	0.40	0.70	1.13	3.79
8935161	*Nandi Hills - Kibweri Tea*	2040	7	0.647	-3.52	0.50	0.68	0.99	4.94
8935186	*Kimwani A.D.C. Farm*	1511	6	0.646	3.72	0.54	0.57	1.21	4.77
8935095	*Nandi Tea Factory*	2010	3	0.639	-5.31	0.51	0.73	0.89	4.96
9035046	*Chemelil Plantation*	1279	7	0.635	3.65	0.55	0.56	1.15	4.62
9034124	*Masaka Apundo's Farm*	1160	6	0.635	7.75	0.69	0.36	1.24	5.26
8935190	*Sitoti Estate*	2043	6	0.626	-2.19	0.51	0.66	1.02	5.41
8935033	*Nandi Hills - Savani Estate*	1889	3	0.605	-1.74	0.63	0.60	0.97	5.01
8935160	*Kapsimotwa Tea Estate*	2021	7	0.553	-8.85	0.55	0.67	0.89	6.45
9034086	*Ahero Irrig. Research Station*	1161	4	0.541	2.04	0.64	0.49	1.06	6.00
9035020	*Kipkelion Railway Station*	1937	4	0.472	5.68	0.76	0.31	1.28	4.93
8935148	*Kipkurere Forest Station*	2236	2	0.417	3.35	0.65	0.50	1.54	5.06
9034121	*Rae Girls' Secondary School*	1143	1	0.371	6.86	0.72	0.41	1.18	5.80
9035002	*Londiani Forest Station*	2315	2	0.346	-4.39	0.80	0.48	0.88	6.56

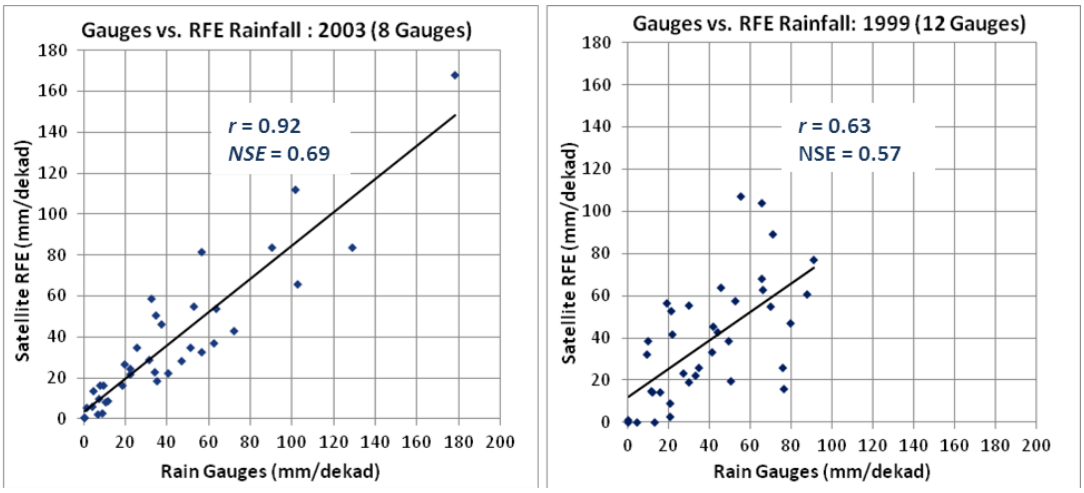

Figure 4.2: Scatter plots of decadal (10-day) average rain gauges (observed) rainfall versus satellite RFE for 1999 and 2003.

Comparison results according to the elevations of the rain gauge stations yielded no definite trend. Table 4.3 gives results of the average indices at elevation ranges classified using natural breaks. The highlands (above 2100 m above sea level) have a slightly better *NSE* of 0.64 and *Bias* of 0.96 between the RFE and rain gauge data than the lower ranges. The mid ranges performed best in the indicating the association between the datasets with the highest correlation coefficient of 0.63 and the lowest mean error, *RMAE* and *RMSE.* The plains showed the worst performance in most indicators.

Table 4.3: Comparison of performance of RFE against rain gauges grouped by elevation of gauges

Rain Gauges Elevation (m above sea level)	*No. of Stations*	*Mean Corr. Coeff. (r)*	*ME*	*RMAE*	*NSE*	*Bias*	*RMSE*
Above 2001	9	0.607	-4.98	0.57	0.64	0.96	5.40
1501-2000	4	0.626	1.80	0.61	0.54	1.11	4.66
1000-1500	5	0.576	4.83	0.60	0.50	1.15	5.09

4.2 Rainfall-Runoff Simulation

From the graphical comparison of the plot of the derived runoff volume vs. observed river levels, it was noticeable that whenever the simulated runoff volume at the gauging position increased significantly, there was, in most cases, a similar incremental trend in the observed level of the river on the same day or one day later. This is illustrated in Figure 4. for Station 1GB11 which is an outlet for a sub-basin of approximately 600 km² in the northern part of the Nyando Basin. This was the only station in the Basin with gap -free data for a continuous calendar year.

The continuous simulation at river gauging station1GD03 run using daily rainfall estimates showed a similar trend. Station 1GD03 is located in a strategic location upstream of the flood plains and almost at the outlet of the catchment. It captures an area of about 2625 km² upstream.

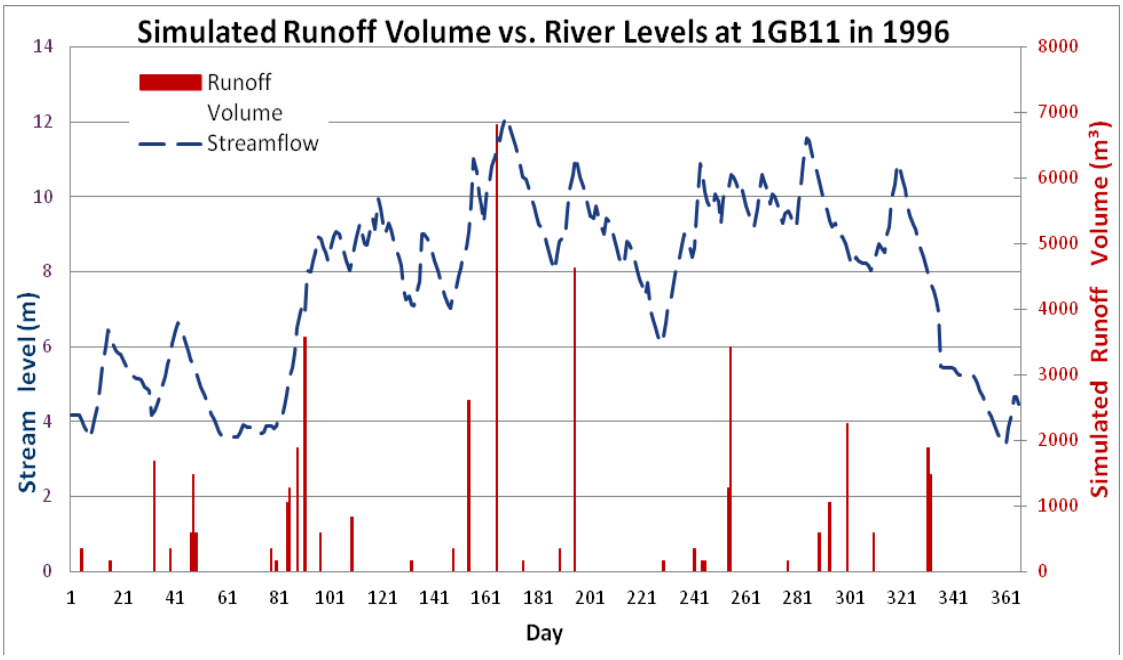

Figure 4.3: A graphical comparison between the simulated runoff volume and observed river levels at flow gauge 1GB11 for the year 1996.

The daily-simulated runoff volumes showed weak correlations to the observed stream levels with values of *r* ranging from -0.120 to + 0.004, with a mean of -0.045 (Table 4.4). While there was a challenge in obtaining real time data on daily stream levels, graphical comparison with the levels when they later became available showed moderate concurrence between the rise in stream level and the rise in simulated runoff volumes during high surges in flow as presented in Figure 4.4.

Table 4.4 Table 4.4: Degree of association between the simulated runoff volume and the daily stream levels at 1GD03 between 2006 and 2012

Year	**Corr. Coeff. (r)**
2006	-0.035
2007	-0.017
2008	-0.093
2009	-0.120
2010	0.004
2011	-0.035
2012	-0.020
Overall Mean	**-0.045**

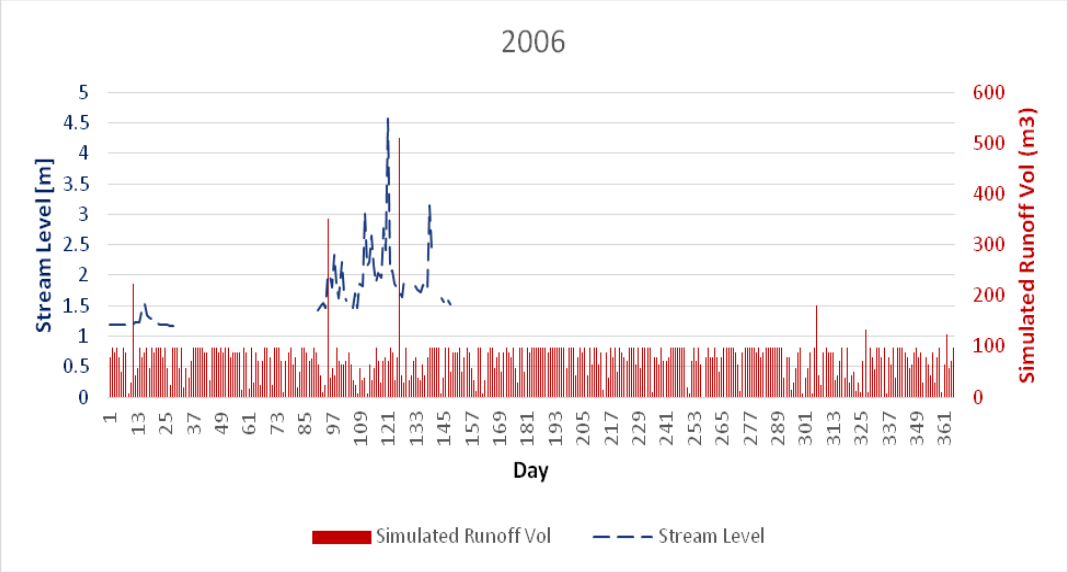

(a)

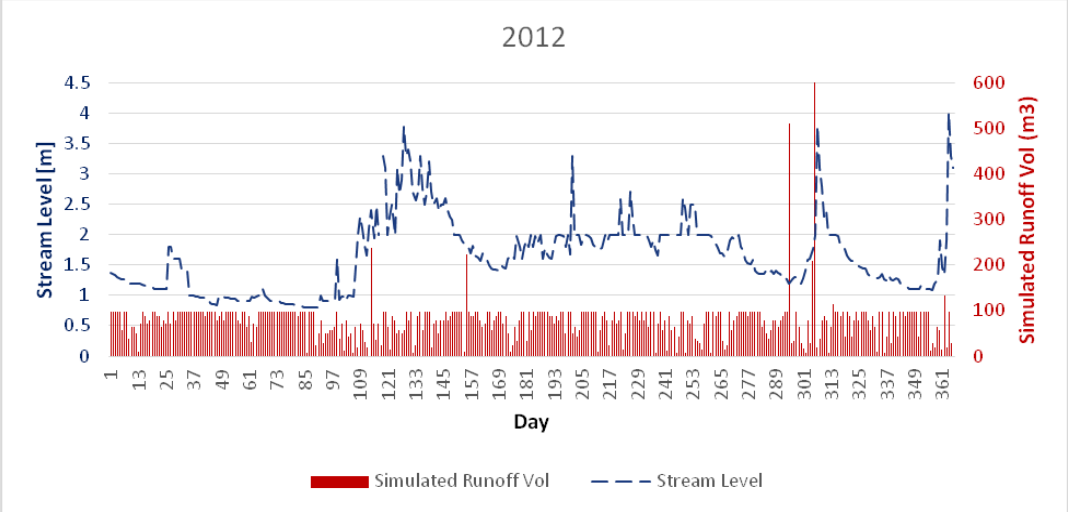

(b)

Figure 4.4: Graphical comparisons between the simulated runoff volume and observed river levels at flow gauge 1GD03 for (a) 2006 and (b) 2012.

4.3 Flood Inundation Mapping

In the study, the overall accuracy of this classification is about 79%. The primary purpose of the classification is to map the flood extent. It is notable that the wetland/ marshland is moderately accurate. The Producer's accuracy for wetland/ marshland is 79% and a site identified as wetland/marshland is also moderately accurate (79% User's accuracy). The Producer's accuracy means 21% errors of omission, but examination of the confusion matrix shows that one-third of the errors of commission (14/36) are mislabeled as water.

Table 4.5: Accuracy assessment for ASTER using Landsat as reference image.

College	Water	Wetland/ Marshland	Crops	Forest	Bare Soil	Urban Areas	**Total**	**User's Accuracy**
Water	32	15	0	6	4	12	**69**	**0.74**
Wetland/ Marshland	14	39	12	9	7	6	**87**	**0.79**
Crops	0	12	49	12	11	5	**89**	**0.80**
Forest	6	9	12	27	8	9	**71**	**0.71**
Bare Soil	4	7	11	8	36	14	**80**	**0.72**
Urban Areas	12	6	5	9	14	23	**66**	**0.90**
Total	**68**	**87**	**89**	**71**	**80**	**64**	**462**	
Producer's Accuracy	**0.72**	**0.79**	**0.80**	**0.71**	**0.72**	**0.91**		

Overall Accuracy: **0.79**

Kappa Coefficient: **0.72**

CHAPTER FIVE

DISCUSSION

5.1 Introduction

In most of Africa, ground-based information is in short supply. Rain gauge networks are sparse with vast areas un-gauged, while weather radar is not a feasible proposition on the grounds of cost, technical infrastructure and topography (Grimes & Diop, 2003). Satellite rainfall estimates can fill in gaps in station observations and are therefore an attractive alternative for providing rainfall information.

5.2 Evaluation of Satellite-Derived Rainfall Estimates (RFE)

The results from the graphical comparison and determination of *Bias* between the satellite estimates with observed rainfall show that the RFE underestimates rainfall in most stations but overestimates in some. The satellite rainfall estimates had a moderate under-estimation/ over-estimation bias. This may have been due to the topography of the region that may have resulted in orographic precipitation (Ouma, Adafre, & Muthama, 2005). On daily time scales, the two rainfall estimates were weakly correlated, whereas the match between dekadal accumulated rainfall values was significant. This agreement between RFE and gauge data is actually distributed in space. A few stations had low or moderate correlation. Overall, as much as the estimates are constrained with gauge data, gauge errors also cause uncertainty (Vieux, 2004). Errors in gauge accumulations may be caused by wind effects and tipping of bucket gauges during heavy rainfall rates.

The results suggest that the satellite rainfall estimates can be a source of rainfall data for modelling processes for 10-day and longer periods (Funk & Verdin, 2003). The gridded rainfall time-series give historical context, and provide a basis for quantitative interpretation of seasonal precipitation forecasts. The RFE data is therefore useful for

hydrologic modelling when the hydrologic model is calibrated with such data (G. Artan et al., 2007). Results herein show better performance in extreme weather events that show that RFE data can be used as the rainfall input in the flood forecasting system. RFE are also used to characterize flood hazards, in both simple indices and stream flow models (Verdin, Funk, Senay, & Choularton, 2005). With the RFE input into a hydrologic model, it is possible to simulate the hydrologic process in order to forecast flooding in the Lake basin.

Ideally, correction for underestimation and overestimation of the total rainfall amount is necessary before the derived rainfall amounts can be applied to model rainfall runoff relations. However, despite the significant correlations obtained, one of the key problems may be the accuracy of the measured rainfall and its reliability.

5.3 GIS-Based Derivation of Runoff Parameters

Just as the correlation between daily observed rainfall and RFE have poor correlation for daily accumulations, the daily simulated volume have a weak correlation with the daily stream gauge level data from visual inspection. This may be attributed to weak association between the daily rainfall and the daily RFE estimates, since the later are used as input to simulate the streamflow. However, during extreme incidents of rise in stream levels, the surges were detectable in the runoff volumes plots. These results show that from the input parameters of satellite rainfall estimates, soil map and land cover map, it is possible to simulate the surface runoff that is fairly indicative of the variation in the stream level. Thus when there is forecast of a drastic surge in the runoff volume, a rise in the river level is to be expected. Depending on the river level before the rise, if the forecast stream level is higher than the historical flood level then it can be marked as warranting an early warning of flooding.

The main cause of uncertainties in runoff modelling using satellite derived rainfall may arise from inaccuracies of the derived satellite rainfall. Therefore, runoff generated in this study may be underestimated or overestimated mainly due satellite underestimation or overestimation of the rainfall amounts. It may, therefore, be necessary to make adjustments to the satellite-derived rainfall before it is applied to model runoff. However this can only be useful if the in situ data can be availed on time and are also accurate in the first place.

5.4 GIS and Remote Sensing Integration for Flood Management

The presence of clouds during rainy seasons when inundation occurs renders the use of optical remote sensors to be limited during a flooding event. Satellite imagery vendors would also normally not deliver imagery products containing more than 20% cloud cover. Radar satellite imagery is therefore recommended for mapping flood inundation areas due to its capabilities of seeing through clouds and rain. The main problem anticipated in operational application of space-borne radar data is the availability of data for near-time monitoring. ERS has a repeat cycle of 35 days and by itself, does not have sufficient temporal coverage. Furthermore, radar imagery coverage of the area is minimal and, when available, is more expensive than other satellite imagery. For example, one scene ERS archival data for the area costs 8 times more than Landsat. Still, getting ERS and other radar data coverage for the date of interest (i.e. during the flooding period) has for a long time been a matter of chance. The introduction Sentinel-1 since 2014 with daily full satellite radar imagery coverage of this region of the world, and its open and free data policy would be extremely beneficial for realising flood inundation mapping in the study area. The study also recognises the potential benefits of integration of a GIS database for the study area in the flood management.

CHAPTER SIX

CONCLUSION AND OUTLOOK

6.1 Conclusions

Rainfall is a major driving force in the runoff generation in any watershed that can lead to flooding. An accurate rainfall data input is therefore required in order to derive accurately the amount of runoff. However, the Sub-Saharan Africa region ranks among the lowest in the world in the density of rainfall monitoring stations. The reliability of the data collected is also a major issue since even where rainfall data are available, weeks can elapse between collection and accessibility to users is poor. For this reason, the possibility of using satellite derived rainfall was explored. However before it was used, it was necessary to verify its suitability to represent the incident rainfall in the study area.

6.1.1 Evaluation of Satellite-Derived Rainfall Estimates (RFE)

In this study, historical rainfall data obtained from the Kenya Meteorological Department for the Nyando basin are used to validate the satellite-derived rainfall estimates (RFE). The RFE raster dataset and the point feature class of gauging stations were first displayed in the GIS user interface. A VBA program was applied in ArcGIS to import each day's RFE raster dataset in turn and loop through each station in the point feature class to obtain the cell value of the raster cell where the point is located. This routine was used to obtain the RFE data for the period 1995 to 2005 corresponding to the locations of 35 gauging stations in the basin.

Time-series graphs were plotted for comparison of RFE and gauge data for each station for daily, 10-day and monthly rainfall. Histograms were plotted of the annual rainfall for each year at each available station by summing the daily precipitation from both sets of

data for a graphical comparison. Simple regression analysis was used to measure the degree of agreement between the observed rainfall and the satellite RFE.

The results for comparisons at daily accumulations of satellite-estimated rainfall when compared with observed rain gauge data are not so good but they performed reasonably well in detecting the occurrence of rainfall. The products show significant results for 10-day accumulation where regression analysis yielded an average correlation coefficient (r) of 0.78.

The validation results show that Satellite rainfall estimates (RFE) can provide a sufficiently reliable estimation of precipitation over the basin for flood forecasting purposes. The Satellite rainfall estimates can therefore be used to fill in the gaps in unavailable station observations or delays in obtaining the observed data.

6.1.2 GIS-Based Derivation of Runoff Parameters

Application of satellite-derived rainfall and the pixel based SCS Curve Number Method for runoff simulation represents one of the key strengths of this study. The study used the fruitful application of the Curve Number method in Geographic Information Systems to derive run-off parameters. For modelling purposes, the infinite variability of the parameters was averaged to a degree of finite elements (20 m square grids), which was then assumed to have uniform parameters (elevation, land cover, soils etc.). These were based on the 20 m resolution of the DEM; generated from contour lines and spot heights of existing topographic maps of the area.

The soil types were classified from their attributes according to the Soil Conservation Service (SCS) into four hydrologic soil groups according to their infiltration rates. The Africover Land Cover map of the area was first translated into meaningful description using the translator in the LCCS software and grouped into the major land cover types against the corresponding LU Code.

The curve numbers were estimated through GIS analysis of existing digital soil maps overlaid with the land cover map on a table look-up basis.

Routines were developed in the GIS to utilise the satellite rainfall estimates (RFE) as daily incident rainfall in running simulations of surface runoff. This was achieved through the incorporation of the RFE raster grid with the derived curve number and surface storage grids to compute the runoff depth by the curve number equation for each cell. This produced a continuous raster representing surface runoff for each day. The runoff depth grid was then used to weight the flow accumulation grid of the Basin to estimate the amount of surface runoff that is incident on the surface, upslope from each cell on a daily basis.

The simulated accumulations of surface runoff volumes driven by the daily rainfall estimates were compared with previous stream level records obtained for two existing river gauging stations, 1 GB11 and 1GD03, for selected periods between 1995 and 2012. The results of graphical comparison of the daily observed, alongside the simulated daily streamflow present a far from perfect relationship. However, reasonable concurrence between the rise in stream level and the rise in simulated runoff volumes was visible from graphical comparison during high flow periods. This simple spatial analysis of the basin drainage parameters integrated with RFE estimates over the basin show the potential to predict the increase in stream levels that may lead to occurrence of floods. The approach may not be useful for quantifying the amount of flooding volumes but can be employed to give alerts of potential flood events.

6.1.3 GIS and Remote Sensing Integration for Flood Management

This research study has identified the usefulness of geospatial tools in the application of flood management. Firstly, geospatial analysis techniques have been applied to simulate the flood runoff volumes using the traditional curve number method. Secondly, the role of Remote Sensing in mapping flood inundation has been demonstrated by mapping

from classified satellite imagery. The applicability of ASTER and Landsat in mapping floods in the Nyando area of Western Kenya were analysed. Landsat images, compared with ASTER gave an overall accuracy of 0.79 and are thus useful for flood mapping provided the cloud cover is minimal.

6.2 Recommendations

A hydrological model for the region can be developed using the simulation process hereby developed. However, the results of this study are far from perfect. This suggests that there are areas of further research that may be explored to provide better refined results.

Satellite rainfall estimation is an attractive option in most of Africa, where rain gauge networks are sparse with vast areas un-gauged, while the use of ground-based weather radar to estimate rainfall is not a feasible proposition on the grounds of cost, technical infrastructure and topography. However, RFE data results should be combined with other satellite products such as TRMM and rain gauge data for better results.

It is intended to use river gauge readings and hydrographs of previous flood events to determine flood warning levels. The simple simulation is to be run daily to provide several days' forecast of the river levels at the various river gauging stations. Using the forecast river levels in conjunction with recorded flood levels of each area, it should be possible to predict the occurrence of floods and issue early warnings.

The accuracy of the simulation can be improved with appropriate channel routing methods and simulation of flood peak discharges. This will definitely require more data to operate and more coefficients and parameters as model inputs. In particular, it will require a higher resolution DEM from which river channel morphology can be obtained. Future studies should also aim at investigating the effects of land cover/use land cover changes on the simulations.

A better resolution DEM will also enable the simulation of flood inundation in the floodplains resulting from the simulated runoff volumes. The recent availability of new and accessible radar coverage of the region, such as Sentinel-1, historical radar data can sourced for inundation mapping.

REFERENCES

Abtew, W., & Melesse, A. M. (2014). The Nile River Basin. In *Nile River Basin: Ecohydrological Challenges, Climate Change and Hydropolitics* (Vol. 9783319027, pp. 7–21).

Adeyewa, Z. D., & Nakamura, K. (2003). Validation of TRMM Radar Rainfall Data over Major Climatic Regions in Africa. *Journal of Applied Meteorology*, *42*(2), 331–347.

Ali, A., Amani, A., Diedhiou, A., & Lebel, T. (2005). Rainfall Estimation in the Sahel. Part II: Evaluation of Rain Gauge Networks in the CILSS Countries and Objective Intercomparison of Rainfall Products. *Journal of Applied Meteorology*, *44*(11), 1707–1722.

Amekudzi, L. K., Osei, M. A., Atiah, W. A., Aryee, J. N. A., Ahiataku, M. A., Quansah, E., … Fink, A. H. (2016). Validation of TRMM and FEWS Satellite Rainfall Estimates with Rain Gauge Measurement over Ashanti Region, Ghana. *Atmospheric and Climate Sciences*, *06*(04), 500–518.

Arkin, A., & Xie, P. (1997). A 17-year monthly analysis based on gauge observations, satellite estimates, and numerical model outputs. *Bulletin of the American Meteorological Society, 78*(11), 2539–2558.

Arkin, P. A., & Ardanuy, P. E. (2002). Estimating Climatic-Scale Precipitation from Space: A Review. *Journal of Climate*.

Arkin, P. A., & Meisner, B. N. (1987). The Relationship between Large-Scale Convective Rainfall and Cold Cloud over the Western Hemisphere during 1982-84. *Monthly Weather Review*.

Artan, B. G. A., Asante, K., Smith, J., Pervez, S., Entenmann, D., Verdin, J., & Survey, U. S. G. (2007). Users Manual for the Geospatial Stream Flow Model (GeoSFM) U . S . Geological Survey. *Director, 605*, 1520.

Artan, G., Gadain, H., Smith, J. L., Kwabena, A., Bandaragoda, C. J., & Verdin, J. P. (2007). Adequacy of Satellite Derived Rainfall Data for Stream Flow Modelling. *Natural Hazards*, *Vol.43*(2), 167–185.

Asadullah, A., McIntyre, N., & Kigobe, M. (2008). Evaluation of five satellite products for estimation of rainfall over Uganda / Evaluation de cinq produits satellitaires pour l'estimation des précipitations en Ouganda. *Hydrological Sciences Journal*,

53(6), 1137–1150.

Bähr, H.-P. (1999). Image Classification (Theory). In H.-P. Bähr & T. Vögtle (Eds.), *GIS for environmental monitoring* (pp. 181–196). E. Schweizerbart'sche Verlagsbuchhandlung.

Bajracharya, S. R., Shrestha, M., & Shrestha, A. B. (2014). Assessment of high-resolution satellite rainfall estimation products in a streamflow model for flood prediction in the Bagmati basin , Nepal Assessment of high-resolution satellite rainfall estimation products in a streamflow model for flood prediction in, (September).

Band, L. E., Tague, C. L., Brun, S. E., Tenenbaum, D. E., & Fernandes, R. A. (2000). Modelling watersheds as spatial object hierarchies: Structure and dynamics. *Transactions in GIS*, *4*(3), 181–196.

Beard, T., Usery, E. L., Scheidt, D. J., Bearden, M., Finn, M. P., & Ruhl, S. (2004). Geospatial data resampling and resolution effects on watershed modeling: A case study using the agricultural non-point source pollution model. *Journal of Geographical Systems*, *6*(3), 289–306. Blasco, F., Bellan, M. F., & Chaudhury, M. U. (1992). Estimating the extent of floods in Bangladesh using SPOT data. *Remote Sensing of Environment*, *39*(3), 167–178.

Bobée, B., & Rasmussen, P. F. (1995). Recent advances in flood frequency analysis. *Reviews of Geophysics*, *33*(S2), 1111–1116. Boonklong, O., & Jaroensutasinee, M. (2007). Computation of D8 Flow Line at Ron Phibun Area, Nakhon Si Thammarat, Thailand. *Proceedings of World*, *8*, 1–4.

Brivio, P. A., National, I., Colombo, R., Maggi, M., Tomasoni, R., & National, I. (2002). Integration of remote sensing data and GIS for accurate mapping of ooded areas, (May 2014).

Budhakooncharoen, S. (2014). Rainfall Estimate for Flood Management Using Meteorological Data from Satellite Imagery, *40722*(June).

Burrough, P. A., McDonnell, R. A., & Lloyd, C. D. (2015). *Principles of geographical information systems*. Oxford university press.

CGIAR-CSI. (n.d.). SRTM 90m DEM Digital Elevation Database. Retrieved April 20, 2019, from http://srtm.csi.cgiar.org/

Chow, V. Te, Maidment, D. R., & Mays, L. W. (1988).

Applied_Hydrology_Chow_1988.

Chow V.T. (1964). *Handbook of Applied Hydrology*. New York: McGraw-Hill.

Clerici, A. (1980). A method for drawing slope maps from contour maps by automatic data acquisition and processing. *Computers & Geosciences*, *6*(3), 289–297.

Condie, R., & Lee, K. A. (1982). Flood frequency analysis with historic information. *Journal of Hydrology*, *58*(1–2), 47–61.

Cornell University. (2008). *Watershed Engineering* (Vol. 2).

D'Asaro, F., & Grillone, G. (2010). Runoff curve number method in Sicily: CN determination and analysis of the initial abstraction ratio. In *2nd Joint Federal Interagency Conference (4th Federal Interagency Hydrologic Modeling Conference and the 9th Federal Interagency Sedimentation Conference):" Hydrology and Sedimentation for a Changing Future: Existing and Emerging Issues"*. Joint Federal Interagency Conference 2010.

Dang, A. T. N., & Kumar, L. (2017). Application of remote sensing and GIS-based hydrological modelling for flood risk analysis: a case study of District 8, Ho Chi Minh city, Vietnam. *Geomatics, Natural Hazards and Risk*, *8*(2), 1792–1811.

Das, G. (2008). *Hydrology and Soil Conservation Engineering*. Prentice-Hall Of India Pvt. Limited.

de Groeve, T. (2010). Flood monitoring and mapping using passive microwave remote sensing in Namibia. *Geomatics, Natural Hazards and Risk*, *1*(1), 19–35.

Deutsch, M., & H. Ruggles Jr, F. (1978). Hydrological Applications of Landsat Imagery Used in the Study of the 1973 Indus River Flood, Pakistan1. *JAWRA Journal of the American Water Resources Association* (Vol. 14).

Dinku, T., Ceccato, P., Grover-Kopec, E., Lemma, M., Connor, S. J., & Ropelewski, C. F. (2007). Validation of satellite rainfall products over East Africa's complex topography. *International Journal of Remote Sensing*, *28*(7), 1503–1526.

Dinku, T., Chidzambwa, S., Ceccato, P., Connor, S. J., & Ropelewski, C. F. (2008). Validation of high-resolution satellite rainfall products over complex terrain. *International Journal of Remote Sensing*, *29*(14), 4097–4110.

DMCN. (2004). *Coping with Floods in Kenya: Vulnerability, Impacts and adaptation*

Options for the Flood Prone areas of Western Kenya.

Endreny, T. A., & Wood, E. F. (2003). Maximizing spatial congruence of observed and DEM-delineated overland flow networks. *International Journal of Geographical Information Science*, *17*(7), 699–713.

ESRI. (2014). Hydrologic and Hydraulic Modeling for Floodplain Delineation. *ESRI International User Conference 2014 Technical Workshops*.

Fernandez, A., Adamowski, J., & Petroselli, A. (2016). Analysis of the behavior of three digital elevation model correction methods on critical natural scenarios. *Journal of Hydrology: Regional Studies*, *8*, 304–315.

Freeman, T. G. (1991). Calculating catchment area with divergent flow based on a regular grid. *Computers & Geosciences*, *17*(3), 413–422.

Funk, C., Nicholson, S. E., Landsfeld, M., Klotter, D., Peterson, P., & Harrison, L. (2015). The Centennial Trends Greater Horn of Africa precipitation dataset. *Scientific Data*

Funk, C., & Verdin, J. (2003). Comparing Satellite Rainfall Estimates and Reanalysis Precipitation Fields with Station Data for Western Kenya. In *Presented at the JRC-FAO International Workshop on Crop Monitoring for Food Security in Africa, January 28-30, 2003, Nairobi, Kenya.* (pp. 89–96). European Commission and FAO.

Gallant, J. C., & Wilson, J. P. (2000). Digital Terrain Analysis. *Terrain Analysis: Principles and Applications*, (1988), 1–21.

Garbrecht, J., & Martz, L. W. (1999). Digital elevation model issues in water resources modeling. In: Proceedings from invited water resources sessions. *ESRI International User Conference*.

García-Pintado, J., Mason, D. C., Dance, S. L., Cloke, H. L., Neal, J. C., Freer, J., & Bates, P. D. (2015). Satellite-supported flood forecasting in river networks: A real case study. *Journal of Hydrology*, *523*.

Gathenya, M., Mwangi, H., Coe, R., & Sang, J. (2011). Climate-and land use-induced risks to watershed services in the Nyando river basin, Kenya. *Experimental Agriculture*, *47*(2), 339–356.

Gaya, C. O., Gachari, M. K., & Gathenya, J. M. (2009a). Managing Floods In the Kano

Plains Using GIS. In *Applied Geoinformatics for Society and Environment: AGSE 2009* (pp. 284–289). Stuttgart: Hochschule für Technik (SUAS.

Gaya, C. O., Gachari, M. K., & Gathenya, J. M. (2009b). Validation of Satellite Rainfall Estimates over the Nyando Basin. *International Journal of Disaster Management and Risk Reduction*, *2*(1), 65–70.

Gaya, C. O., Gachari, M. K., & Gathenya, J. M. (2011). Construction of a Geodatabase for Use as a Decision Support Tool in the Floodplains of the Nyando Basin. *Journal of Science Technology Education and Management (JSTEM)*, *2*(1), 57–65.

Gaya, C. O., Gachari, M. K., & Gathenya, J. M. (2012). Use of Satellite Rainfall Estimates in Flood Early-Warning: Case of Nyando Basin., Journal of Earth Science and Engineering, Vol. 2, No.5, Serial No.8, 292 – 316, davidpublishing.com.

Griffith, C. G., Augustine, J. A., & William, L. (2014). Real time inference of convective rainfall from satellite data Real time inference of convective rainfall from satellite data, (July).

Grimes, D. I. F., Pardo-Iguzquiza, E., & Bonifacio, R. (1999). *Optimal Areal Rainfall Estimation Using Raingauges and Satellite Data*. *Journal of Hydrology* (Vol. 222).

Harris, A., Rahman, S., Hossain, F., Yarborough, L., Bagtzoglou, A. C., & Easson, G. (2007). Satellite-based Flood Modeling Using TRMM-based Rainfall Products, 3416–3427.

Hawkins, R. H., Ward, T. J., & Woodward, D. E. (2009). *Curve Number Hydrology: State of the Practice*. American Society of Civil Engineers.

Herman, A., Kumar, V. B., Arkin, P. A., & Kousky, J. V. (1997). Objectively determined 10-day African rainfall estimates created for famine early warning systems. *International Journal of Remote Sensing*, *18*(10), 2147–2159.

Hermance, J. F., & Sulieman, H. M. (2014). Assessing daily and seasonal satellite rainfall estimates using local gauges for the anomalous 2012 monsoon season in the African East Sahel. *International Journal of Remote Sensing*, *35*(1), 253–288.

Hijazi, J., & Geomatics, P. C. I. (2001). Elevation extraction from satellite data using PCI software. In *First Symposium on Space Observation Technologies for Defense Applications, Abu Dhabi, United Arab Emirates* (p. 6).

Jain, S. K., Mani, P., Jain, S. K., Prakash, P., Singh, V. P., Tullos, D., … Dimri, A. P. (2018). A Brief review of flood forecasting techniques and their applications. *International Journal of River Basin Management*, *16*(3), 329–344.

Jenson, S. K., & Domingue, J. O. (1988). Extracting topographic structure from digital elevation data for geographic information system analysis. Photogrammetric Engineering and Remote. *Photogrammetric Engineering and Remote Sensing*, *54*(11), 1593–1600.

JICA. (2009). *The Study on Integrated Flood Management for Nyando River Basin in the Republic of Kenya: Final Report Volume II* (Vol. II).

Jr. Sabins, F. F. (1997). *Remote Sensing Principles and Interpretation*. *XF2006166912*.

Jung, Y., Kim, D., Kim, D., Kim, M., & Lee, S. O. (2014). Simplified flood inundation mapping based on flood elevation-discharge rating curves using satellite images in gauged watersheds. *Water (Switzerland)*, *6*(5), 1280–1299.

Keenan, P. B., & Jankowski, P. (2019). Spatial Decision Support Systems: Three decades on. *Decision Support Systems*, *116*(October 2018), 64–76.

Kenny, F., & Matthews, B. (2005). A methodology for aligning raster flow direction data with photogrammetrically mapped hydrology. *Computers & Geosciences*, *31*(6), 768–779.

Kidd, C., & Huffman, G. (2011). Global precipitation measurement. *Meteorological Applications*, *18*(3), 334–353.

Kidson, R., & Richards, K. S. (2005). Flood frequency analysis: Assumptions and alternatives. *Progress in Physical Geography*.

KNBS. (2009). Population Distribution by Sex, Number of Households, Area and Density by County and District. *Kenya Census 2009*, 1–5.

KNBS. (2018). Highlights of the 2015/16 Kenya Integrated Household Budget Survey (KIHBS) Reports. Retrieved from https://www.knbs.or.ke/download/statistics-abstract-2018/

Kourgialas, N. N., & Karatzas, G. P. (2011). Flood management and a GIS modelling method to assess flood-hazard areas—a case study. *Hydrological Sciences Journal*, *56*(2), 212–225.

Krajewski, W. F., Ciach, G. J., McCollum, J. R., & Bacotiu, C. (2000). Initial Validation of the Global Precipitation Climatology Project Monthly Rainfall over the United States. *Journal of Applied Meteorology*, *39*(7), 1071–1086.

Lance, K. (2004). Hydrologic Process. Nairobi: USGS.

Laurent, H., Jobard, I., & Toma, A. (1998). *Validation of satellite and ground-based estimates of precipitation over the Sahel*. *Atmospheric Research* (Vol. 47–48).

Levy, J. K., Gopalakrishnan, C., & Lin, Z. (2005). Advances in decision support systems for flood disaster management: Challenges and opportunities. *International Journal of Water Resources Development*, *21*(4), 593–612.

Li, Z. (2014). Watershed modeling using arc hydro based on DEMs: a case study in Jackpine watershed. *Environmental Systems Research*, *3*(1), 11.

Liang, C., & MaCkay, D. S. (2000). A general model of watershed extraction and representation using globally optimal flow paths and up-slope contributing areas. *International Journal of Geographical Information Science*, *14*(4), 337–358.

Liu, X., & Li, J. (2008). Application of SCS model in estimation of runoff from small watershed in loess plateau of China. *Chinese Geographical Science*, *18*(3), 235–241.

Liu, Y. B., & De Smedt, F. (2005). Flood modeling for complex terrain using GIS and remote sensed information. *Water Resources Management*, *19*(5), 605–624.

LP DAAC. (n.d.). Land Processes Distributed Active Archive Center (LP DAAC). Retrieved April 2, 2019, from https://lpdaac.usgs.gov/dataset_discovery/aster/

Luchetta, A., & Manetti, S. (2003). *A real time hydrological forecasting system using a fuzzy clustering approach*. *Computers & Geosciences* (Vol. 29).

M. Lillesand, T., Kiefer, R., & W Chipman, J. (2004). *Remote Sensing and Image Interpretation (Fifth Edition)*. *The Geographical Journal* (Vol. 146).

Maidment, R. I., Grimes, D., Black, E., Tarnavsky, E., Young, M., Greatrex, H., … Alcántara, E. M. U. (2017). A new, long-term daily satellite-based rainfall dataset for operational monitoring in Africa. *Scientific Data*, *4*, 1–19.

Michener, W. K., & Houhoulis, P. F. (1997). Detection of Vegetation Changes Associated with Extensive Flooding in a Forested Ecosystem, (December).

Mitsova, D. (n.d.). Supporting Natural Hazards Management With Geospatial Technologies. Oxford University Press.

Moore, I. D. (1996). Hydrologic modeling and GIS. *GIS and Environmental Modeling: Progress and Research Issues*, 143–148.

Muthusi, F. M., Gathenya, M., Gadain, H., Kaluli, W., & Lenga, F. K. (2005). Application of the Usgs Streamflow Model to the Nyando Basin, Western Kenya. *European Journal of Scientific Research*, *12*(1), 9–19.

NASA. (n.d.). Distributed Active Archive Centers (DAACs). Retrieved April 20, 2019, from https://nssdc.gsfc.nasa.gov/earth/daacs.html

Nash, J. E., & Sutcliffe, J. V. (1970). River flow forecasting through conceptual models part I—A discussion of principles. *Journal of Hydrology*, *10*(3), 282–290.

Nicholson, S. E., Some, B., McCollum, J., Nelkin, E., Klotter, D., Berte, Y., … Traore, A. K. (2003a). Validation of TRMM and Other Rainfall Estimates with a High-Density Gauge Dataset for West Africa. Part II: Validation of TRMM Rainfall Products. *Journal of Applied Meteorology*, *42*(10), 1355–1368.

Nicholson, S. E., Some, B., McCollum, J., Nelkin, E., Klotter, D., Berte, Y., … Traore, A. K. (2003b). Validation of TRMM and Other Rainfall Estimates with a High-Density Gauge Dataset for West Africa . Part I : Validation of GPCC Rainfall Product and Pre-TRMM Satellite and Blended Products. *Journal of Applied Meteorology*, *42*(October), 1337–1354.

Njoroge, M., Muthama, N. J., Ouma, G. O., & Lukorito, C. B. (2010). Validation of satellite derived rainfall estimates over Kenya Résumé. In *Second RUFORUM Biennial Meeting 20 - 24 September 2010, Entebbe, Uganda* (pp. 1445–1449).

North, G. R. (1994). The Ground-Truth Problem for Satellite Estimates of Rain Rate, *0426*(September 2015).

Nyakundi, H., Mogere, S., Mwanzo, I., & Yitambe, A. (2012). Community perceptions and response to flood risks in Nyando District, Western Kenya. *Jàmbá: Journal of Disaster Risk Studies*, *3*(1).

O'Callaghan, J. F., & Mark, D. M. (1984). The extraction of drainage networks from digital elevation data. *Computer Vision, Graphics, and Image Processing*, *28*(3), 323–344.

Ogrosky, H. O., & Mockus, V. (1957). The hydrology guide. *National Engineering Handbook, Section*, *4*.

Olang, L. O., & Fürst, J. (2011). Effects of land cover change on flood peak discharges and runoff volumes: Model estimates for the Nyando River Basin, Kenya. *Hydrological Processes*, *25*(1), 80–89.

Olugunorisa, T. (2011). Strategies for Mitigation of Flood Risk in the Niger Delta, Nigeria. *Journal of Applied Sciences and Environmental Management*, *13*(2).

Onyango, L. (2004). Effects of flooding in the lower Nyando River Basin. In D. Mungai, S. Brent, J. Mburu, L. Onyango, & A. Njui (Eds.), *Reversing Environmental and Agricultural Decline in the Nyando River Basin* (pp. 41–51). 2004 World Agroforestry Centre.

Opere, A. (2013). *Floods in Kenya*. *Kenya: A Natural Outlook* (1st ed., Vol. 16). Elsevier B.V.

Oswald, H., & Raetzsch, H. (1984). A system for generation and display of digital elevation models. *Geo-Processing*, *2*, 197–218.

Otiende, B. (2009). The economic impacts of climate change in Kenya: Riparain Flood Impacts and Cost of Adaptation, (September), 16.

Ouma, G. O., Adafre, C. ., & Muthama, N. J. (2005). Validation of Satellite-Derived Rainfall Estimates: The Ethiopian Case Study. In *7th Kenya Meteorological Society Workshop on Meteorological Research, Applications and Services*. Nairobi.

Petty, G., Morissey, M., Adler, R. F., Goodman, H. M., & Kidd, C. (2002). Intercomparison of Global Precipitation Products: The Third Precipitation Intercomparison Project (PIP–3). *Bulletin of the American Meteorological Society*, *82*(7), 1377–1396.

Ponce, V. M., & Hawkins, R. H. (2002). Runoff Curve Number: Has It Reached Maturity? *Journal of Hydrologic Engineering*, *1*(1), 11–19.

Rao, A. R., & Hamed, K. H. (2000). *Flood Frequency Analysis*. CRC Press LLC.

Saunders, W. (2000). *Preparation of DEMs for use in environmental modeling analysis*. *Hydrologic and Hydraulic Modeling Support with Geographic Information Systems*.

SCS. (1972). *National Engineering Handbook (NEH), Section 4, Hydrology*. Washington DC: US Department of Agriculture.

SCS, H. U. and T. T. S. S. (1992). Technical Release 20: Computer Program for Project Formulation Hydrology (TR-20). *Program*.

Sindhu, K., & Durga Rao, K. H. V. (2017). Hydrological and hydrodynamic modeling for flood damage mitigation in Brahmani–Baitarani River Basin, India. *Geocarto International*, *32*(9), 1004–1016.

Soulis, K. X., Valiantzas, J. D., Dercas, N., & Londra, P. A. (2009). Analysis of the runo generation mechanism for the investigation of the SCS-CN method applicability to a partial area experimental watershed. *Soil Conservation*, 605–615.

Stedinger, J. R., & Griffis, V. W. (2011). Getting from here to where? Flood frequency analysis and climate. *Journal of the American Water Resources Association*, *47*(3), 506–513.

Swallow, B., Onyango, L., & Meinzen-Dick, R. (2003). Catchment Property Rights and the Case of Kenya's Nyando Basin'. *Preparing for the Next Generation of Watershed Management Programmes And Projects*, 123–136.

Tarboton D.G. (1997), A New Method for Determination of Flow Directions and Upslope Areas in Grid Digital Elevation Models, Water Resources Research, 32, pp 309-319

Tarboton, D. G., Bras, R. L., & Rodriguez-iturbet, I. (1991). On Extraction of Channel Networks From Digital Elevation Data, *Hydrological Processes 5* (September 1990), 81–100.

Tarruella, R., & Jorge, J. (2003). Comparison of three infrared satellite techniques to estimate accumulated rainfall over the Iberian Peninsula. *International Journal of Climatology*, *23*(14), 1757–1769.

Tehrany, M. S., Pradhan, B., Mansor, S., & Ahmad, N. (2015). Flood susceptibility assessment using GIS-based support vector machine model with different kernel types. *Catena*, *125*, 91–101.

Thiemig, V., de Roo, A., & Gadain, H. (2011). Current status on flood forecasting and early warning in Africa. *International Journal of River Basin Management*, *9*(1), 63–78.

Thorne, V., Coakeley, P., Grimes, D., & Dugdale, G. (2001). Comparison of TAMSAT and CPC rainfall estimates with raingauges, for southern Africa. *International Journal of Remote Sensing*, *22*(10), 1951–1974.

Tobler, W. R. (1970). A Computer Movie Simulation Urban Growth in Detroit Region. *Economic Geography*, *46*, 234–240.

Torres, R., Snoeij, P., Geudtner, D., Bibby, D., Davidson, M., Attema, E., … Floury, N. (2012). GMES Sentinel-1 mission. *Remote Sensing of Environment*, *120*, 9–24.

Toté, C., Patricio, D., Boogaard, H., Funk, C., Tarnavsky, E., & van der Wijngaart, R. (2015). Evaluation of Satellite Rainfall Estimates for Drought and Flood Monitoring in Mozambique. *Remote Sensing*, *7*(2), 1758–1776.

Tucker, M. R., & Sear, C. B. (2001). A comparison of Meteosat rainfall estimation techniques in Kenya. *Meteorological Applications*, *8*(1), 107–117.

Ulubay, A., & Altan, M. O. (2002). A Different Approach to the Spatial Data Integration. *Symposium on Geospatial Theory, Processing and Applications*, 6.

USDA. (1986). *Urban Hydrology for Small Watersheds TR-55*. *TR-55*. https://doi.org/Technical Release 55

USGS FEWSNET. (n.d.). FEWS Home | Early Warning and Environmental Monitoring Program. Retrieved April 20, 2019, from https://earlywarning.usgs.gov/fews

van der Meer, F., Schmidt, K. S., W., B., & W., B. (2002). New environmental remote sensing systems. In A. Skidmore (Ed.), *Environmental Modelling with GIS and Remote Sensing* (pp. 26–51). London: Taylor& Francis.

van Dijk, M. ., Boekelman, R. H., & Rientjes, T. H. M. (1999). Modelling of hydrological processes. In P. Bähr & T. Vögtle (Eds.), *GIS for environmental monitoring* (pp. 283–306). Schweizerbart'sche Verlagsbuchhandlung.

van Westen, C. J. (2002). Remote Sensing and Geographic Information Systems for Natural Disaster Management. In A. Skidmore (Ed.), *Environmental Modelling with GIS and Remote Sensing* (pp. 200–226). London: Taylor& Francis.

Verdin, J., Funk, C., Senay, G., & Choularton, R. (2005). Climate science and famine early warning. *Philosophical Transactions of the Royal Society B: Biological Sciences*, *360*(1463), 2155–2168.

Vieux, B. E. (2004). *Distributed Hydrological Modeling Using GIS* (2nd ed.). Dordrecht: Kluwer Academic Publishers.

Wang, J., Li, L., Hao, Z., & Gourley, J. J. (2011). Stream guiding algorithm for deriving flow direction from DEM and location of main streams. *IAHS-AISH Publication*, *346*(July), 198–206.

WMO. (2011a). *Manual on Flood Forecasting and Warning: WMO-No. 1072*. Retrieved from http://www.wmo.int/pages/prog/hwrp/publications/flood_forecasting_warning/WMO 1072_en.pdf

WMO. (2011b). WMO Flood Forecasting Initiative. Retrieved April 20, 2019, from https://www. wmo.int/pages/prog/hwrp/FFI-index.php

Yoeli, P. (1982). *Cartographic drawing with computers*. Department of Geography, University of Nottingham.

Yoeli, P. (1984). Computer-assisted determination of the valley and ridge lines of digital terrain models. *International Yearbook of Cartography*, *24*, 197–206.

Zhang, W., & Montgomery, D. R. (1994). Digital elevation model grid size, landscape representation, and hydrologic simulations. *Water Resources Research*, *30*(4), 1019–1028.

APPENDICES

Appendix I: VBA Code for Extraction of RFEValues at Rain Gauge Positions

```
Sub RFEvsGAUGES()

'

'Macro: Comparison of RFE data with observed raingauge data

'



Dim pWorkspaceFactory As IWorkspaceFactory

Set pWorkspaceFactory = New ShapefileWorkspaceFactory

Dim pWorkSpace As IFeatureWorkspace

Dim pMxDoc As IMxDocument

'Dim pActiveView As IActiveView

Set pMxDoc = ThisDocument

'---------------------------------------------

'ATTRIBUTIVE QUERY TO SELECT RAINGAUGE STATIONS

'- - - - - - - - - - - - - - - - - - - - - - -

'Find the Stations layer

Dim pMap As IMap

Dim pFeatLyr As IFeatureLayer

Dim i As Integer

Set pMap = pMxDoc.FocusMap

For i = 0 To pMap.LayerCount - 1

 Set pFeatLyr = pMap.Layer(i)
```

```
 If pFeatLyr.Name = "AvailableStns" Then
' Found it and exit loop
 Exit For
End If
Next i
' Create a string to use in the query
Dim queryStr As String
queryStr = "ID = 1"
' Create the query filter
Dim pQueryFltr As IQueryFilter
Set pQueryFltr = New QueryFilter
pQueryFltr.WhereClause = queryStr
' Perform the selection
Dim pFeatSeln As IFeatureSelection
' QI for IFeatureSelection from the IFeatureLayer
Set pFeatSeln = pFeatLyr
pFeatSeln.SelectFeatures pQueryFltr, esriSelectionResultNew, False
'MsgBox "num features:" & pFeatLyr.FeatureClass.FeatureCount(Nothing)
'Flag the area of the new selection to invalidate
pMxDoc.ActiveView.PartialRefresh esriViewGeoSelection, Nothing, Nothing
'_____
'to form a single geometry from the selected features in a layer.
```

```
Dim pSelnSet As ISelectionSet

Set pSelnSet = pFeatSeln.SelectionSet

Dim pEnumGeom As IEnumGeometry

Dim pEnumGeometryBind As IEnumGeometryBind


Set pEnumGeom = New EnumFeatureGeometry

Set pEnumGeometryBind = pEnumGeom

pEnumGeometryBind.BindGeometrySource Nothing, pSelnSet

Dim pGeomFactory As IGeometryFactory

Set pGeomFactory = New GeometryEnvironment

Dim pGeom As IGeometry

Set pGeom = pGeomFactory.CreateGeometryFromEnumerator(pEnumGeom)

'_____

'open the RFE polygon of the date and add to view

Set pWorkSpace = pWorkspaceFactory.OpenFromFile("D:\DATABANK\Hydro\Rainfall\Processed", 0)

Dim pClass As IFeatureClass

Set pClass = pWorkSpace.OpenFeatureClass("rain_2003111v")

Dim pLayer As IFeatureLayer

Set pLayer = New FeatureLayer

Set pLayer.FeatureClass = pClass

pLayer.Name = pClass.AliasName


pMxDoc.AddLayer pLayer
```

```
'----------------------

' SPATIAL QUERY TO SELECT RFE "CELLS" THAT AT THE LOCATIONS OF THE GAUGES

'

Dim pSpatialFilter As ISpatialFilter

Set pSpatialFilter = New SpatialFilter

With pSpatialFilter


Set .Geometry = pGeom

.GeometryField = pFeatLyr.FeatureClass.ShapeFieldName

.SpatialRel = esriSpatialRelIntersects

End With

Dim pFeatureSelection As IFeatureSelection

Set pFeatureSelection = pLayer

pFeatureSelection.SelectFeatures pSpatialFilter, _

esriSelectionResultNew, False


End Sub

'_

'_____________________________________________________________________

Public Sub GetSelectedFeature()

Dim pMxDoc As IMxDocument

Dim pMap As IMap
```

```
Dim pEnumFeature As IEnumFeature

Dim pFeature As IFeature

Set pMxDoc = Application.Document

Set pMap = pMxDoc.FocusMap

Set pEnumFeature = pMap.FeatureSelection

pEnumFeature.Reset

Set pFeature = pEnumFeature.Next

End Sub
```

```
'RASTER import (still under construction)

Sub RasterRFE()

Dim pMxDoc As IMxDocument

Set pMxDoc = ThisDocument

Dim pRFE As IRasterDataset


Dim pRasLayer As IRasterLayer

Set pRasLayer = New RasterLayer



'open RFE the raster file for the date

Set pRFE = OpenRasterDataset("D:\DATABANK\RFE Data\rfe_2003", "rain_20031")

pRasLayer.CreateFromDataset pRFE

pMxDoc.FocusMap.AddLayer pRasLayer
```

```
End Sub

'CLIPPING RFE Raster (still under construction)

Sub ClipRaster()

Dim pMxDoc As IMxDocument

Set pMxDoc = ThisDocument

Dim pFeatLyr As IFeatureLayer

Dim pRasLayer As IRasterLayer

Set pRasLayer = New RasterLayer

Dim pMap As IMap

Dim i As Integer

Set pMap = pMxDoc.FocusMap

For i = 0 To pMap.LayerCount - 1

 Set pRasLayer = pMap.Layer(i)


 If pRasLayer.Valid = True Then

' Found it and exit loop

 Exit For

End If

Next i

'Dim pClip As IRasterLayer

'Set pClip = New RasterLayer

'pClip = pRasLayer.AreaOfInterest

'#Set pRasLayer.AreaOfInterest.Envelope = pFeatLyr.SpatialReference
```

```
End Sub

Public Function OpenFeatureClass(sPath As String, sFile As String)

Dim pWorkspaceFactory As IWorkspaceFactory

Set pWorkspaceFactory = New ShapefileWorkspaceFactory

Dim pFeatureWorkspace As IFeatureWorkspace

Set pFeatureWorkspace = _

pWorkspaceFactory.OpenFromFile(sPath, 0)

Dim pFeatureClass As IFeatureClass

Set pFeatureClass = pFeatureWorkspace.OpenFeatureClass(sFile)

MsgBox "There are " & pFeatureClass.FeatureCount(Nothing) & " polygons"

End Function


Public Function SetRasterWorkspace(sName As String) As IRasterWorkspace

' Given a pathname, returns the raster workspace object for that path

' If not a valid raster workspace returns nothing. Caller must test!!

On Error GoTo ErrorSetWorkspace

Dim pWKSF As IWorkspaceFactory

Set pWKSF = New RasterWorkspaceFactory

Dim pWKS As IRasterWorkspace

Set pWKS = pWKSF.OpenFromFile(sName, 0)

Set SetRasterWorkspace = pWKS

Exit Function

ErrorSetWorkspace:
```

```
Set SetRasterWorkspace = Nothing

End Function

Public Function OpenRasterDataset(sPath As String, sFile As String) _

As IRasterDataset

' Given a path and filename, returns the raster dataset object

' If not a valid raster dataset returns nothing. Caller must test!!

On Error GoTo ErrorOpenRasterDataset

Dim pRasWKS As IRasterWorkspace

Set pRasWKS = SetRasterWorkspace(sPath)

Dim pRasDS As IRasterDataset

Set pRasDS = pRasWKS.OpenRasterDataset(sFile)

Set OpenRasterDataset = pRasDS

ErrorOpenRasterDataset:

Set OpenRasterDataset = Nothing

End Function
```

Appendix II: The Procedure of Using Satellite Rainfall Estimates (RFE) to Simulate Surface Runoff in GIS

1. Clipping Satellite Rainfall Estimates to Basin Boundary

To reduce on the size of raster files being handled in the simulation, a routine was developed to clip all RFE global raster to the coverage of the study area. This was performed iteratively for each day of each year used using the model shown in Figure II.1.

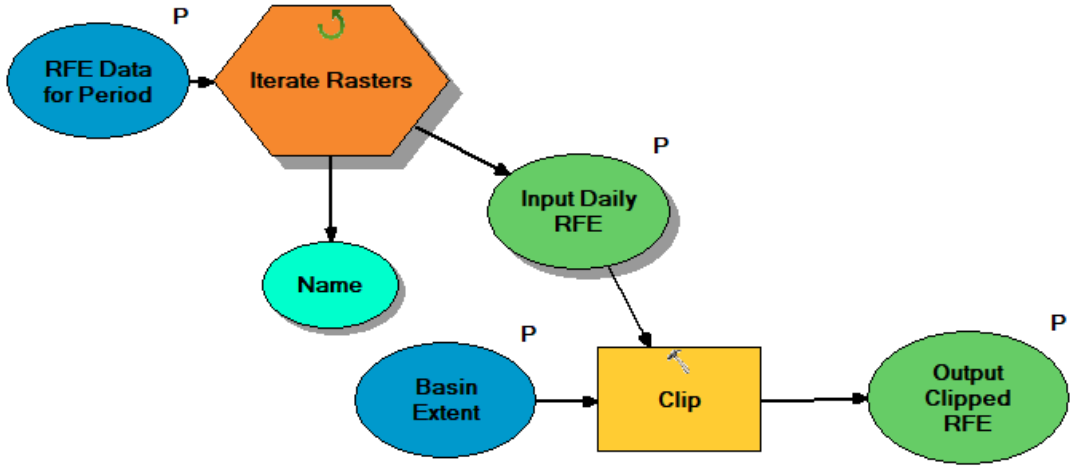

Figure II.1: This model clips the input global raster rainfall estimates to the river basin of interest.

The inputs were the daily global RFE data for a year and the shapefile of the basin extent. The output was the clipped daily RFE raster for the year.

2. Converting Satellite Rainfall from mm to inches

In order to use the Curve Number method Eqn 3.9. to compute runoff volume, the RFE rainfall values, P for each cell must first be converted from millimeters to inches using the model shown in Figure II.2.

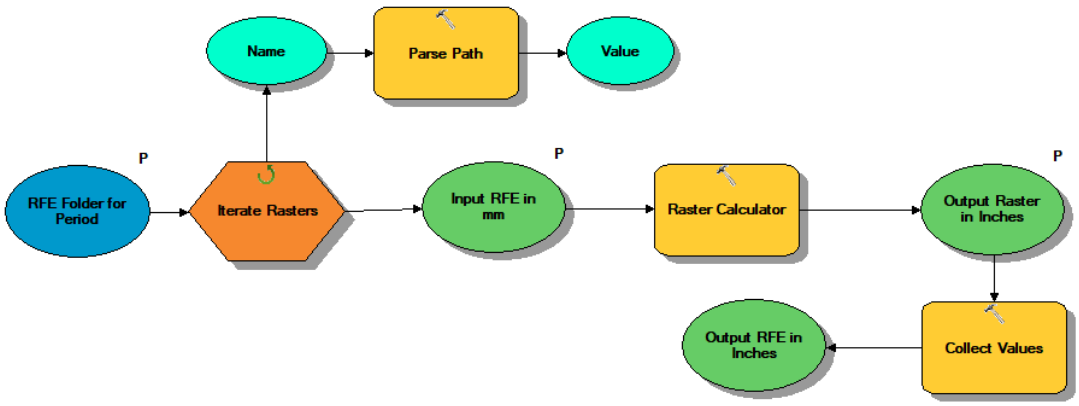

Figure II.2: Converting unit of display of satellite rainfall estimates from millimetres to inches for each cell, for each day.

The input was the daily clipped RFE data for a year in millimetres. This was iteratively subjected to the expression: *"%Input RFE in mm%" / 25.4* in the raster calculator. The output was the clipped daily RFE raster for the year in inches.

3. Computing Runoff Depth in mm

Using the converted rainfall estimates in mm, the runoff depth, Q was computed for each cell using Eqn 3.11`through the expression: 25.4*Square("%Input RFE in

Inches%" -"%Initial Abstraction%")/ ("%Initial Abstraction%"+0.8*"%Surface Storage%") in the Raster Calculator.

The inputs were the initial abstraction raster and surface storage rasters for the basin and the daily RFE estimate in inches for a year. The daily RFE is introduced iteratively. The output was the runoff depth in mm for each cell, for each day of the year. The model used to achieve this is shown in Figure II.3.

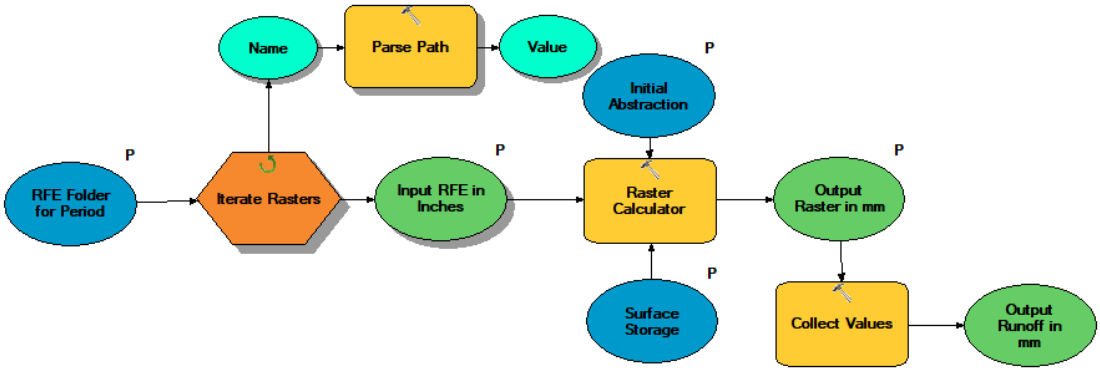

Figure II.3: Model computes runoff (mm) from initial abstraction, surface storage and satellite rainfall estimates for each cell, for each day.

4. Computing Runoff Volume

The runoff depth for each cell on each day was used to assign weights to the upstream cells contributing drainage to each cell in the basin using the flow direction grid. This was used to generate a weighted flow accumulation grid to record how much volume of runoff is incident to each cell for each day, the areal unit being one cell. This was done using the model shown in Figure II.4

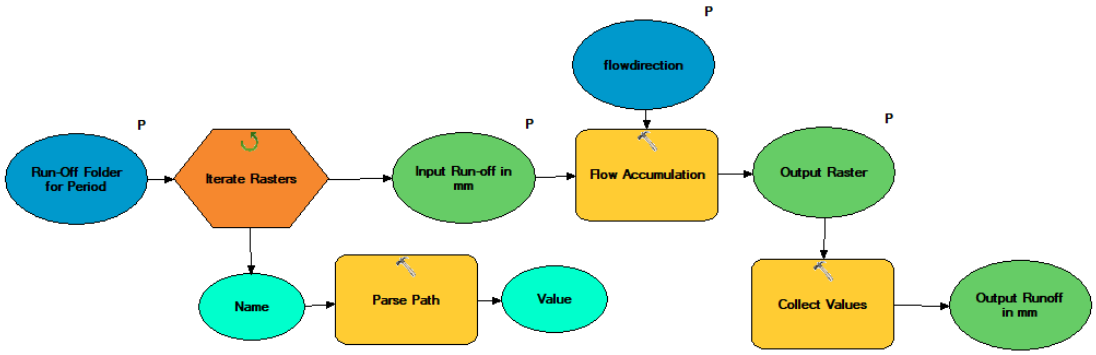

Figure II.4: Model computes runoff volume from flow direction and satellite rainfall estimates for each cell, for each day.

The inputs were the flow direction raster for the basin and the daily RFE estimates in mm. The output was a continuous raster of runoff volume for each day.

5. Extracting Runoff Values at Flow Gauge Positions

Finally, the runoff volumes obtained were exported to tabular form for analysis using the shapefile of positions of the flow gauges to extract the runoff values at those points. This was done using the model shown in Figure II.5.

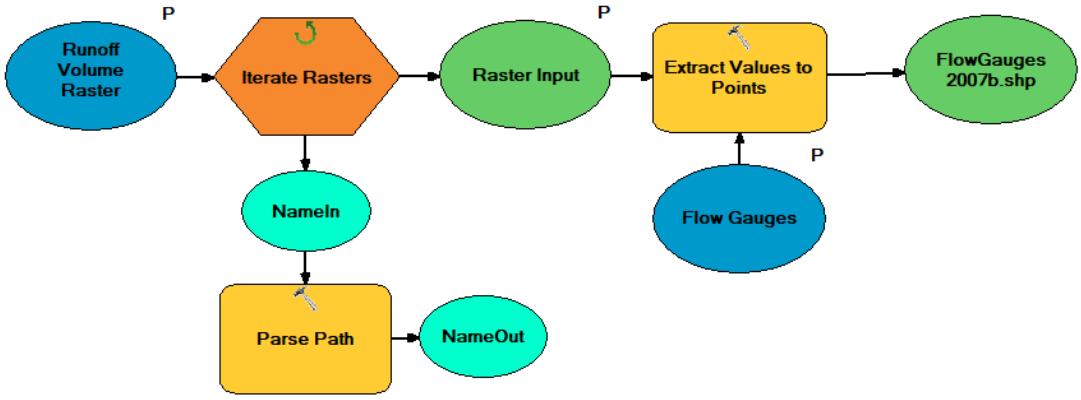

Figure II.5: This model extracts cell values of the runoff volume raster at positions of the flow gauges.

The inputs were the run off volume raster and the shapefile of flow gauges. The output was an updated flow gauges attribute table that contains new fields and data on the runoff volume for each day for each gauge. This data was exported to Excel spreadsheets for analysis.